IOWA STATE UNIVERSITY
Digital Repository

Retrospective Theses and Dissertations

Iowa State University Capstones, Theses and Dissertations

1997

Photodissociation dynamics of polyatomic molecules

Hequan Zhao
Iowa State University

Follow this and additional works at: https://lib.dr.iastate.edu/rtd

 Part of the Physical Chemistry Commons

Recommended Citation
Zhao, Hequan, "Photodissociation dynamics of polyatomic molecules " (1997). *Retrospective Theses and Dissertations*. 11581.
https://lib.dr.iastate.edu/rtd/11581

This Dissertation is brought to you for free and open access by the Iowa State University Capstones, Theses and Dissertations at Iowa State University Digital Repository. It has been accepted for inclusion in Retrospective Theses and Dissertations by an authorized administrator of Iowa State University Digital Repository. For more information, please contact digirep@iastate.edu.

www.manaraa.com

INFORMATION TO USERS

This manuscript has been reproduced from the microfilm master. UMI films the text directly from the original or copy submitted. Thus, some thesis and dissertation copies are in typewriter face, while others may be from any type of computer printer.

The quality of this reproduction is dependent upon the quality of the copy submitted. Broken or indistinct print, colored or poor quality illustrations and photographs, print bleedthrough, substandard margins, and improper alignment can adversely affect reproduction.

In the unlikely event that the author did not send UMI a complete manuscript and there are missing pages, these will be noted. Also, if unauthorized copyright material had to be removed, a note will indicate the deletion.

Oversize materials (e.g., maps, drawings, charts) are reproduced by sectioning the original, beginning at the upper left-hand corner and continuing from left to right in equal sections with small overlaps. Each original is also photographed in one exposure and is included in reduced form at the back of the book.

Photographs included in the original manuscript have been reproduced xerographically in this copy. Higher quality 6" x 9" black and white photographic prints are available for any photographs or illustrations appearing in this copy for an additional charge. Contact UMI directly to order.

UMI

A Bell & Howell Information Company
300 North Zeeb Road, Ann Arbor MI 48106-1346 USA
313/761-4700 800/521-0600

Photodissociation dynamics of polyatomic molecules

by

Hequan Zhao

A dissertation submitted to the graduate faculty
in partial fulfillment of the requirements for the degree of
DOCTOR OF PHILOSOPHY

Major: Physical Chemistry
Major Professor: Cheuk-Yiu Ng

Iowa State University
Ames, Iowa
1997

UMI Number: 9814718

UMI Microform 9814718
Copyright 1998, by UMI Company. All rights reserved.

This microform edition is protected against unauthorized
copying under Title 17, United States Code.

UMI
300 North Zeeb Road
Ann Arbor, MI 48103

Graduate College

Iowa State University

This is to certify that the Doctoral dissertation of

Hequan Zhao

has met the dissertation requirements of Iowa State University

Signature was redacted for privacy.

Major Professor

Signature was redacted for privacy.

For the Major Program

Signature was redacted for privacy.

For the Graduate College

TABLE OF CONTENTS

ACKNOWLEDGMENTS

Many people have assisted me during my Ph.D. studies at Iowa State University. At this time, I would like to express my cordial appreciation.

First, I deeply thank Dr. Cheuk-Yiu Ng for his support, understanding and assistance in my research. I am strongly impressed by his insight in science and his enthusiastiasm for work. I have greatly benefited from his guidance.

I would like to thank Dr. Chung-Lin Liao and Mr. Chu-Xiong Liao for their assistance to my experiments. We worked together to repair the excimer laser to increase laser energy. I am grateful to Mr. Jerry Flesch for helping me to use the mass spectrometer and the leak detector. I also thank Mr. Eldon Ness, Terry Soseman, and Dick Egger in the chemistry machine shop for their invaluable service. I am grateful to Y.-S. Cheung for conducting the *ab initio* calculations in order to explain my experimental data. I also thank Dave Baran, Dan Heck and Troy Tetzlaff for editing my writing. I have enjoyed my time with them.

Finally, I deeply thank my family for their support and understanding. My wife, Guijuan Wang, took a lot of time to take care of our son. Whenever I felt upset about my experiments, she always encouraged me.

GENERAL INTRODUCTION

Introduction

The study of the photodissociation dynamics of polyatomic molecules has attracted great interest. The measurement of maximum translational energy release can be used to calculate the specific bond energy of molecules, which is essential in determining the chemical reaction enthalpy.[1] The pathway identifications of photodissociation molecules provide information for the photochemical reaction mechanisms. Furthermore, photodissociation can produce radicals in a pure state to be used in studies of the interactions or reactions between radicals and molecules.

Photodissociation of polyatomic molecules generally involves more than one product process, resulting from the multi-dimensional nature of the excited potential energy surfaces and the efficient energy redistribution between the internal degrees of motion of the excited precursor molecules. Because of the accessibility of multi-channel dissociation pathways, the identification of nascent products, as well as data analysis for such dissociation processes, poses a great challenge to experimentalists.[2] Photodissociation of acetophenone (a model of the polyatomic molecule) at 193 nm and 248 nm has been conducted. Due to two unequivalent C-C bonds, two primary processes have been observed.

For a symmetric molecule, such as acetone [$(CH_3)_2CO$], two equivalent C-C bonds can be broken. In this case the question of whether the products $CH_3 + CO + CH_3$ are formed sequentially or concertedly[3] needs to be answered.[4-6] Dimethylsulfoxide [$(CH_3)_2SO$] is a sulfur analog of acetone [$(CH_3)_2CO$]. Being the simplest sulfoxide, the

photochemistry of $(CH_3)_2SO$ represents a model system for understanding sulfoxide photochemistry. Therfore, we choose DMSO as another model for the study of the photodissociation dynamics of polyatomic molecules.[7]

Dissertation Organization

The thesis is composed of five papers prepared in a format ready for publication. The tables, figures, and references mentioned in each paper pertain only to that paper. The first paper is a typical example for studies of photodissociation of polyatomic molecules. In this paper, photodissociation studies of acetophene ($C_6H_5COCH_3$) at 193 nm and 248 nm are presented. Due to the multi-process property, experimental and data fitting techniques were applied to identify the processes. The second paper is the photodissociation study of dimethylsulfoxide [DMSO, $(CH_3)_2SO$] at 193 nm. DMSO is a sulfur analog of acetone in which two chemical bonds may be broken with one photon. In this study, the CH_3SO radical was directly detected. Evidently, this is a stepwise dissociation process. The third paper is the photodissociation study of $HSCH_2CH_2SH$. The C-S bond energy of this compound is reported for the first time. The fourth paper is the photodissociation of thiophene (C_4H_4S), which is a cyclic organic molecule containing a sulfur atom. Since the primary dissociation products cannot be observed due to the kinematic constraints, the biradical (•C4H4S•) decay dynamics were studied. The fifth paper is a study of the radical and atomic interactions using the photodissociation products obtained from the photodissociation of SO_2.

References

(1) H.-Q Zhao, Y.-S. Cheung, C.-X. Liao, C. Y. Ng, Wai-Kee Li, and See-Wing, *J. Chem. Phys.* **104**, 130(1996).

(2) C.-W. Hsu, C.-L. Liao, Z.-X. Ma, and C. Y. Ng, *J. Phys. Chem.* **99**, 1760 (1995).

(3) C. E. M. Strauss and P. L. Houston, *J. Phys. Chem.* **94**, 8751 (1990).

(4) K. A. Trentelman, S. H. Kable, D. B. Moss, and P. L. Houston, *J. Chem. Phys.* **91**, 7498 (1989).

(5) S. W. North, D. A. Blank, J. D. Gezelter, C. A. Longfellow, and Y. T. Lee, *J. Chem. Phys.* **102**, 4447 (1995).

(6) S. K. Kim, S. Pederson, and A. H. Zewail, *J. Chem. Phys.* **103**, 477 (1995).

(7) H.-Q. Zhao, Y.-S.Cheung, D. P. Heck, C. Y. Ng, T. Tetzlaff, and W. Jenks, *J. Chem. Phys.* ***106***, 86 (1997).

A LASER PHOTOFRAGMENTATION TIME-OF-FLIGHT MASS SPECTOROMETRIC STUDY OF ACETOPHENONE AT 193 AND 248 NM

A paper accepted by the Journal of chemical Physics

Zhao, H.Q., Cheung, Y-S., Liao, C-L., Liao, C-X., Ng, C.Y.

Abstract

The photodissociation of acetophenone ($C_6H_5COCH_3$) at 193 and 248 nm has been studied using the time-of-flight (TOF) mass spectrometric technique. For hν=193 nm, two major primary processes, $C_6H_5COCH_3 + h\nu \rightarrow C_6H_5CO + CH_3$ [process (1)] and $C_6H_5 + CH_3CO$ [process (2)], are observed with comparable cross sections. Data analysis shows that ≈30-50% of primary C_6H_5CO and CH_3CO radicals further decomposes, yielding secondary products C_6H_5 + CO and CH_3 + CO, respectively. The translational energy release measurements indicate that for both processes (1) and (2) at 193 nm, ≈25-30 % of the available energy is channeled into kinetic energies of the primary photofragments. Measurements at hν=248 nm reveal that the branching ratio of process (2) to process (1) is ≈0.01. For process (1) at hν=248 nm, ≈42% of the available energy is directed as the kinetic energy of the photofragments. The observed maximum kinetic energy release for process (1) at 248 nm yields a value of 85.0±2.2 kcal/mol for the C_6H_5CO-CH_3 bond dissociation energy at 0 K (D_0). The photofragment angular distributions are found to be isotropic for both processes (1) and (2) at hν= 193 nm and for process (1) at hν= 248 nm. A minor photodissociation process $C_6H_5COCH_3 + h\nu \rightarrow C_6H_5CH_3 + CO$ is identified at both hν=193 and 248 nm. The energetics for the dissociation reactions of acetophenone have also been investigated using *ab initio* Gaussian-2-type procedures. The heats of formation at 0 K

($\Delta_fH°_0$) for C_6H_5CO and C_6H_5 calculated using the isodesmic reaction scheme are 33.9±1.3 and 87.6±1.0 kcal/mol, respectively. These results suggest that the literature $\Delta_fH°_0$ values for C_6H_5CO and C_6H_5 are likely to be high by 3-4 kcal/mol. These theoretical $\Delta_fH°$ values for C_6H_5CO and C_6H_5 yield a theoretical $D_0(C_6H_5CO\text{-}CH_3)$ value of 85.1±1.4 kcal/mol, which is in excellent accord with the experimental results obtained in the present study.

Introduction

The ultraviolet (UV) photochemistry of alkyl ketones[1-5] and related molecules[5-9] has been the subject of many recent laser excitation studies. Upon absorption of a UV photon, ketone is known to dissociate efficiently via C-CO bond cleavage, resulting in acyl and alkyl radicals.[1-5,10] Since the C-CO bond of an acyl radical is weak, excited acyl radicals formed at a sufficiently high internal energy have been found to undergo further decomposition, producing CO and alkyl radicals.[1,5,7,11] Acyl and alkyl radicals are important intermediates in combustion and atmospheric process.[12] The knowledge of the UV photochemistry of ketone is relevant for the preparation of these radicals for spectroscopic and reactivity studies. Recent excimer laser photofragmentation time-of-flight (TOF) mass spectrometric experiments have provided detailed information concerning the dissociation mechanism of acetone (CH_3COCH_3).[1,2] Both acetyl (CH_3CO) and methyl (CH_3) radicals are observed in the 248 nm photodissociation of CH_3COCH_3, whereas CO + $2CH_3$ are identified to be products at 193 nm.[1] A analysis of the TOF spectra for CH_3 and CO has established that the formation of CO + $2CH_3$ from CH_3COCH_3 at 193 nm is governed by a stepwise mechanism.[1]

The photochemistry of acetophenone ($C_6H_5COCH_3$), the simplest aromatic ketone, has received little attention compared to that of CH_3COCH_3. Early photochemical studies of acetophenone were motivated by the search for a convenient source of phenol radicals.[13,14] The gas phase absorption spectrum for $C_6H_5COCH_3$ in the region of 210-380 nm exhibits three broad peaks centered at 325, 275, and 230 nm, which are assigned to the $S_0 \rightarrow S_1$, $S_0 \rightarrow S_2$, and $S_0 \rightarrow S_3$ transitions, respectively.[10,15] The absorption cross section for the $S_0 \rightarrow S_3$ peak is significantly stronger than that of the $S_0 \rightarrow S_2$ peak, which is in turn stronger than that of the $S_0 \rightarrow S_1$ peak. The first excited singlet S_1 or $^1(n, \pi^*)$ state of acetophenone is formed by an electron from the nonbonding orbital (n) localized at the O atom being excited to the antibonding π^* orbital of the carbonyl group. The existence of an aromatic ring adjacent to the carbonyl group in simple aromatic ketones, such as acetophenone, is likely to facilitate intramolecular energy transfer, and hence inhibits the dissociative channels. Due to a small energy gap between the S_1 and T_1 [or $^3(n, \pi^*)$] states, the S_1 states of simple aromatic ketones are known to undergo rapid intersystem crossing to the T_1 state, resulting in high phosphorescence quantum yields.[10,15] Similar intersystem crossing processes are expected to follow the S_2 and S_3 states. Thus, the photochemistry of S_1 as well as S_2 and S_3 states may actually take place from triplet potential energy surfaces.

The present work deals with the measurement and analysis of photofragment translational energy distributions and recoil anisotropies for the photodissociation of acetophenone at 193 nm and 248 nm. The photon wavelength of 248 nm falls between the $S_0 \rightarrow S_2$ and $S_0 \rightarrow S_3$ absorption peaks.[15] The previous kinetic study concluded that following $S_0 \rightarrow S_2$ excitation,

triplet acetophenone dissociates exclusively into C_6H_5CO (benzoyl radical) + CH_3.[15] The absorption cross section for acetophenone at 193 nm is not available. However, judging from the trend of the absorption cross sections measured near 210 nm, the absorption cross section at 193 nm is likely to be much higher than that for the $S_0 \rightarrow S_3$ peak. Excited states higher than S_3 are likely responsible for the photohemistry of acetophenone at 193 nm. In accordance with the known UV photochemistry of ketone,[1-5,10,15] we find that the dissociation of $C_6H_5COCH_3$ at 193 and 248 nm is dominated by processes (1) and (2).

$$C_6H_5COCH_3 + h\nu \rightarrow C_6H_5CO + CH_3 \quad (1)$$

$$\rightarrow C_6H_5 + CH_3CO \quad (2)$$

$$\rightarrow C_6H_5CH_3 + CO \quad (3)$$

Evidence is found for the very minor occurrence of process (3).

Accurate energetic information about process (1) and (2) is essential for the analysis of the photofragment TOF spectra observed in this experiment. The heats of formation at 0 K (298K), $D_fH°_0$ ($D_fH°_{298}$) for the radical fragments formed in processes (1) and (2) are not well-established. Thus, we have conducted a theoretical study of the energetics of C_6H_5CO, C_6H_5, and CH_3CO using established *ab initio* quantum chemical schemes, such as the Gaussian-2 (G2) theory and its variances.[16-19] We note that the G2 and G2(MP2) calculations of the heat of formation for the acetyl radical has been reported previously.[20] The errors associated with G2 predictions for $D_fH°_0$ ($D_fH°_{298}$) values of larger polyatomic species, such as C_6H_5CO and

C_6H_5, may be higher than that of CH_3CO.[20] Recent G2-type schemes, which combine the G2-type calculations and appropriate isodesmic reactions, have shown to provide accurate $D_fH°_0$ ($D_fH°_{298}$) predictions even for large polyatomic species.[21-24]

Experimental And Theoretical Methods

A. Experiment

The rotatable beam source laser photofragmentation TOF apparatus used in this study has been described in detail.[25-28] The apparatus consists of three main components: an ArF excimer laser, a photodissociation chamber in which a rotatable supersonic molecular beam intersects with the excimer laser beam, and a linearly movable ultrahigh vacuum electron ionization quadrupole mass spectrometer (QMS).

A continuous molecular beam of $C_6H_5COCH_3$ (about 3% seeded in He) was produced by supersonic expansion through a nozzle (diameter = 0.125 mm) at a total stagnation pressure (P_o) of 360 Torr for 193 nm excitation and 560 Torr for 248 nm excitation. For the TOF measurement of C_6H_5 formed at 248 nm and θ_{lab} (the angle between the molecular beam and the detector axis) = 10°, P_o was reduced to 260 Torr in order to minimize the influence of dimers and clusters. The nozzle stagnation temperature (T_o) was maintained at ≈180 °C for 193 nm measurements and at ≈130 °C for 248 nm measurements. During the experiment, the beam source, differential pumping, and photodissociation chambers were maintained at pressures of ≈$1x10^{-4}$, $2x10^{-6}$, and ≤$1x10^{-7}$ Torr, respectively.

The energy of the excimer laser (Questek model 2460) used was in the range of 60-80 mJ/pulse at 193 nm or 100-140 mJ/pulse at 248 nm. The laser beam entered the photodissociation chamber through a MgF_2 focusing lens and intersected the seeded $C_6H_5COCH_3$ beam and the central axis of the QMS at 90°. The spot size of the excimer laser beam was estimated to be ≈5 mm^2 at the photodissociation region.

The electron energy and emission current of the ionizer used were 75 eV and 1.2 mA, respectively. During the experiment, the ionization chamber pressure was maintained at $\leq 5 \times 10^{-11}$ Torr. Unless specified, the TOF spectra were taken at a flight path (the distance between the photodissociation region and the ionizer) of 65.5 cm. The TOF spectra were recorded on a multichannel scaler (Stanford Research model SRT430), which was usually set to a channel width of 1.28 μs.

The velocity distribution of the parent $C_6H_5COCH_3$ molecular beam was measured by recording the laser hole burning spectra at the mass corresponding to $C_6H_5COCH_3^+$ (or $C_6H_5^-$) at $\theta_{lab} = 0°$. The measured speed profile of a species was then fitted to an assumed functional form, $f(v) \sim v^2 \exp[-(v-v_o)^2/\alpha^2]$, where v_o is the most probable speed and α is a measure of the width of the speed profile.[25,29] For 193 nm excitation, these constants were determined to be v_o = 1.79×10^5 cm/s and $\alpha = 0.91 \times 10^4$ cm/s. In the case of 248 nm excitation, $v_o = 1.73 \times 10^5$ cm/s and α = 0.79x104 cm/s for P_o = 560 Torr, while $v_o = 1.44 \times 10^5$ cm/s and $\alpha = 1.15 \times 10^5$ cm/s for P_o = 260 Torr.

The ion drift times through the quadrupole mass filter were determined in a hole burning experiment. By recording the hole burning spectra of different ions, $C_6H_5COCH_3^+$, $C_6H_5CO^+$,

CH_3CO^+, $C_6H_5^+$, and CH_3^+ formed in electron impact ionization of $C_6H_5COCH_3$, the corresponding arrival times (t) and masses (m) of these ions were used to fit the equation: $t=Am^{1/2} + t_o$, where t_o is the flight time of $C_6H_5COCH_3$ from the photodissociation region to the ionizer and A is a constant. The procedure yielded a value of 4.114 for A. That is, the ion drift time through the QMS is determined as $4.114m^{1/2}$ μs. The actual flight times of photofragments were corrected for the corresponding ion drift times.

The analysis of the TOF data was performed by a forward simulation method.[30,31] Briefly, the procedure began with a trial kinetic energy distribution $P(E_{c.m.})$, which was transformed to a TOF spectrum for comparison with the experimental TOF spectrum. Here, $E_{c.m.}$ represents the center-of-mass kinetic energy of the photofragment. The $P(E_{c.m.})$ distribution was adjusted until satisfactory agreement between the experimental and calculated TOF data was obtained. For the determination of the threshold (maximum) $E_{c.m.}$ threshold of a dissociation process, the $P(E_{c.m.})$ distribution near the $E_{c.m.}$ onset was also obtained by direct transformation[25] of the TOF data.

In the measurements of the angular distribution, the laser light was polarized by a stack of ten quartz plates set at the Brewster angle. The electric vector **E** of the polarized laser beam was set perpendicular to the detector and then rotated to the desired angle with a 193 nm (or 248 nm) half-wave retarder. The laser energy was measured by a pyroelectric detector, and was kept at 10 mJ/pulse at 193 nm and 15 mJ/pulse at 248 nm.

B. *Ab initio* calculations

The G2 *ab initio* theoretical procedure has been described in detail by Curtiss *et al.*[16]

It is effectively corresponds to the QCISD(T)/6-311+G(3df,2p)//MP2/6-31G(d) level of theory. Briefly, at the G2 level of theory, molecular structures are optimized with the Hartree-Fock (HF) approach and the second-order Møller-Plesset perturbation theory (MP2), with all electrons included using the 6-31G(d) basis set [i.e., at the HF/6-31G(d) and MP2(full)/6-31G(d) levels]. Harmonic vibrational frequencies are calculated at the HF/6-31G(d) geometries for stationary point characterization. All subsequent single-point calculations at higher levels involved are based on the MP2/6-31G(d) optimized structures. Approximations of QCISD(T)/6-311+G(3df,2p) energies are obtained with frozen-core single-point calculations at the QCISD(T)/6-311G(d,p), MP4/6-311G(d,p), MP4/6-311+G(d,p), MP4/6-311G(2df,p), and MP2/6-311+G(3df,2p) levels. A small semiempirical correction is applied to account for high level correlation effects to obtain the total electronic energy (E_e). The HF/6-31G(d) harmonic vibrational frequencies, scaled by 0.8929, are used for zero-point vibrational energy (ZPVE) correction. The total energy at 0 K (E_0) is equal to E_e + ZPVE.[33] All calculations are performed on IBM RS6000-320h and RS6000/340 workstations using the Gaussian 94 package of program.[32] Unless specified, the $D_fH°_0$ and $D_fH°_{298}$ values for the molecules are derived by evaluating the atomization energies and using the known experimental $D_fH°_0$ values of C (170.0 kcal/mol), O(^{3}P) (59.0 kcal/mol), and H (51.63 kcal/mol).[21,33]

The G2(MP2) theory[17] is a variation of the G2 procedure in which the single-point energies are calculated only at the QCISD(T)/6-311G(d,p) and MP2/6-311+G(3df,2p) levels. In this study, we have obtained E_0[G2(MP2)] values for C_6H_5, CH_3CO, CH_3 and CO.

In view of the large size of $C_6H_5COCH_3$ and C_6H_5CO, the QCISD(T)/6-311G(d,p) single-point energy calculations are computationally very demanding. Here, we have calculated the E_0 values for $C_6H_5COCH_3$, C_6H_5CO, CH_3CO, CH_3 and CO using the approximated G2(MP2,SVP) scheme introduced by Radom and co-workers.[34] In the G2(MP2,SVP) scheme, the QCISD(T)/6-311G+(3d,2p) energies are calculated using an additivity approximation,

$$E[\text{QCISD(T)/6-311G+(3df,2p)}] \approx E[\text{QCISD(T)/6-31G(d)}] + E[\text{MP2/6-311+G(3df,2p)}] - E[\text{MP2/6-31G(d)}]. \quad (4)$$

The G2(MP2,SVP) calculations have been shown to reproduce proton affinities for a set of reference molecules to within the G2 target accuracy of 2 kcal/mol but at significantly lower computational cost. Surprisingly, it is found that G2(MP2,SVP) performs better than G2 for hydrocarbons and radicals.[34,35] Thus, we have applied the G2(MP2,SVP) procedure to calculate the $D_fH°_0$ ($D_fH°_{298}$) values of $C_6H_5COCH_3$, C_6H_5CO, C_6H_5, CH_3CO, CH_3, and CO.

Results and Discussion

A. Thermochemistry

The theoretical E_0, $D_fH°_0$, and $D_fH°_{298}$ values for $C_6H_5COCH_3$, C_6H_5CO, C_6H_5, CH_3CO, CH_3, and CO obtained here and in previous calculations[20,33] at the G2, G2(MP2), and G2(MP2,SVP) levels of theory are compared with the experimental[21,22,36] values in Table I. In the case when only the $D_fH°_0$ ($D_fH°_{298}$) value for a species is known, the corresponding $D_fH°_{298}$ ($D_fH°_0$) value are obtained using the calculated HF/6-31G(d) vibrational frequencies.

The $D_fH°_0$ (-0.55±0.6 kcal/mol) and $D_fH°_{298}$ (-2.2±0.6 kcal/mol) values for CH_3CO have been determined at high levels of theory using an isodesmic reaction.[20] This calculation supports the recent experimental $D_fH°_{298}$ value of -2.39 ±0.29 kcal/mol for CH_3CO.[22] The $D_fH°_0$ ($D_fH°_{298}$) values calculated for CH_3CO following the normal G2, G2(MP2), and G2(MP2,SVP) procedures are in satisfactory agreement with those of Ref. 20, with the G2(MP2,SVP) $D_fH°_0$ ($D_fH°_{298}$) value closest to the experimental finding. The G2(MP2,SVP) $D_fH°_{298}$ value of -20.8 kcal/mol for $C_6H_5COCH_3$ is essentially identical to the literature value.[21] However, the G2(MP2,SVP) $D_fH°_0$ ($D_fH°_{298}$) value of 32.5 (29.9) kcal/mol for C_6H_5CO is higher than the experimental value of 30±2 (26±2) kcal/mol by ≈3 kcal/mol. In a recent study of the C-H bond energy of benzene, values of 84.3±0.6 and 81.2 ±0.6 kcal/mol are recommended for $D_fH°_0(C_6H_5)$ and $D_fH°_{298}(C_6H_5)$, respectively.[36] These latter values are significantly lower than the corresponding G2(MP2) $D_fH°_0$ (93.0 kcal/mol) and $D_fH°_{298}$ (90.3 kcal/mol) values for C_6H_5. It is known that there is an accumulation of errors in the application of G2-type approaches to larger molecules.[34,35,37,38] For example, the $D_fH°_0$ and $D_fH°_{298}$ values for benzene (C_6H_6) are too low compared to known experimental values by 3.9 and 5.1 kcal/mol, respectively.[34,38] It is interesting that the $D_fH°_0$[G2(MP2,SVP)] (87.7 kcal/mol) and $D_fH°_{298}$[G2(MP2,SVP)] (85.0 kcal/mol) values for C_6H_5, though still higher, are in better agreement with the experimental values. This observation is consistent with the previous finding that G2(MP2,SVP) performs better than G2 for hydrocarbons and radicals.[35]

Table I. E_0[G2(MP2)], $\Delta_fH°_0$[G2(MP2)], $\Delta_fH°_{298}$[G2(MP2)], $\Delta_fH°_0$[G2(MP2,SVP)], $\Delta_fH°_{298}$[G2(MP2,SVP)], and $\Delta_fH°_0$(expt) values for $C_6H_5COCH_3$, C_6H_5CO, C_6H_5, CH_3CO, and CH_3.

	Theory[a]		Experiment[b]		
Species	E_0 (hartree)	$\Delta_fH°_0$ (kcal/mol)	$\Delta_fH°_{298}$ (kcal/mol)	$\Delta_fH°_0$ (kcal/mol)	$\Delta_fH°_{298}$ (kcal/mol)
$C_6H_5COCH_3$	-384.18059	-16.0[c]	-20.8[c]	-15.9	-20.7±0.4
$C_6H_5CH_3$	–	–	–	17.5±0.1	12.0±0.1
C_6H_5CO	-344.30374	32.5[c]	29.9[c]	29±2[d]	26.1±2[d]
		33.9±1.3[g]	30.6±0.7[g]	33.3±2.2[h]	29.4±2.3[h]
C_6H_5	-231.09198	93.0[e]	90.3[e]	84.3±0.6	81.2±0.6
	-231.08923	87.7[c]	85.0[c]		
		87.6±1.0[g]	84.5±0.6[g]		
CH_3CO	-152.93546[d]	-1.3[f]		-0.74±0.29	-2.39±0.29
		-0.55±0.6[i]	-2.2±0.6[i]		
	-152.93156	-1.5[e]			
	-152.92757	-0.9[c]	-2.05[c]		
CH_3	-39.74390	35.7[f]	35.1[f]	35.8±0.1	35.0±0.1
	-39.73695	36.2[e]	35.6[e]		
	-39.74119	36.3[c]	35.7[c]		
CO	-113.17749	-29.0[f]	-28.2[f]	-27.20±0.04	-26.4±0.0
	-113.17540	-30.1[e]	-29.3[e]		
	-113.17908	-30.4[c]	-29.6[c]		

a). The theoretical $\Delta_fH°_0$ and $\Delta_fH°_{298}$ values are calculated using the $\Delta_fH°_0$(expt) values of C (170.0 kcal/mol), O(^{3}P) (59.0 kcal/mol), and H (51.63 kcal/mol) from Ref. 21, and theoretical E_0 values calculated at the G2, G2(MP2), or G2(MP2,SVP) level.

b). Unless specified, experimental values are from Ref. 21.

c). G2(MP2,SVP) values.

d). Reference 23;

e). G2(MP2) values;

f). G2 values.

g). Calculated using isodesmic reactions of Table II.

h). This work; i) Reference 20. Calculated using an isodesmic reaction.

It has been demonstrated that more accurate heats of formation can be calculated by the use of isodesmic reactions rather than atomization energies as in standard G2-type procedures.[34,37,38] The cancellation of errors in cases involving similar chemical bonds improves the agreement with experiment. In G2-type approaches, a semiempirical high level correction is involved. It was pointed out that the high level corrections can be canceled exactly for isodesmic schemes.[38] In order to obtain reliable theoretical $D_fH°_0$ ($D_fH°_{298}$) values for C_6H_5CO and C_6H_5, we have examined the variation of their calculated $D_fH°_0$ ($D_fH°_{298}$) values at the G2(MP2) and G2(MP2,SVP) level by the use of selected isodesmic reactions shown in Table II. We find that for reactions involving radicals, such as C_6H_5CO and C_6H_5, the "bond separation" isodesmic reactions are not unique (see Table II, reactions i-iii for C_6H_5 and reactions v-viii for C_6H_5CO).[38] These reactions are selected because the energetics of all species involved are well known, except those for C_6H_5CO and C_6H_5. The uncertainties for $D_fH°_0$ ($D_fH°_{298}$) thus determined using individual isodesmic reactions are lower limits determined only by the uncertainties of the experimental $D_fH°_0$ ($D_fH°_{298}$) values used in the calculations. We have also calculated the G2(MP2,SVP) $D_fH°_0$ ($D_fH°_{298}$) values of C_6H_5 and C_6H_5CO and using isodesmic reactions iv and ix, respectively, (see Table II). As shown in the table, the $D_fH°_0$ ($D_fH°_{298}$) values of C_6H_5 and C_6H_5CO, thus derived are highly consistent, with the maximum deviations of 1.3 and 2.2 kcal/mol for $D_fH°_0$ ($D_fH°_{298}$) of C_6H_5 and C_6H_5CO, respectively. We recommend the average values 87.6±1.0 (84.5±0.6) kcal/mol for $D_fH°_0$ ($D_fH°_{298}$) of C_6H_5 and 33.9±1.3 (30.6±0.7) kcal/mol for $D_fH°_0$ ($D_fH°_{298}$) of C_6H_5CO. We have conservatively assigned the uncertainties to be the maximum of the

Table II. Values for $\Delta_f H°_0$ and $\Delta_f H°_{298}$ of C_6H_5 and C_6H_5CO calculated using selected isodesmic reactions.[a]

Isodesmic reactions	G2(MP2)		G2(MP2,SVP)	
	$\Delta_f H°_0$	$\Delta_f H°_{298}$	$\Delta_f H°_0$	$\Delta_f H°_{298}$
C_6H_5				
i. $C_6H_5 + 6CH_4 \rightarrow 2C_2H_4 + C_2H_5 + 3C_2H_6$	88.2	84.8	88.0	84.6
ii. $C_6H_5 + 6CH_4 \rightarrow 3C_2H_4 + C_2H_5 + 2C_2H_6$	87.3	84.3	86.4	83.9
iii. $C_6H_5 + 7CH_4 \rightarrow 3C_2H_4 + 3C_2H_6 + CH_3$	88.6	85.1	87.4	84.6
iv. $C_6H_5\text{-}COCH_3 + CH_4 \rightarrow C_6H_5 + CH_3\text{-}COCH_3$			87.0	84.2
C_6H_5CO				
v. $C_6H_5CO + 8CH_4 \rightarrow 2C_2H_4 + C_2H_5 + 4C_2H_6 + H_2CO$			34.6	31.0
vi. $C_6H_5CO + 8CH_4 \rightarrow 3C_2H_4 + C_2H_5 + 3C_2H_6 + H_2CO$			33.5	30.3
vii. $C_6H_5CO + 8CH_4 \rightarrow 3C_2H_4 + 4C_2H_6 + HCO$			34.2	30.6
viii. $C_6H_5CO + 9CH_4 \rightarrow 3C_2H_4 + 4C_2H_6 + H_2CO + CH_3$			34.8	31.0
xi. $C_6H_5CO\text{-}CH_3 + CH_3 \rightarrow C_6H_5CO + H_3C\text{-}CH_3$			32.6	29.9

a) $\Delta_f H°_0$(kcal/mol, expt) and $\Delta_f H°_{298}$(kcal/mol, expt) values used are from Refs. 21 and 35

differences between individually calculated $D_fH°_0$ ($D_fH°_{298}$) values and the corresponding averages. Again, we note that these recommended $D_fH°_0$ ($D_fH°_{298}$) values for C_6H_5 and C_6H_5CO are in excellent agreement with the $D_fH°_0$[G2(MP2,SVP)] and $D_fH°_{298}$[G2(MP2,SVP)] predictions. Comparing these values and the experimental results (Table I) indicates that the literature $D_fH°_0$ ($D_fH°_{298}$) values for C_6H_5 and C_6H_5CO are likely on the low side.

In Table III, we have compared the theoretical G2(MP2,SVP) and experimental D_0 (D_{298}) values for the C_6H_5CO-CH_3, C_6H_5-$COCH_3$, C_6H_5-CO, and CH_3-CO bonds. The experimental D_0 (D_{298}) values for the C_6H_5CO-CH_3 and C_6H_5-$COCH_3$ bonds are 4.4 (5.0) and 2.3 (4.4) kcal/mol lower than the corresponding theoretical predictions, while the experimental D_0 (D_{298}) values for the C_6H_5-CO and CH_3-CO bonds are higher than the respective theoretical predictions by 4.8 (3.2) and 1.5 (1.7) kcal/mol.

B. Newton diagrams for photodissociation at 193 and 248 nm

Based on the conservation of energy,

$$E(h\nu) + E_{int}(C_6H_5COCH_3) = D_0(C_6H_5CO\text{-}CH_3 \text{ or } C_6H_5\text{-}COCH_3) + E_{int}[(C_6H_5CO + CH_3) \text{ or } (C_6H_5 + CH_3CO)] + E_{c.m.} \quad (5)$$

where E(hν) is the dissociation photon energy (147.9 kcal/mol for hν = 193.3 nm and 115.3 kcal/mol for hν = 248 nm); and E_{int} is the initial internal energy of $C_6H_5COCH_3$ or its photofragments ($C_6H_5CO + CH_3$ or $C_6H_5 + COCH_3$). Using the HF/6-31G(d) vibrational

Table III. Comparison of theoretical and experimental selected bond dissociation energies at 0 (298 K) for $C_6H_5COCH_3$, C_6H_5CO, and CH_3CO.[a]

Reactions	Theory [G2(MP2,SVP)]		Experiment	
	D_0 (kcal/mol)	D_{298} (kcal/mol)	D_0 (kcal/mol)	D_{298} (kcal/mol)
$C_6H_5COCH_3 \rightarrow C_6H_5CO + CH_3$	85.1	86.8	80.7 85.0±2.2[b]	81.8
$C_6H_5COCH_3 \rightarrow C_6H_5 + CH_3CO$	102.8	103.8	99.5	99.5
$C_6H_5CO \rightarrow C_6H_5 + CO$	23.3	25.5	28.1	28.7
$CH_3CO \rightarrow CH_3 + CO$	6.8	8.2	9.3	11.0

a) Calculated using the experimental and theoretical G2(M2,SVP) $\Delta_fH°_0$ ($\Delta_fH°_{298}$) values of Table I.

b) This work.

frequencies for $C_6H_5COCH_3$, the total thermal energy at 298 K for $C_6H_5COCH_3$ is estmated to be 5.7 kcal/mol. Considering the mild expansion conditions used in this experiment, we expect that the vibrational relaxation is inefficient and the rotational relaxation is incomplete. For an initial nozzle temperature of 130-180 °C (403-453 K), we estimate that the effective beam temperature for $C_6H_5COCH_3$ is most likely in the range of 250-350 K. Thus, after expansion, the parent $C_6H_5COCH_3$ molecules may contain ≈5.7 kcal/mol of thermal energy.

Using Eq. (5) and the literature D_0 values [$D_0(C_6H_5CO\text{-}CH_3)$ = 80.7 kcal/mol and $D_0(C_6H_5\text{-}COCH_3)$ = 99.5 kcal/mol] (see Table III), we have constructed the Newton diagrams for the $C_6H_5CO + CH_3$ and $C_6H_5 + COCH_3$ processes. The Newton diagrams corresponding to 193 nm and 248 nm photodissociation are shown in Figs. 1(a) and 1(b), respectively, where v_{lab} and $v_{c.m.}$ are the laboratory and center-of-mass velocities for the photofragments, and θ_{lab} and $\theta_{c.m.}$ are the laboratory and center-of-mass angles, defined by the angles between the detector axis and molecular beam axis and between $v_{c.m.}$ and the molecular beam axis, respectively. The v_0 values are 1.79×10^5 cm/s for 193 nm excitation and 1.73×10^5 cm/s for 248 nm excitation. The maximum $v_{c.m.}$ circles are calculated assuming $E_{int}[(C_6H_5CO + CH_3)$ or $(C_6H_5 + CH_3CO)] = 0$. Also shown in Figs. 1(a) and 1(b) are γ and ε, which are defined as the angles between the laser electric field **E** and $v_{c.m.}$ and between **E** and the detector axis, respectively.

C. Photodissociation at 193 nm

Figures (2a) and (2b) show the TOF spectra for CH_3 observed at θ_{lab} = 15° and 30°, respectively. The TOF spectrum for C_6H_5CO at θ_{lab} = 15° is depicted in Fig. 3. The direct detection of C_6H_5CO and CH_3 signals confirms the occurrence of process (1). The $P(E_{c.m.})$ for process (1) (solid curve) shown in Fig. 4(a) is derived from the fast peaks in the CH_3 TOF

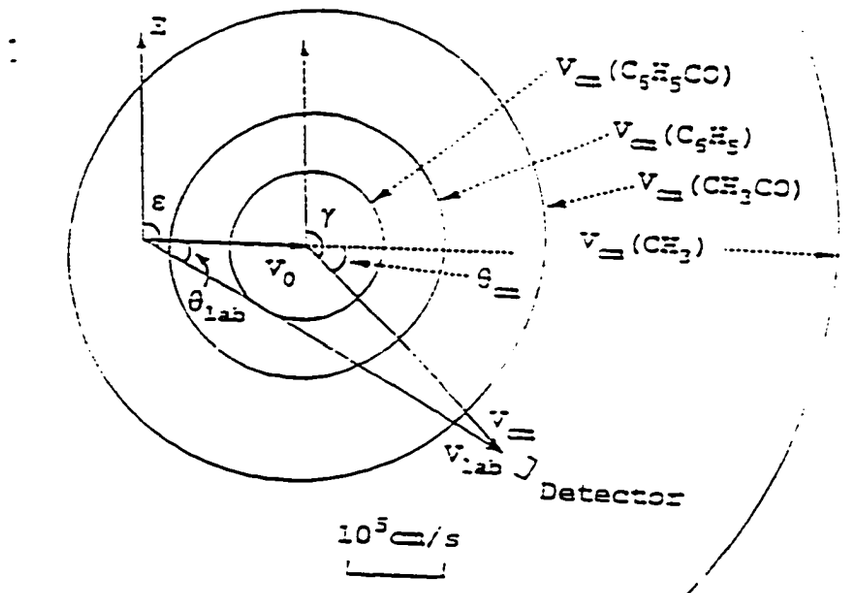

Figure 1(a)

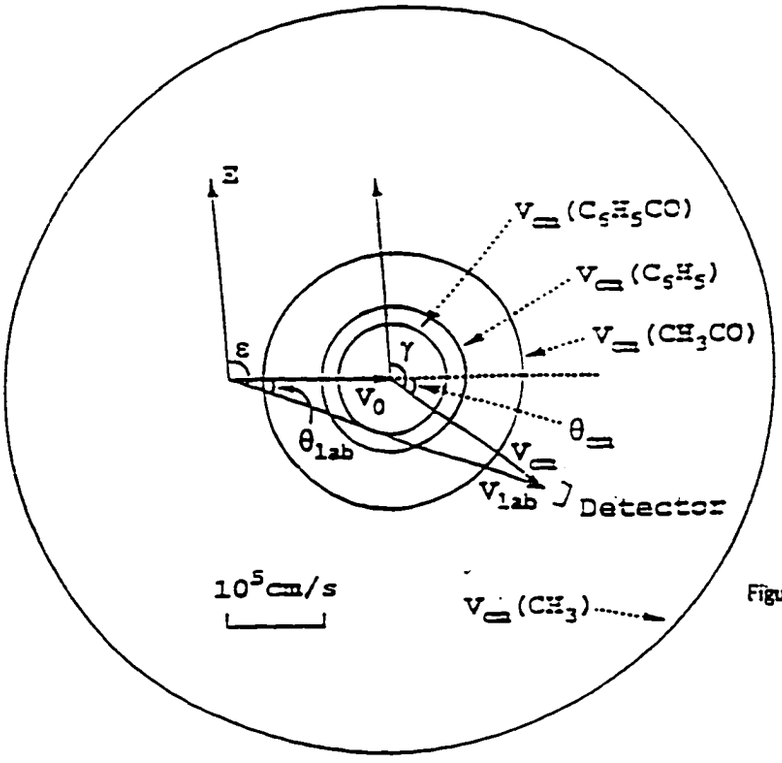

Figure 1(b)

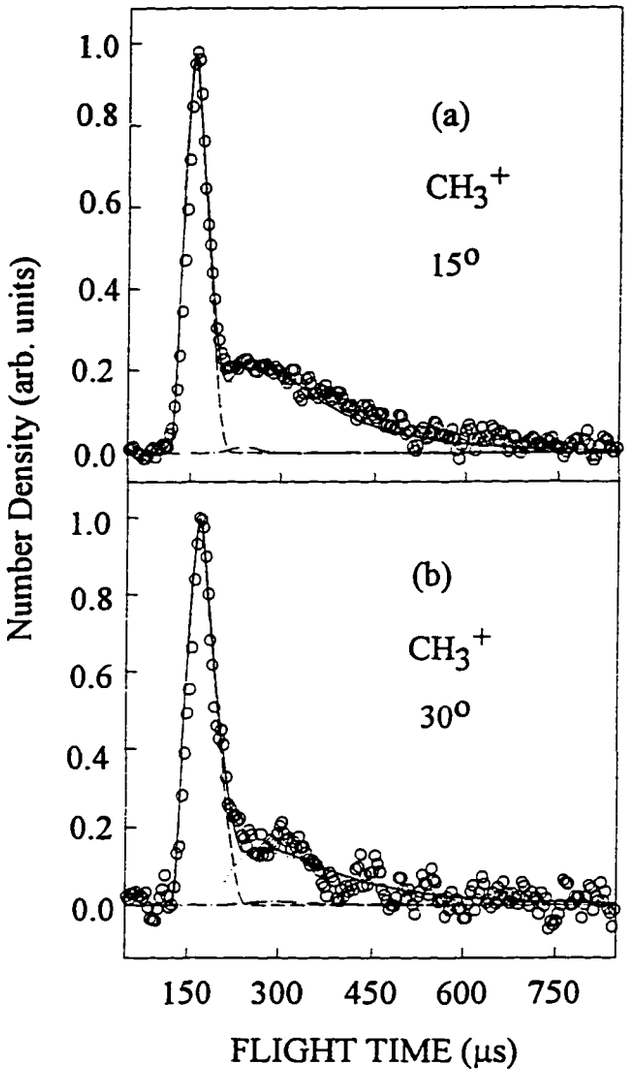

Figure 2 TOF spectra for CH_3 at (a) $\theta_{lab}=15°$ and (b) $\theta_{lab}=30°$. Circles represent experimental data. Contributions are shown for CH_3 (dashed line) from process (1), CH_3CO (dot-dashed line) from process (2), and CH_3 (dotted line) from process (8).

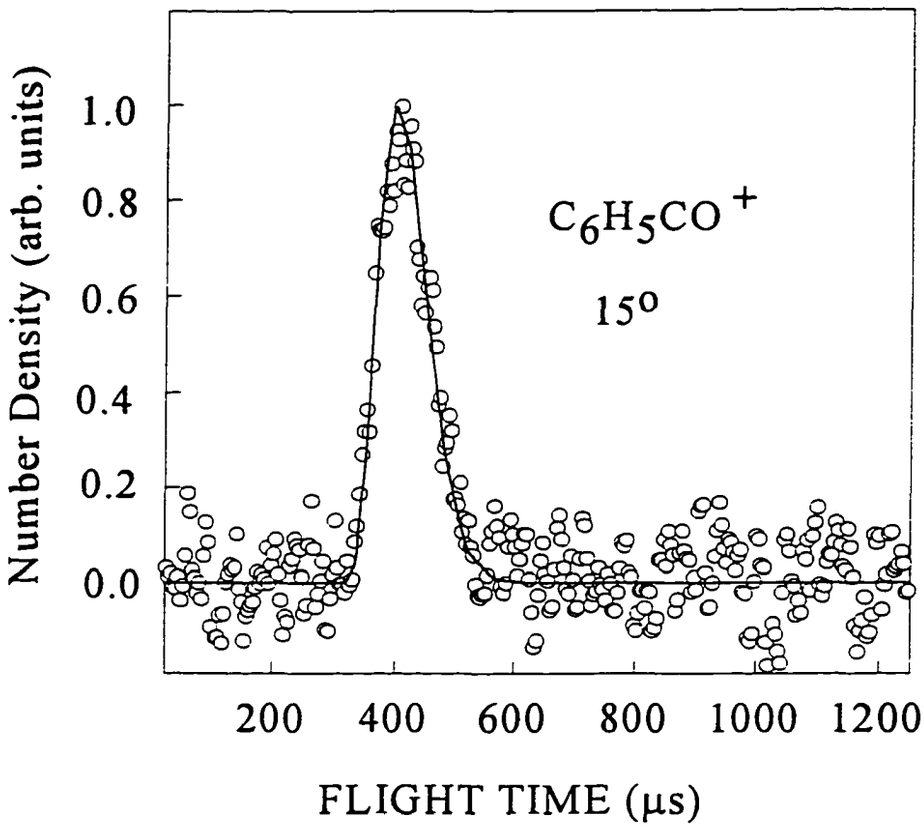

Figure 3 TOF spectrum for C_6H_5CO at θ_{lab}=15°. Circles represent experimental data.

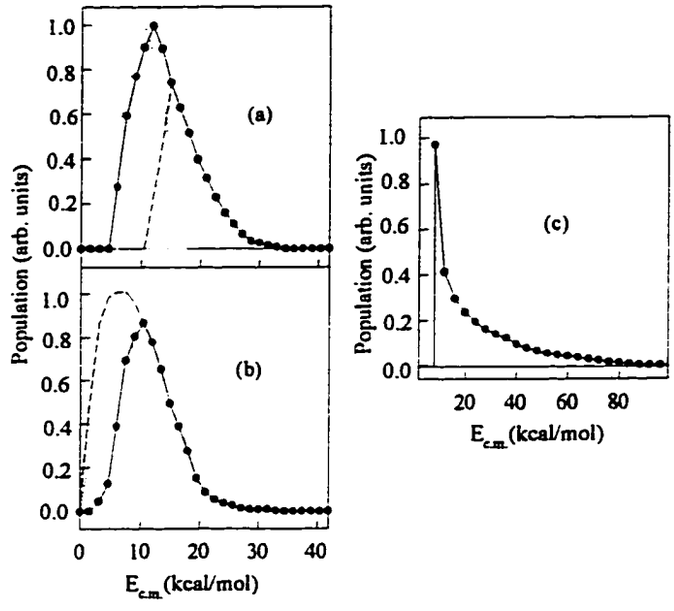

Figure 4 (a) The $P(E_{c.m.})$ for process (1) derived by the TOF spectra for CH_3 is shown as the solid curve. The part of the $P(E_{c.m.})$ to the right of the dashed line fits the TOF spectrum for C_6H_5CO of Fig. 3. The $P(E_{c.m.})$ for the secondary dissociation process (6) derived by the TOF spectra for C_6H_5 and CO is shown by the dotted line. (b) The solid curve is the approximated $P(E_{c.m.})$ for process (2) derived by the TOF of CH_3CO at θ_{lab}=15°. The modified $P(E_{c.m.})$ for process (2) (dashed curve) at $E_{c.m.}$ < 11 kcal/mol is obtained by fitting the TOF spectrum for C_6H_5 at θ_{lab}=15°. Thus, the complete $P(E_{c.m.})$ for process (2) is the combined dashed curve at $E_{c.m.}$< 11 kcal/mol and the solid curve at $E_{c.m.}$ ≥ 11 kcal/mol. The $P(E_{c.m.})$ for the secondary dissociation of CH_3CO obtained by fitting the slow peak the CH_3 TOF spectra of Figs. 2(a) and 2(b) is shown by the dotted curve (c) $P(E_{c.m.})$ derived by the TOF spectrum of $C_6H_5CH_3$ of Fig. 8. The TOF spectrum of $C_6H_5CH_3$ does not contain information for $P(E_{c.m.})$ at $E_{c.m.}$<8 kcal/mol due to the kinematic constraint.

spectra. This $P(E_{c.m.})$ peaks near 12 kcal/mol and has a $E_{c.m.}$ onset of 34 kcal/mol. The latter value is significantly lower than the thermochemical $E_{c.m.}$ threshold of 67 kcal/mol. The average kinetic energy release of 13.8 kcal/mol for process (1) is ≈20% of the total available energy.

We attempt to use the $P(E_{c.m.})$ derived from the CH_3 spectrum to fit the TOF spectrum for C_6H_5CO, and find that the $P(E_{c.m.})$ at $E_{c.m.}$>15 kcal/mol [indicated by the dashed curve in Fig. 4(a)] satisfactorily fits the C_6H_5CO TOF spectrum. This observation indicates that a fraction of excited C_6H_5CO radicals initially formed with $E_{c.m.}$<15 kcal/mol [or $E_{int}(C_6H_5CO + CH_3)$ > 52 kcal/mol] by process (1) undergoes further dissociation in the time scale of the present experiment. If the internal energy distributed in C_6H_5CO and CH_3 is proportional to the internal degrees of freedom, the internal energy for C_6H_5CO is expected to be >41.6 kcal/mol at $E_{c.m.}$<15 kcal/mol. Since the $D_0(C_6H_5\text{-}CO)$ is <29 kcal/mol (see Table III), excited C_6H_5CO radicals with internal excitation >29 kcal/mol are expected to dissociate according to

$$C_6H_5CO \rightarrow C_6H_5 + CO. \qquad (6)$$

On the basis of the $P(E_{c.m.})$'s derived from the TOF spectra of CH_3 and C_6H_5CO, we conclude that ≈50 % of the primary C_6H_5CO radicals [corresponding to the shaded area in Fig. 4(a)] undergoes further dissociation according to process (6).

The TOF spectrum for CH_3CO measured at θ_{lab} = 15° and a flight path of 84.5 cm is shown in Fig. 5(a). We have also observed the TOF spectrum for CH_2CO as shown in Fig. 5(b). Figures 6(a) and 6(b) depict the TOF spectra for C_6H_5 at θ_{lab} = 15° and 30°, respectively. The

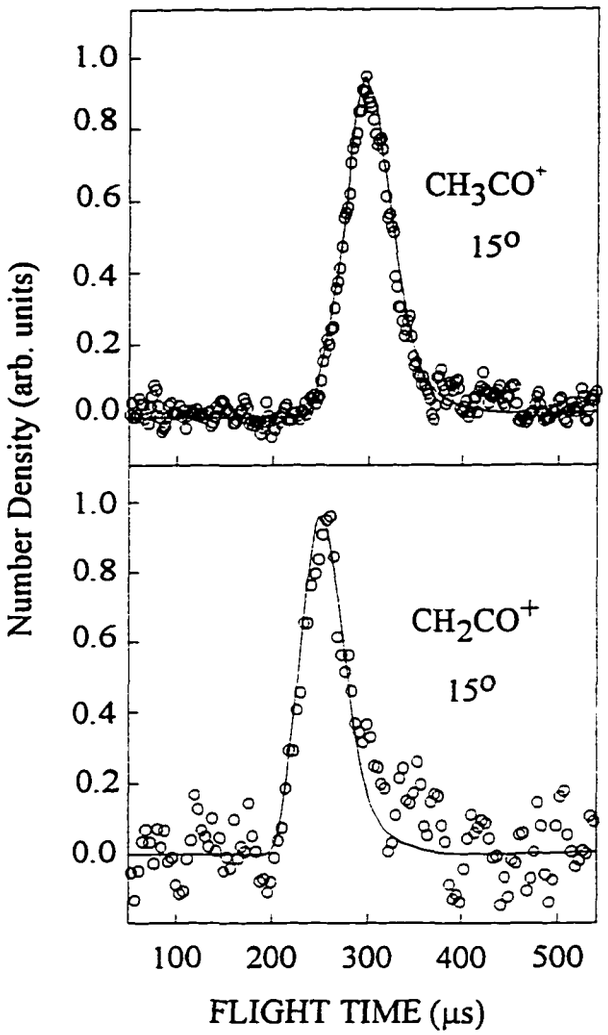

Figure 5 TOF spectrum for (a) CH_3CO and (b) CH_2CO at θ_{lab}=15°. The spectrum for CH_3CO is measured at a flight path of 84.5 cm. Circles represent the experimental data.

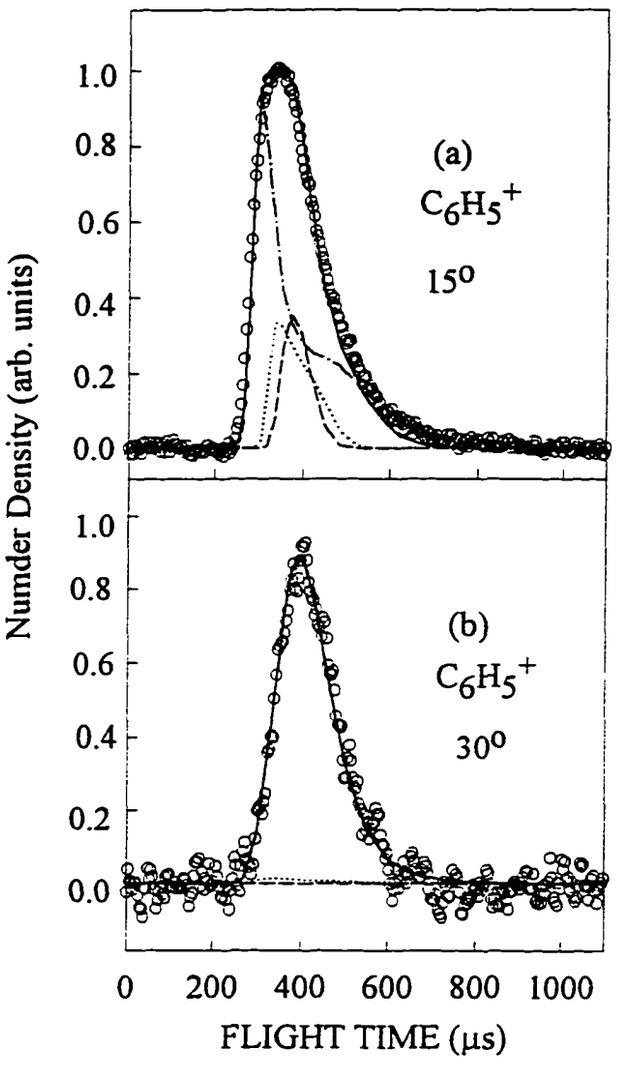

Figure 6 TOF spectra for C_6H_5 at (a) θ_{lab}=15° and (b) θ_{lab}=30°. Circles represent experimental data. Contributions are shown for C_6H_5 (dot-dashed line) from process (2), C_6H_5CO (dashed line) from process (1), and C_6H_5 (dotted line) from process (6).

observation of the CH_3CO and C_6H_5 spectra indicates the occurrence of process (2). The TOF spectrum for CH_3CO is used to derive the approximated $P(E_{c.m.})$ for process (2), shown as the solid curve in Fig. 4(b). The $P(E_{c.m.})$ thus obtained fits the TOF spectrum for CH_2CO, indicating that the CH_2CO^+ signal arises from the dissociative electron ionization of CH_3CO.

We expect that CH_3^+ fragment ions formed in the dissociative electron ionization of CH_3CO [process (7)] contribute to the TOF spectra for CH_3 (Fig. 2).

$$CH_3CO + e^- \rightarrow CH_3^+ + CO + 2e^- \qquad (7)$$

However, the $P(E_{c.m.})$ derived from the TOF spectrum of CH_3CO cannot account for the slow, broad peaks shown in Figs. 2(a) and 2(b). Since $D_0(CH_3\text{-}CO)$ is <11 kcal/mol (see Table III), the further dissociation of some internally excited CH_3CO radicals according to process (8) is expected.

$$CH_3CO \rightarrow CH_3 + CO \qquad (8)$$

Process (8) has been observed for acetyl radicals initially formed in the photodissociation of acetone and acetyl chloride.[1,7] The approximated $P(E_{c.m.})$ for process (2) derived from the TOF spectrum peaks at $E_{c.m.} \approx 10.5$ kcal/mol,[39] indicating that the most probable internal energy for $CH_3CO + C_6H_5$ is ≈38 kcal/mol, which is ≈79% of the available energy. Assuming that this internal energy is partitioned according to the internal degrees of freedom of the photofragments,

the most probable internal energy for CH_3CO is estimated to be 19 kcal/mol, which is above the $D_0(CH_3\text{-}CO)$ value of 9.3 kcal/mol (see Table III). Since the portion of excited CH_3CO radicals originally formed by process (2) with internal energy greater $D_0(CH_3\text{-}CO)$ is expected to dissociate according to process (8), the true $P(E_{c.m.})$ at lower $E_{c.m.}$ for process (2) should be higher than that indicated by the approximated $P(E_{c.m.})$ derived by the TOF spectrum of CH_3CO. However, the high $E_{c.m.}$ portion of the approximated $P(E_{c.m.})$ based on the CH_3CO spectrum represents the true $P(E_{c.m.})$ for process (2). The $E_{c.m.}$ onset of $\approx$35 kcal/mol observed is more than 10 kcal/mol lower than the thermochemical $E_{c.m.}$ threshold 48.5 kcal/mol for process (2).

Using the secondary $P(E_{c.m.})$ shown as the dotted curve in Fig. 4(b) for the dissociation process (8), we find that the slow, broad peaks observed in the TOF spectra of CH_3 at $\theta_{lab} = 15°$ and 30° are satisfactorily accounted for by process (8) [see dotted curves in Figs 2(a) and 2(b)]. We note that the secondary $P(E_{c.m.})$ for process (8) thus obtained peaks at 6 kcal/mol and is similar to that derived in the 193 nm photodissociation study of acetone.[7] This latter observation can be taken as support for the present attribution of the slow peaks of Figs. 2(a) and 2(b). Based on this attribution, the contribution due to the dissociative electron ionization process (7) is small [see dot-dashed curve in Figs. 2(a) and 2(b)]. The simulation of the CH_3 spectra reveals that the cross sections for process (1) to (2) at $h\nu = 193$ nm are comparable.

As a result of the kinematic constraint, C_6H_5CO cannot be observed beyond 27° [see Fig. 1(a)]. Thus, $C_6H_5^+$ ions formed in the dissociative electron ionization process (9),

$$C_6H_5CO + e^- \rightarrow C_6H_5^+ + CO + 2e^-, \qquad (9)$$

should not contribute to the TOF spectrum for C_6H_5 at 30° shown in Fig. 6(b). We find that this latter spectrum can be accounted for by the $P(E_{c.m.})$ derived from the CH_3CO spectrum [Fig. 4(b)] at $E_{c.m.} \geq 16.5$ kcal/mol. However, the TOF spectrum for C_6H_5 at 15°, shown in Fig. 6(a), may contain contributions from the primary process (2), the secondary dissociation process (6), and the dissociative electron ionization process (9). The fitting due to processes (2) and (9) are fixed by the $P(E_{c.m.})$'s of the primary processes (1) and (2). The fact that the spectrum of Fig. 6(a) cannot be fitted by processes (2) and (9) indicates the occurrence of secondary process (6). As pointed out above, the approximated $P(E_{c.m.})$ of process (2) derived from the TOF spectrum for CH_3CO represents only the stable part of CH_3CO formed by process (2). The complete $P(E_{c.m.})$ for process (2) should include the secondary dissociation part according to process (8). Therefore, we have adjusted the approximated $P(E_{c.m.})$ at lower $E_{c.m.}$ values to fit the TOF spectrum for C_6H_5 at 15°. The best fit is achieved by taking into account contributions form process (2) (dot-dashed curve), process (6) (dotted curve), and process (9) (dashed curve). The secondary $P(E_{c.m.})$ for process (6) (dotted curve) used is shown in Fig. 4. The complete $P(E_{c.m.})$ for process (2) [Fig. 4(b)] is thus the combined dashed curve at $E_{c.m.} < 10.5$ kcal/mol and the solid curve at $E_{c.m.} \geq 10.5$ kcal/mol. The shaded area between the solid and dashed curve represents the portion of excited CH_3CO (≈40%) undergoing further dissociation. We note that the portion of the $P(E_{c.m.})$ at $E_{c.m.} < 10.5$ kcal/mol derived by fitting the C_6H_5 spectrum of Fig. 6(a) has considerable uncertainties. Nevertheless, the fitting of the C_6H_5 spectrum at 15° is consistent with the conclusion obtained in the simulation of the TOF spectra for CH_3: the cross sections for processes (1) and (2) are comparable.

Figures 7(a) and 7(b) show the TOF spectra for CO observed at $\theta_{lab} = 15°$ and 30°. In addition to contributions from the secondary dissociation processes (6) and (8), the TOF spectra for CO also contain contributions from the primary processes (1) and (2) due to the dissociative electron ionization processes (10) and (11), respectively.

$$C_6H_5CO + e^- \rightarrow C_6H_5 + CO^+ + 2e^- \quad (10)$$

$$CH_3CO + e^- \rightarrow CH_3 + CO^+ + 2e^- \quad (11)$$

Contributions from processes (1) + (10) (dashed line) and processes (2) + (11) (dot-dashed line) are found to be small. This can be understood by the low efficiencies for CO^+ production in processes (10) and (11) as a result of the significantly higher IE(CO) value than those for C_6H_5 and CH_3.[21] The gross features of the CO TOF spectra of Figs. 7(a) and 7(b) can be fitted by adjusting the portions of process (6) (dot-dot-dashed line) and process (8) (dotted line).

Figure 8 shows the TOF spectrum for toluene ($C_6H_5CH_3$) at 15° obtained by more than one million laser shots. The direct detection of $C_6H_5CH_3$ can be taken as evidence that process 3) also occurs. Since the breakage of the CH_3-CO and C_6H_5-CO bonds is compensated by the formation of the C_6H_5-CH_3 bond (see Table I for the $\Delta_fH°_0$ value of $C_6H_5CH_3$) and an additional π-bond in CO, the endothermicity at 0 K for process (3) is only 6.2 kcal/mol. However, the activation energy for this dissociation process, which neccessarily involves a tight transition complex, is likely to be high. The $P(E_{c.m.})$ for process (3) derived from the TOF spectrum for $CH_3C_6H_5$ is shown in Fig. 4(c). This $P(E_{c.m.})$ decreases rapidly as $E_{c.m.}$ is increased from $E_{c.m.} = 8$ (kcal/mol toward higher $E_{c.m.}$, exhibiting the feature expected of a statistical dissociation process.

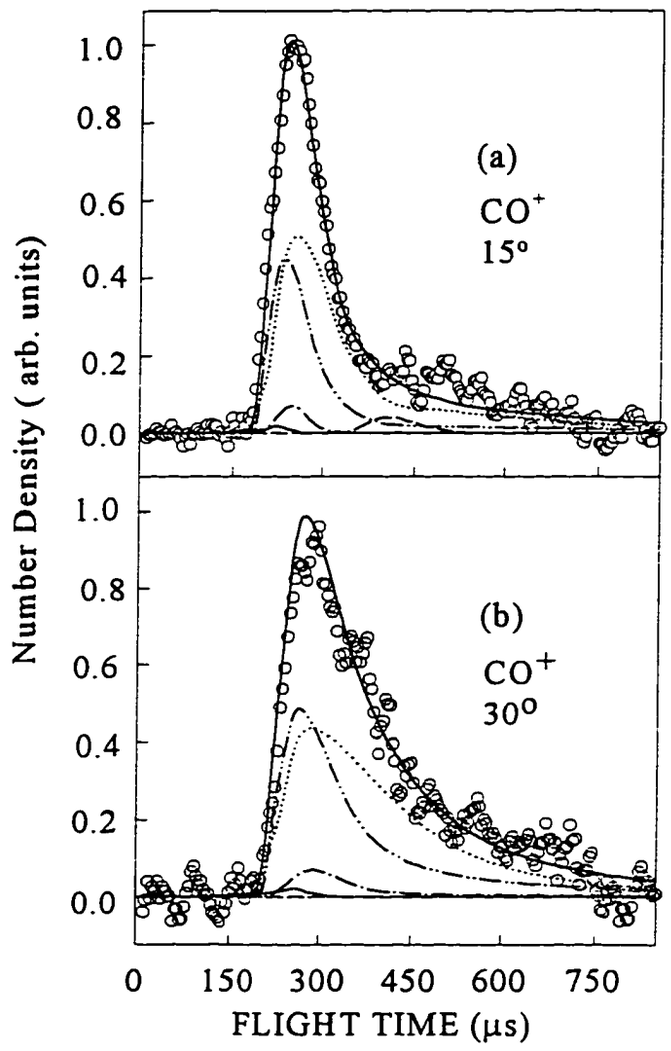

Figure 7 TOF spectra for CO at (a) θ_{lab}=15° and (b) θ_{lab}=30°. Circles represent experimental data. Contributions are shown C_6H_5CO (dashed line) from process (1), CH_5CO (dash-dotted line) from process (2), CO (solid line) from process (3), CO (dot-dot-dashed line) from process (6), and CO (dotted) from process (8).

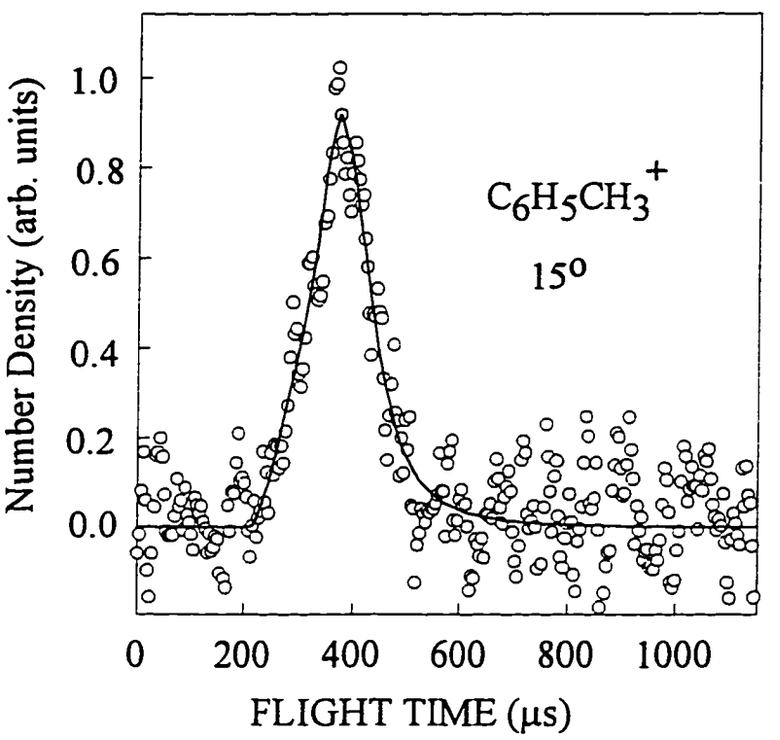

Figure 8 TOF spectrum for $C_6H_5CH_3$ at θ_{lab}=15°. Circles represent experimental data. This spectrum was obtained from more than one million laser shots.

Due to the kinematic constraint, the TOF spectrum for $C_6H_5CH_3$ at 15° contains no information for the $P(E_{c.m.})$ at $E_{c.m.} < 8$ kcal/mol. The $E_{c.m.}$ onset for the $P(E_{c.m.})$ of process (3) is >90 kcal/mol. Comparing the observed $C_6H_5CH_3$, C_6H_5, and CH_3 signals, we estimate the cross section for process (3) is <0.1% of those for processes (1) and (2) at hν = 193 nm. The contribution of process (3) to the TOF spectra for CO at 15° and 30° is negligibly small [see the small solid curves in Fig. 7(a) and 7(b)]. The statistical appearance of the $P(E_{c.m.})$ for process (3) is in consistent with the long time scale involved in CH_3 rearrangement for the formation of $C_6H_5CH_3$ from $C_6H_5COCH_3$.

The angular distribution of the photodissociation fragments has the form:[40,41]

$$P(\gamma) = (1/4\pi)[1 + \beta P_2(\cos\gamma)] \qquad (12)$$

Where $P_2(\cos\gamma)$ is the second Legendre polynomial and β is the anisotropy parameter. We have measured the TOF spectra for $C_6H_5^+$ at polarization angles ε = 0°, 20°, 50°, 70°, 100° and 150° and TOF spectra for CH_3^+ at ε = 0°, 40°, 90°, 130° (Fig. 9). Within experimental error limits, no difference in the spectra is observed. Therefore, we conclude that the photofragment angular distributions for processes (1) and (2) at hν=193 nm are isotropic. i.e., β=0. This observation is consistent with the conclusion that the 193 nm photodissociation of acetophenone involves a predissociation mechanism with a dissociation lifetime longer than the rotational period of photoexcited $C_6H_5COCH_3$.

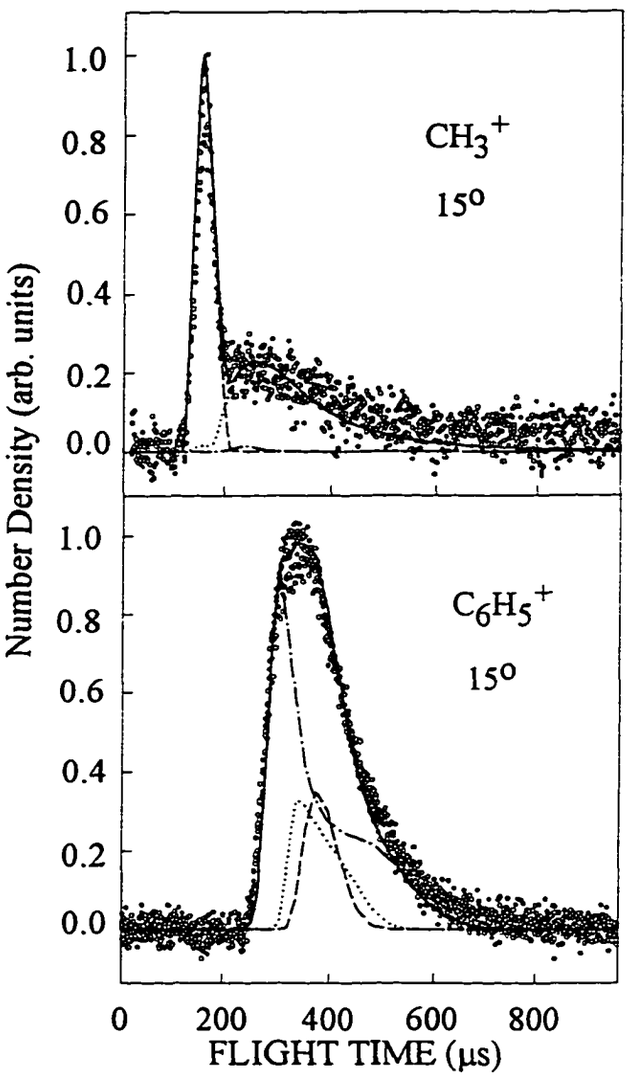

Figure 9 (a) TOF spectra for CH_3 at θ_{lab}=15° and ε=0°, 40°, 90° and 130°.
(b) TOF spectra for C_6H_5 at θ_{lab}=15° and ε=0°, 20°, 50°, 70°, 100°, and 150°.

D. Excitation at 248 nm

Upon the absorption of a 248 nm photon, $C_6H_5COCH_3$ may dissociate according to processes (1) and (2). Since a 248 nm photon corresponds to an energy of 115.2 kcal/mol, and the dissociation of $C_6H_5COCH_3$ into C_6H_5 + CO + CH_3 requires 110 kcal/mol, finite dissociation of excited primary C_6H_5CO and CH_3CO radicals according to processes (6) and (8) are still possible. Thus, we have searched for the TOF signals of C_6H_5CO, $C_6H_5CH_3$, C_6H_5, CH_3CO, CH_3, and CO as in the 193 nm photodissociation experiment described above.

However, the measurements of the TOF spectra for C_6H_5CO, CH_3CO, and CH_2CO were unsuccessful despite a long and careful search for $C_6H_5CO^+$, CH_3CO^+, and CH_2CO^+ signals at θ_{lab}=15°, 20°, 25°, and 30°. The absorption cross section of $C_6H_5COCH_3$ at 248 nm is more than 10% of that at 193 nm.[10,15] Thus, the intensities for C_6H_5CO and CH_3CO at 248 nm are much lower than those at 193 nm. The dissociative ionization processes (7) and (9) are expected to reduce the CH_3CO^+ and $C_6H_5CO^+$ signals. Hoping to minimize the effect of processes (7) and (9), we have also searched for the CH_3CO^+ and $C_6H_5CO^+$ signals at ionizing electron energies lower than 75 eV. However, under such conditions, the signals for CH_3CO^+ and $C_6H_5CO^+$ are too weak to measure the TOF spectra of C_6H_5CO and CH_3CO.

The TOF spectra for CH_3 at θ_{lab} = 15°, 20°, and 30° are depicted in Figs. 10 (a), 10(b), and 10(c), respectively. Figures 11(a), 11(b), 11(c), and 11(d) show the respective TOF spectra for C_6H_5 at θ_{lab} = 10°, 15°, 20°, and 25°. The TOF spectra for CO and $C_6H_5CH_3$ are shown in Figs. 12(a) and 12(b), respectively. We note that the TOF spectra for C_6H_5 at θ_{lab}=25°,

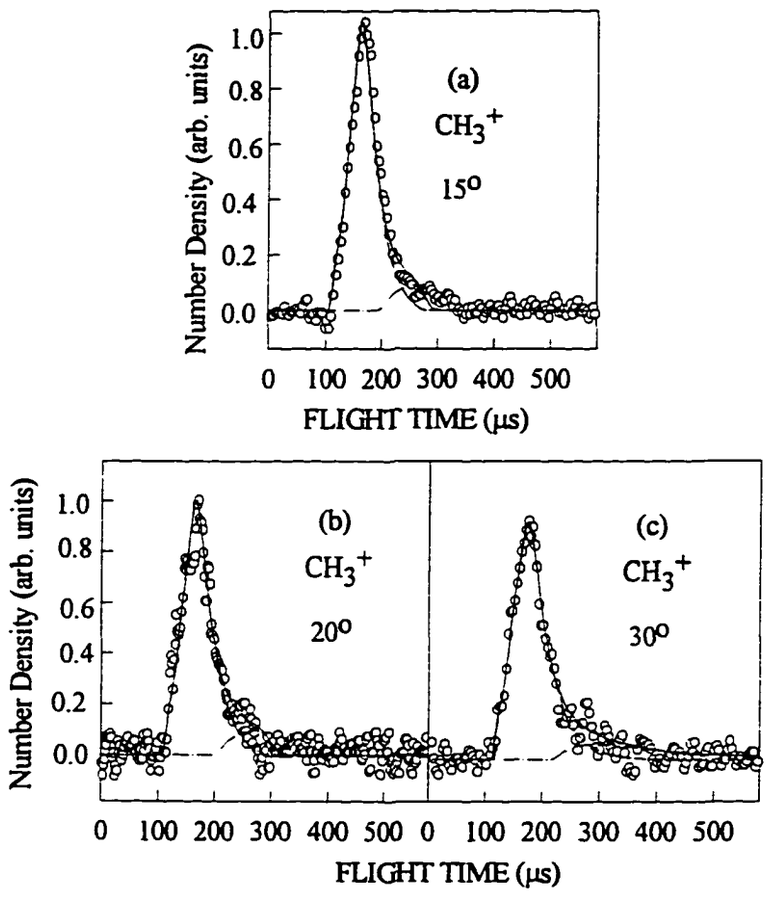

Figure 10 TOF spectra for CH_3 at (a) θ_{lab}= 15°, (b) θ_{lab}= 20°, and (c) θ_{lab}= 30°. Circles represent experimental data. Contributions are shown for CH_3 (dashed curve) from process (1) and CH_3CO (dot-dashed curve) from process (2).

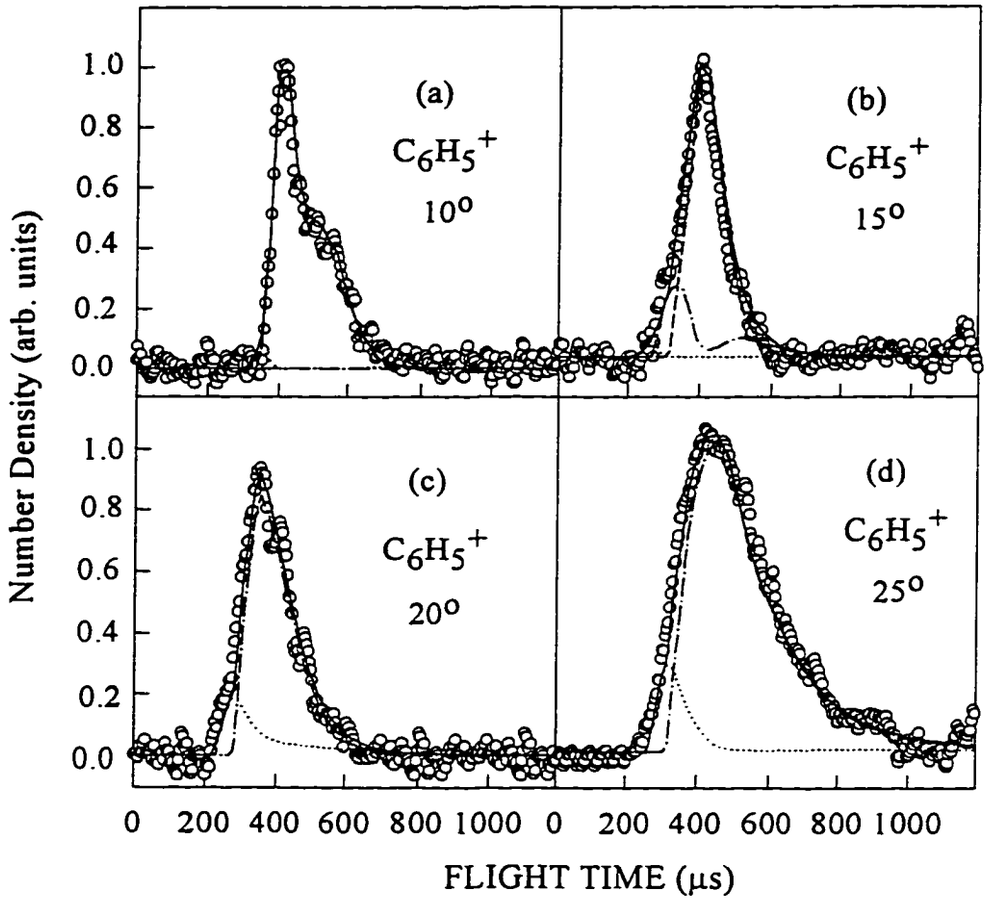

Figure 11 TOF spectra for C_6H_5 at (a) θ_{lab}=10°, (b) θ_{lab}= 15°, (c) θ_{lab}= 20°, and (d) θ_{lab}= 25°. The TOF spectrum for C_6H_5 at θ_{lab}= 25° was obtained from more than one million laser shots. Circles represent experimental data. Contributions are shown for C_6H_5CO (dashed curve) from process (1), C_6H_5 (dot-dash curve) from process (2), and $C_6H_5CH_3$ (dotted curve) process (3).

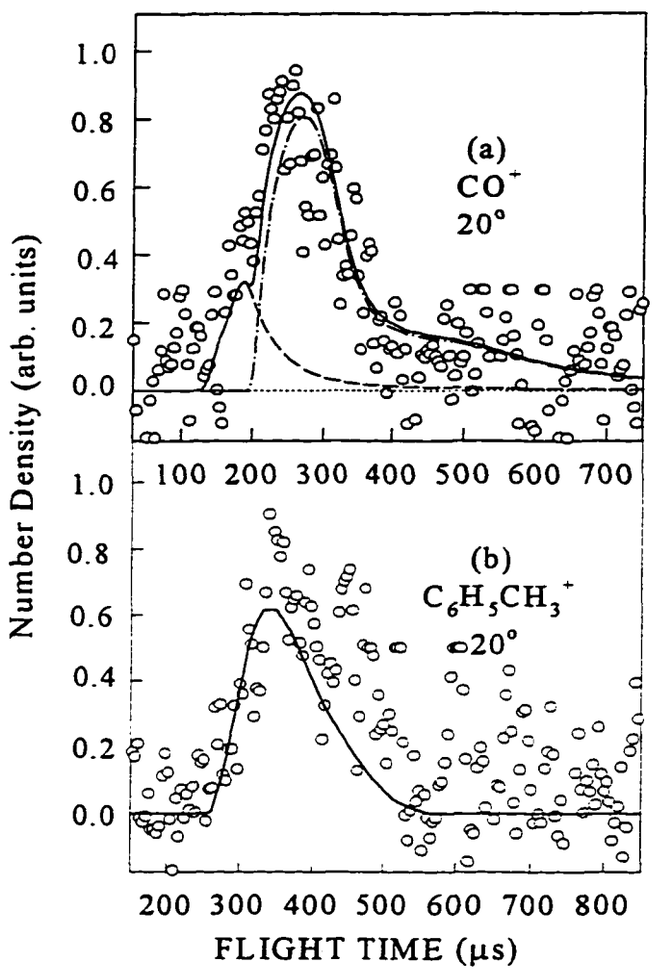

Figure 12 (a) TOF spectrum for CO at θ_{lab}= 20°. Circles represent experimental data. Contributions are shown from CH_3CO (dot-dashed line) formed in process (2) and CO (dashed line) from process (3). (b) TOF spectrum for $C_6H_5CH_3$ at θ_{lab}=20°. Circles represent experimental data. Both spectra were obtained from more than one million laser shots.

$C_6H_5CH_3$ at θ_{lab}= 20°, CO at θ_{lab}= 20° result from the accumulation of more than one million laser shots.

Because of the kinematic constraint, C_6H_5CO produced by process (1) cannot be observed at $\theta_{lab} > 20°$ [see Fig. 1(b)]. Thus, the translational energy distribution for process (2) at 248 nm can be derived from the TOF spectrum for C_6H_5 at θ_{lab}= 25°. However, in this spectrum a very fast onset appears as a shoulder, which cannot be due to process (2) based on the known $D_0(C_6H_5\text{-}COCH_3)$. We have attributed this to $C_6H_5^+$ formed in the dissociative electron ionization of $C_6H_5CH_3$. The $P(E_{c.m.})$ for process (2) at hν=248 nm derived from the TOF spectrum for C_6H_5 at 25° is shown in Fig. 13(b), which increases monotonically as $E_{c.m.}$ is decreased from the onset at $E_{c.m.} \approx 19$ kcal/mol to $E_{c.m.}$= 6 kcal/mol. Due to the overlap with the $C_6H_5^+$ signal from $C_6H_5CH_3$, the $E_{c.m.}$ onset for the $P(E_{c.m.})$ of process (2) cannot be determined. The onset for the $P(E_{c.m.})$ of Fig. 13(b) is fixed by the known $D_0(C_6H_5\text{-}COCH_3)$ of 99.5 kcal/mol and the estimated thermal energy of ≈4.8 kc/mol for parent $C_6H_5COCH_3$. The spectrum for C_6H_5 at 25° provides information only about the $P(E_{c.m.})$ at $E_{c.m} \geq 6$ kcal/mol. As shown in the analysis below, the $C_6H_5^+$ signal observed at $\theta_{lab} \leq 15°$ results overwhelmingly from the dissociative electron ionization of C_6H_5CO, i.e., processes (1) + (9). Thus, the TOF spectrum for C_6H_5 at smaller θ_{lab}'s does not provide reliable information about the $P(E_{c.m.})$ for process (2) at $E_{c.m.} < 6$ kcal/mol.

On the basis of the $P(E_{c.m.})$ for process (2) shown in Fig. 13(b), we conclude that the CH_3^+ signal originating from the dissociative electron ionization of CH_3CO [process (7)] contributes only a small component to the tail of the CH_3 spectra of Figs. 10(a)-10(c). Thus, the $P(E_{c.m.})$ for process (1) can be reliably determined from the TOF spectra of CH_3. The $P(E_{c.m.})$ of

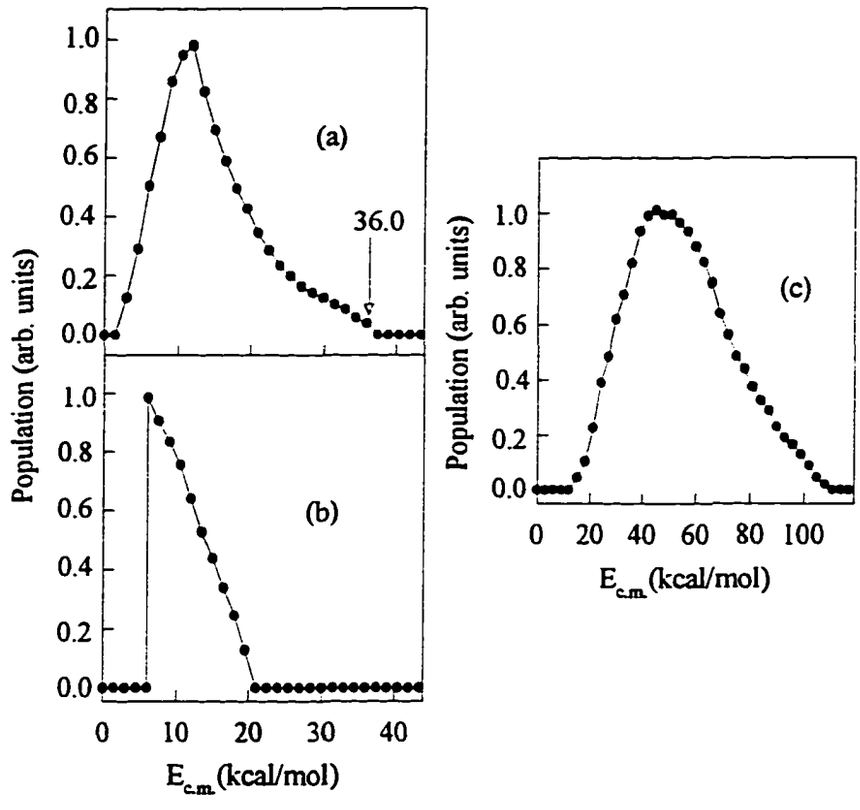

Figure 13 (a) $P(E_{c.m.})$ for process (1) derived by fitting TOF spectra for CH_3.
(b) $P(E_{c.m.})$ for process (2) derived by fitting the TOF spectra for C_6H_5.
(c) $P(E_{c.m.})$ for process (3) derived by fitting the TOF spectra for $C_6H_5CH_3$.

process (1) thus determined is shown in Fig. 13(a), and peaks near 12 kcal/mol. The average $E_{c.m.}$ energy release is 14.6 kcal/mol, which corresponds to 42% of the available energy of ≈35 kcal/mol. The $E_{c.m.}$ onset for the $P(E_{c.m.})$ of process (1) is 36.0±1.5 kcal/mol. Since this experiment uses a nozzle temperature of 130 °C (403 K), the onset observed here is affected by the hot band effect. Without consideration of the hot band effect, we determine a lower bound of 79.3 kcal/mol for $D_0(C_6H_5CO\text{-}CH_3)$. Using the HF/6-31G vibrational frequencies, the thermal energy for $C_6H_5COCH_3$ at 403 K is estimated to be 9.5 kcal/mol. Thus, the true $D_0(C_6H_5CO\text{-}CH_3)$ value should fall in the range of 79.3-88.8 kcal/mol. As mentioned above, we estimate that the effective temperature for $C_6H_5COCH_3$ after the mild beam expansion is in the range of 250-350 K, corresponding to a thermal energy range of 4.2-7.4 kcal/mol. Taking into account the thermal energy for $C_6H_5COCH_3$, we arrive at a value of 85.0±2.2 kcal/mol for $D_0(C_6H_5CO\text{-}CH_3)$. The uncertainties of ±2.2 kcal/mol given for $D_0(C_6H_5CO\text{-}CH_3)$ include the uncertainties of the $E_{c.m.}$ onset and the possible spread in the thermal energy of the parent $C_6H_5COCH_3$. The $D_0(C_6H_5CO\text{-}CH_3)$ value obtained here is between the literature value of 80.7 kcal/mol and the theoretical value of 85.1 kcal/mol (see Table III). Using $D_0(C_6H_5CO\text{-}CH_3)$ = 85.0±2.2 kcal/mol determined here, together with the known $\Delta_fH°_0(C_6H_5COCH_3)$ = -15.9±0.4 kcal/mol and $\Delta_fH°_0(CH_3)$ = 35.8±0. kcal/mol (see Table I), we obtain $\Delta_fH°_0(C_6H_5CO)$ = 33.3±2.2 kcal/mol, which is in excellent agreement with the G2(MP2, SVP) prediction of 32.5 kcal/mol and the value of 33.9±0.4 kcal/mol calculated based on the selected set of isodesmic reactions (see Table I and reactions v-xi in Table II).

The $P(E_{c.m.})$'s for process (1) and (2) of Figs. 13(a) and 13(b) have been used successfully to fit the TOF spectra for C_6H_5 at θ_{lab}=10° 15°, and 20° [Figs. 11(a), 11(b), and 11c)]. The TOF spectrum for C_6H_5 at $\theta_{lab.}$=20° is mostly due to process (2), with minor contribution from process (3), whereas the TOF spectra for C_6H_5 at θ_{lab}= 10° and 15° are largely due to process (1), with minor contribution from process (2). We note that the contribution of process (2) to the TOF spectrum for C_6H_5 at θ_{lab}= 15° has a bimodal structure, which results from the forward and backward scattered components of the C_6H_5 fragments.

The simulation of the TOF spectra for CH_3 at $\theta_{lab.}$= 15°, 20° and 25° [Figs. 10(a), 10(b), and 10(c)] shows that the branching ratio of process (2) to process (1) is small at 248 nm. This ratio can also be estimated from the simulation of the TOF spectrum for C_6H_5 at θ_{lab}=10° [Fig. 11(a)]. As we have shown in a previous photodissociation study of CS_2,[25] the photofragments resulting from photodissociation of dimmers and clusters are mainly confined to small θ_{lab} values because of kinematic constraints. In order to avoid the influence of dimers and clusters on the TOF measurement at 10°, we have decreased the stagnation pressure of $C_6H_5COCH_3$ to 260 Torr to reduce the effect of supersonic cooling. Under such molecular beam expansion conditions, no signals from electron ionization of dimers and clusters of $C_6H_5COCH_3$ are observed at $\theta_{lab.}$=10°. As shown in Fig. 11(a), the simulation indicates that the TOF spectrum for C_6H_5 at $\theta_{lab.}$=10° is predominantly accounted for by process (1). On the basis of the simulation of the CH_3 and C_6H_5 TOF spectra, we estimate that the branching ratio of process (2) to process (1) is ≈ 0.01.

The $P(E_{c.m.})$ for process (3) at hν=248 nm derived from the TOF spectrum for $C_6H_5CH_3$ [Fig. 12(b)] is depicted in Fig.13(c). This $P(E_{c.m.})$ is different from that obtained at hν=193 nm [Fig. 4(c)]. The observed $E_{c.m.}$ onset of ≈106 kcal/mol for the $P(E_{c.m.})$ of Fig. 13(c) is close to the thermochemical threshold of 109 kcal/mol for process (3) at hν = 248 nm. The $P(E_{c.m.})$ is nearly symmetrical about the maximum at $E_{c.m.} \approx 50$ kcal/mol, indicating that the available energy of 109 kcal/mol for process (3) is about equally partitioned into internal and translational energies of the photofragments. This $P(E_{c.m.})$ of Fig. 13(c) has been used satisfactorily to fit the fast shoulder observed in the TOF spectra for C_6H_5 at θ_{lab}= 20° and 25° [Figs. 11(c) and 11(d)]. The simulation of the C_6H_5 TOF spectra indicates that the branching ratio for process (2) to process (3) is ≈0.08 without considering the difference in the efficiency for the formation of $C_6H_5^+$ by electron ionization of C_6H_5 and that by the dissociative electron ionization of $C_6H_5CH_3$.

Due to the high N_2 background in the ionizer of the QMS, the signal-to-noise ratio is poor for the CO TOF spectrum observed at θ=20° [Fig. 14(a)] even after accumulating more than one million laser shots. According to dissociative electron ionization processes (10) and (11), CO^+ from the primary photofragments C_6H_5CO and CH_3CO should also contribute to the CO TOF spectrum. However, as pointed out above, the CO^+ signals from processes (10) and (11) are expected to be small because of the high ionization energy of CO. The simulation of the CO TOF spectrum at θ=20° shows that the major contribution is by processes (2) + (11) (dot-dashed curve), and process (3) contributes as a smaller fast peak (dashed curve). We note that process (1) cannot be seen at θ=20° due to the kinematic constraints.

The angular distribution for process (1) is probed by measuring the TOF spectrum for C_6H_5 at θ_{lab}=12° and ε = 10°, 30°, 50°, 70°, 90°, 100°, 130°, 150°, and 170° (see Fig. 14). These spectra are essentially identical, indicating that the photofragment angular distribution for process (1) is isotropic, i.e., $\beta = 0$. Again, this observation indicates that the dissociation lifetime of the excited state of $C_6H_5COCH_3$ involved is longer than that of the rotational period, and that a predissociation mechanism is operative for process (1) at $h\nu = 248$ nm. Since process (2) is a minor channel, the low TOF signal for CH_3 makes it difficult to measure the photofragment angular distribution for process (2).

Conclusion

The TOF spectra for CH_3 and C_6H_5 resulting from the 193 nm and 248 nm photofragmentation of $C_6H_5COCH_3$ has been measured. At 193 nm, processes (1) and (2) occur with comparable cross sections. The cross section for process (3) at 193 nm is estimated to be < 0.1% of those for processes (1) and (2). Approximately 30-50% of the CH_3CO and C_6H_5CO radicals initially formed at 193 nm by processes (1) and (2) are found to undergo further dissociation according to processes (6) and (8). At 248 nm, process (1) is overwhelmingly the dominant channel. The branching ratios for process (1) : process (2) : process (3) are estimated as 1.0: 0.01: 0.0008. The energy releases for these dissociation processes have also been determined. The photofragment angular distributions for these processes are isotropic, possibly indicative of a predissociative mechanism. From the $E_{c.m.}$ onset for process (2) at 248 nm, we determine $D_0(C_6H_5CO\text{-}CH_3) = 8.5 \pm 2.2$ kcal/mol and $\Delta_f H°_0(C_6H_5CO) = 33.3 \pm 2.2$ kcal/mol.

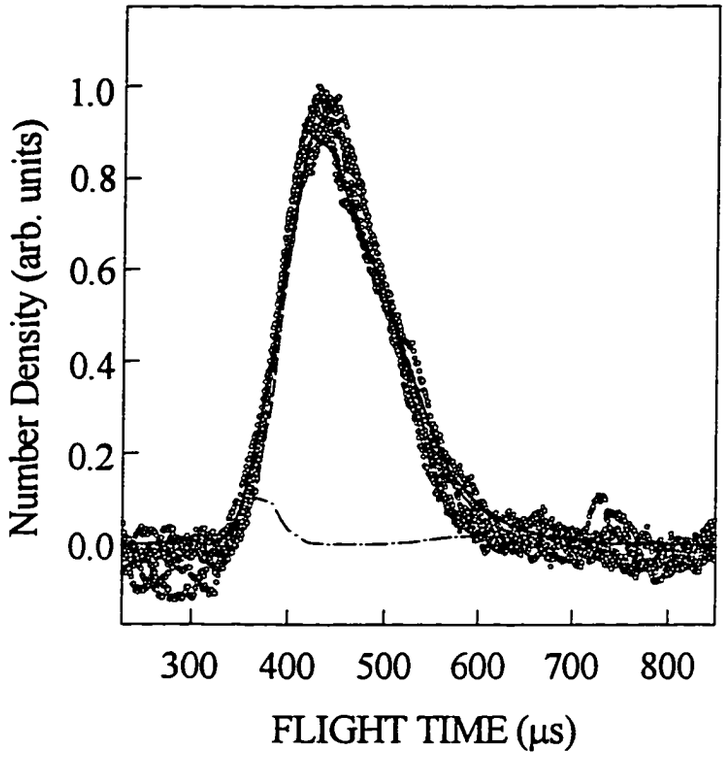

Figure 14 TOF spectra for C_6H_5 at θ_{lab}=12° and ε = 10°, 30°, 50°, 70°, 90°, 110°, 130°, 150°, and 170°.

We have also conducted an *ab initio* study of the energetics for C_6H_5CO, and C_6H_5 formed in processes (1) and (2) using the G2-type procedures together with isodesmic reaction scheme. The theoretical value $\Delta_fH°_0(C_6H_5CO) = 33.9\pm1.3$ kcal/mol is in good accord with the experimental result of the present study. The theoretical values $\Delta_fH°_0(C_6H_5) = 87.6\pm1.0$ kcal/mol and $\Delta_fH°_0(C_6H_5CO) = 33.9\pm1.3$ kcal/mol indicate the literature $\Delta_fH°_0$ values for C_6H_5CO and C_6H_5 are likely high by 3-4 kcal/mol.

References

1. S. W. North, D. A. Blank, J. D. Gezelter, C. A. Longfellow, and Y. T. Lee, *J. Chem. Phys.* **102**, 4447 (1995).

2. S. K. Kim, S. Pederson, and A. H. Zewail, *J. Chem. Phys.* **103**, 477 (1995).

3. K. A. Trentelman, S. H. Kable, D. B. Moss, and P. L. Houston, *J. Chem. Phys.* **91**, 7498 (1989).

4. P. D. Lightfoot, S.P.Kirwan, and M.J.Pilling, *J.Phys.Chem.* **92**, 4938, (1988)

5. H. Li, Q. Li, W. Mao, Q. Zhu, and F. Kong, *J. Chem. Phys.* **106**, 5943 (1997).

6. P. W. Kash, G. C. G.Waschewsky, R. E. Morss, and L. J. Butler, *J.Chem. Phys.* **100**, 3463(1994)

7. S. W. North, D. A. Blank, and Y. T. Lee, *Chem. Phys. Lett.* **224**, 38 (1994).

8. S. Deshmukh and W. P. Hess, *J. Chem. Phys.* **100**, 6429 (1994).

9. S. Deshmukh, J. D. Myers, S. S. Xantheas, and W. P. Hess, *J. Phys. Chem.* **98**, 12535 (1994).

10. J. G. Calvert and J. N. Pitts, "Photochemistry" (Wiley, New York, 1966).

11. N. C. Baird and H. B. Kathpal, *Can. J. Chem.* **55**, 863 (1977).

12. W. C. Brider, "Combustion Chemistry" (Springer, New York, 1984).

13. H. H. Glazebrook and T G. Pearson, *J. Chem. Soc.* 589 (1939).

14. F. J. Duncan and A. F. Trotman-Dickenson, *J. Chem. Soc.* 4672 (1962).

15. M. Berger and C. Steel, *J. Am. Chem. Soc.* **97**, 4817 (1975).

16. L. A. Curtiss, K. Raghavachari, G. W. Trucks, and J. A. Pople, *J. Chem. Phys.* **94**, 7221 (1991).

17. L. A. Curtiss, K. Raghavachari, and J. A. Pople, *J. Chem. Phys.* **98**, 1293 (1993).

18. B. J. Smith and L. Radom, *J. Phys. Chem.* **99**, 6468 (1995).

19. Y. S. Cheung, Y.-J. Chen, C.-L. Liao, C. Y. Ng, and W.-K. Li, *J. Amer. Chem. Soc.*, **117**, 9725 (1995).

20. C. W. Bauschlicher, Jr., J. Phys. Chem. **98**, 2564 (1994).

21. S. G. Lias, J. E. Bartmess, J. F. Liebman, . L. Holmes, R. D. Levin, and W. G. Mallard, *J. Phys. Chem. Ref. Data* **17**, Suppl. No. 1 (1988).

22. J. T. Niiranen, D. Gutman, and L. N. Krasnoperov, *J. Phys. Chem.* **96**, 5881 (1992).

23. R. K. Solly and S. W. Benson, *J. Am. Chem. Soc.* **93**, 1592 (1971).

24. S. W. Benson, "Thermochemical Kinetics" (Wiley, new York, 1968).

25. W.-B Tzeng, H.-M Yin, W.-Y. Leung, J.-Y. Luo, S. Nourbakhsh, G.D.Flesch and C. Y. Ng; *J. Chem. Phys.* **88**, 1658 (1988).

26. H.-Q. Zhao, Y.-S. Cheung, C.-X. Liao, C. Y. Ng, W.-K. Li, and S.-W. Chiu, *J. Chem. Phys.* **104**, 130 (1996).

27. H.-Q. Zhao, Y.-S. Cheung D. P. Heck, C. Y. Ng, T. Tetzlaff, and W. S. Jenks, *J. Chem. Phys.* **106**, 86 (1997).

28. C. Y. Ng, *Adv. Photochem.* **22**, 1 (1997).

29. T.K.Minton, G.M.Nathanson, and Y.T.Lee, *J.Chem.Phys.* **86**,1991 (1987)

30. E. J. Hintsa, X.Zhao, and Y.T.Lee, *J.Chem.Phys.* **92**,2280 (1990).

31. X. Zhao, Ph.D. Thesis, University of California, Berkeley,CA (1988).

32. M. J. Frisch *et al.*, GAUSSIAN 94 (Gaussian, Pittsburgh, PA, 1994).

33. S.-W. Chiu, W.-K. Li, W.-B. Tzeng, and C. Y. Ng, *J. Chem. Phys.* **97**, 6557 (1992).

34. A. Nicolades and L. Radom, *Mol. Phys.* **88**, 759 (1996).

35. L. A. Curtiss, K. Raghavachari, P. C. Redfern, and J. A. Pople, *J. Chem. Phys.* **106**, 1063 (1997).

36. G. E. Davico, V. M. Bierbaum, C. H. DePuy, G. B. Ellison, and R. R. Squires, *J. Am. Chem. Soc.* **117**, 2590 (1995).

37. M. N. Glukhovtsev and S. Laiter, *Theor. Chim. Acta* **92**, 32 (1995).

38. K. Raghavachar, B. B. Stefanov, L. A. Curtiss, *J. Chem. Phys.* **106**, 6764 (1997).

39. The portion of the true $P(E_{c.m.})$ at $E_{c.m.}$<10.5 kcal/mol for process (2) is higher than that shown by the approximated $P(E_{c.m.})$. Thus, the true $P(E_{c.m.})$ is expected to peak at a $E_{c.m.}$ lower than 10.5 kcal/mol.

40. R. N. Zare, Mol. Photochem. **4**, 1(1972)

41. J. G. Frey and P. Felder, Mol. Phys. **75**,1419(1992)

A 193 NM LASER PHOTOFRAGMENTATION TIME-OF-FLIGHT MASS SPECTROMETRIC STUDY OF DIMETHYLSULFOXIDE

A paper accepted by Journal of Chemical Physics

H.-Q. Zhao, Y.-S. Cheung, D. P. Heck, and C. Y. Ng

Abstract

The photodissociation of dimethylsulfoxide [$(CH_3)_2SO$] at 193.3 nm has been investigated using the molecular beam time-of-flight (TOF) mass spectrometric technique. In addition to CH_3 and SO, CH_3SO is also observed as a stable primary product, indicating that $CH_3SO + CH_3$ is an important product channel for the 193.3 nm photodissociation of $(CH_3)_2SO$. The analysis of the TOF data provides evidence that SO is formed via a stepwise mechanism: $(CH_3)_2SO + h\nu(193.3\ nm) \rightarrow CH_3SO + CH_3 \rightarrow 2CH_3 + SO$. The analysis also indicates that $\approx$ 53% of the primary CH_3SO radicals undergo further dissociation to produce $CH_3 + SO$, yielding a quantum yield of $\approx$ 1.53 for CH_3. Within the sensitivity of our experiment, the product channel of $CH_3SCH_3 + O$ is not found. The angular distribution for the formation of $CH_3SO + CH_3$ is found to be isotropic, an observation consistent with a predissociation mechanism, in which the dissociation of photoexcited $(CH_3)_2SO$ is slow compared to its rotational period. The energetics for selected dissociation reactions of $(CH_3)_2SO$ have also been investigated by *ab initio* calculations at the G2(MP2) level of theory. The experimental dissociation energy at 0 K (53 $\pm$ 2 kcal/mol) for the CH_3-$SOCH_3$ bond obtained here is in excellent agreement with the theoretical prediction of 52.6 kcal/mol.

Introduction

Photodissociation of polyatomic molecules generally involves more than one product channel, resulting from the multi-dimensional nature of the excited potential energy surfaces and the efficient energy redistribution between the internal degrees of motion of the excited precursor molecules. Because of the accessibility of multi-channel dissociation pathways, the identification of nascent products for such dissociation processes poses a great challenge to experimentalists.[1] In the case when the final products are known, such as in the 193.3 nm photodissociation of acetone [$(CH_3)_2CO$], the question of whether the products CH_3 + CO + CH_3 are formed sequentially or concertedly[2] has only been answered recently.[3-5] This photodissociation reaction involves two equivalent C-C bonds, both of which can be broken at 193.3 nm. By measurements of the fragment kinetic energy distributions, the laser photofragmentation time-of-flight (TOF) study of North *et al.*[4] has provided strong evidence that the 193.3 nm photodissociation of acetone proceeds via a stepwise mechanism. The stepwise mechanism is also found in the most recent ultrafast photofragmentation study of Kim *et al.*, which examined the bond breaking process in real time.[5] Despite the beauty of a concerted symmetric mechanism, the phase space associated with excited surfaces which leads to such a photodissociation process may not be high.

Dimethylsulfoxide [$(CH_3)_2SO$] is a sulfur analog of acetone [$(CH_3)_2CO$]. Being the simplest sulfoxide, the photochemistry of $(CH_3)_2SO$ represents a model system for the understanding of sulfoxide photochemistry. In previous photochemical studies of $(CH_3)_2SO$

at hν = 253.7 nm in solution, evidence is found indicating that the primary step is a C-S bond breaking process.[6-9]

$$(CH_3)_2SO + h\nu \rightarrow CH_3SO + CH_3 \qquad (1)$$

Secondary reactions involving CH_3SO, CH_3, and $(CH_3)_2SO$ are ascribed to the formation of a series of sulfur-containing compounds, such as dimethylsulfide (CH_3SCH_3).[7] Since the production of $2CH_3 + SO$ from $(CH_3)_2SO$ requires 104 kcal/mol at 0 K,[6] the energy of 112 kcal/mol corresponding to a 253.7 nm photon is adequate for breaking the two equivalent C-S bonds in $(CH_3)_2SO$.

Absorption at 193.3 nm is assumed to be due to a $p \rightarrow p^*$ transition in the S-O group.[7-9] Since a 193.3 nm photon corresponds to 147.9 kcal/mol, which is well above the energy required to break the two C-S bonds in $(CH_3)_2SO$, the formation of $2CH_3 + SO$ may be of considerable importance. This expectation is confirmed by recent photodissociation studies of $(CH_3)_2SO$ in the gas phase,[10,11] in which were detected both CH_3 and SO as the primary products. The rovibrational energy distributions for CH_3 and SO in their ground states have also been measured using the resonance enhanced multiphoton ionization and laser induced fluorescence (LIF) techniques, respectively.[10,11] On the basis of this information, together with the unity quantum yield measured for SO, Chen *et al.* favor the concerted three-body fragmentation mechanism as the sole photodissociation pathway.[11]

In accordance with the known photochemistry of $(CH_3)_2CO$ at 193.3 nm,[4,5] it is logical to suggest that the formation of SO and CH_3 from $(CH_3)_2SO$ at 193.3 nm results from a stepwise mechanism, i.e., internally excited CH_3SO radicals initially formed by process (1) undergo spontaneously dissociation according to process (2).

$$CH_3SO \rightarrow CH_3 + SO \qquad (2)$$

If this sequential mechanism is a realistic pathway for the production of SO, finite concentration of CH_3SO initially formed by process (1) at 193.3 nm may be stable. However, the direct identification of primary CH_3SO radicals formed in such a process has not been made previously.

We have undertaken a 193.3 nm laser photofragmentation TOF mass spectrometric study of $(CH_3)_2SO$. In addition to identifying CH_3, SO, and CH_3SO as the primary photoproducts, we have also obtained the energy release spectra for these radicals. The analysis of the experimental results supports that processes (1) and (2) are the dominant pathways in the 193.3 nm photodissociation of $(CH_3)_2SO$. Cleavage of the S-O bond in $(CH_3)_2SO$ to yield CH_3SCH_3 and O atom requires 85.3 kcal/mol.[6]

$$(CH_3)_2SO + h\nu \rightarrow CH_3SCH_3 + O(^3P) \qquad (3)$$

Since process (3) is exothermic by 62.7 kcal/mol for $h\nu$ = 193.3 nm,[6] we have also search for the formation of CH_3SCH_3 and O atom.

To our knowledge, the heat of formation at 0 K [$D_fH°_0$] for CH_3SO is not well known.[6,12] In order to interpret the TOF data obtained in this study, we have also conducted an *ab initio* quantum chemical study on selected dissociation processes of $(CH_3)_2SO$, which involves the energetic and structural calculations of $(CH_3)_2SO$, CH_3SCH_3, CH_3SO, and CH_2SO at the G2(MP2) level[13,14] of theory.

Experimental and Theoretical Methods

A. Experiment

The rotatable beam source laser photofragmentation TOF apparatus used in this study has been described in detail.[15] The apparatus consists of three main components: an ArF excimer laser, a photodissociation chamber in which a rotatable supersonic molecular beam intersects with the excimer laser beam, and a linearly movable ultrahigh vacuum electron ionization quadrupole mass spectrometer (QMS).

In this experiment, a pulsed beam of $(CH_3)_2SO$ (3 or 3.8% seeded in He) is produced by supersonic expansion through a commercial pulsed valve (General Valve, No. 9) with a nozzle diameter of 0.5 mm at 323 K and a total stagnation pressure of ≈ 1535 Torr. The pulsed valve is operated at 40 Hz. The seeded $(CH_3)_2SO$ beam has an angular divergence of 3° which is defined by the opening of the conical skimmer and the circular aperture as it passes through the differential chamber into the photodissociation chamber. The 3° angular spread of the beam corresponds to a beam width of 3 mm at the photodissociation region. During the experiment, the photodissociation chamber is maintained at a pressure of $1x10^{-8}$ Torr.

The excimer laser (Questek model 2460) was operated at 35-50 mJ. The laser beam enters the photodissociation chamber through a MgF_2 focusing lens and is perpendicular to the seeded $(CH_3)_2SO$ beam and the central axis of the QMS. The spot size of the excimer laser beam is estimated to be ≈ 5 mm^2 at the photodissociation region.

All TOF spectra are taken at a flight path of 65.5 cm which is defined by the distance between the photodissociation region and the ionizer. The emission current of the ionizer is about 1.25 mA and the ionization electron energy is about 75 eV.

The TOF spectra presented here were recorded on a multichannel scaler (Stanford Research model SRT430) with a channel width of 1.28 μs. The ion drift times through the QMS were determined to be 4.114 $m^{1/2}$, where m is the ion mass. The actual flight times of photofragments were corrected for the corresponding ion drift times. The velocity distribution of the parent $(CH_3)_2SO$ beam was determined by taking laser hole burning spectra of $(CH_3)_2SO$ at $\theta_{lab} = 0°$, where θ_{lab} is the angle between the $(CH_3)_2SO$ beam and the detector axis. The measured speed profile of species was then fitted to an assumed functional form,[15,16] $f(v) \sim v^2\exp[-(v-v_o)^2/\alpha^2]$, where v_o is the most probable speed and α is a measure of the width of the speed profile. In this experiment, the values of v_o and α for a beam of 3% $(CH_3)_2SO$ seeded in He are determined to be 1.64×10^5 and 5.5×10^3 cm/s, respectively. For a beam of 3.8% $(CH_3)_2SO$ seeded in He, the respective v_o and α values are 1.56×10^5 and 5.2×10^3 cm/s.

The analysis of the TOF data was performed by a forward simulation method.[17,18] Briefly, the procedure began with a trial center-of-mass (c.m.) kinetic energy ($E_{c.m.}$)

distribution, i.e., $P(E_{c.m})$, which was transformed to a TOF spectrum for comparison with the experimental TOF spectrum. The $P(E_{c.m.})$ distribution was adjusted until satisfactory agreement between the experimental and calculated TOF data was obtained. For the determination of the kinetic energy threshold for process (1), the $P(E_{c.m.})$ distribution near the $E_{c.m.}$ onset was obtained by direct transformation of the TOF data.

In angular distribution measurements, the laser light was polarized by a stack of ten quartz plates set at the Brewster angle. The electric vector **E** of the polarized laser beam was set perpendicular to the detector and then rotated into the desired direction with a half-wave retarder. The laser energy was measured by a pyroelectric detector, and was kept at 10 mJ/pulse. The θ_{lab} value was set at 15° or 30° with respect to the detector axis. In order to determine the angular distribution for process (1), the TOF spectra for CH_3SO and SO was recorded as a function of ε with each spectrum accumulated for a fixed number of laser shots, where ε is the angle between **E** and the direction of the molecular beam. In this experiment, the detector axis, the molecular beam axis, and **E** are in the same plane, which is perpendicular to the laser propagation direction.

B. *Ab initio* calculations

The Gaussian-2 (G2) *ab initio* theoretical procedure has been described in detail by Curtiss *et al.*[13] Briefly, at the G2 level of theory, molecular structures are optimized with the Hartree-Fock (HF) approach and the second-order Møller-Plesset perturbation theory (MP2) with all electrons included using the 6-31G(d) basis set [i.e., at the HF/6-31G(d) and MP2(full)/6-31G(d) levels]. Harmonic vibrational frequencies are calculated at the HF/6-

31G(d) geometries for stationary point characterization. All subsequent single-point calculations at higher levels involved are based on the MP2/6-31G(d) optimized structures. Approximations of QCISD(T)/6-311+G(3df,2p) energies are obtained with frozen-core single-point calculations at the QCISD(T)/6-311G(d,p), MP4/6-311G(d,p), MP4/6-311+G(d,p), MP4/6-311G(2df,p), and MP2/6-311+G(3df,2p) levels. A small semiempirical correction is applied to account for high level correlation effects to obtain the total electronic energy (E_e). The HF/6-31G(d) harmonic vibrational frequencies, scaled by 0.8929, are used for zero-point vibrational energy (ZPVE) correction. The total energy at 0 K (E_0) is equal to E_e + ZPVE.

The G2(MP2) theory[14] is a variation of the G2 procedure in which the single-point energies are only calculated at the QCISD(T)/6-311G(d,p) and MP2/6-311+G(3df,2p) levels. In this study, the E_0[G2(MP2)] values for $(CH_3)_2SO$, CH_3SCH_3, CH_3SO, CH_2SO, CH_3 and SO were calculated using the Gaussian-94 for Windows package.[19] All calculations were performed on a Pentium (166 MHz) PC. In the following sections, the structural parameters refer to those from calculations obtained at the MP2(full)/6-31G(d) level unless otherwise specified.

The optimized geometries of $(CH_3)_2SO$ (C_s), CH_3SCH_3 (C_{2v}), CH_3SO (C_s), and *planar*-CH_2SO (C_s) in their ground states are depicted in Figs. 1(a), 1(b), 1(c), and 1(d). Calculations show that CH_2SO has a higher energy cyclic isomer, the structure of which is shown in Fig. 1(e). The structural parameters of these species are summarized in Table I. The E_0[G2(MP2)], $D_fH°_0$[G2(MP2)], and the experimental $D_fH°_0$ [$D_fH°_0$(expt)] values[6] for

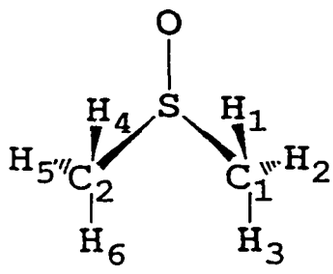

(a) $(CH_3)_2SO$ (C_s)

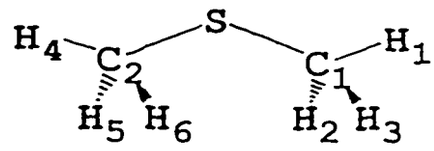

(b) $(CH_3)_2S$ (C_{2v})

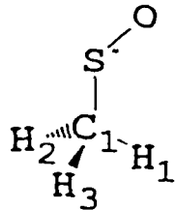

(c) CH_3SO (C_s)

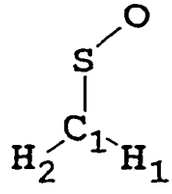

(d) *planar*-CH_2SO (C_s)

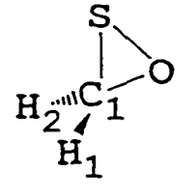

(e) *cyclic*-CH_2SO (C_s)

Figure 1. The structures of (a) $(CH_3)_2SO$ (C_s), (b) CH_3SCH_3 (C_{2v}), (c) CH_3SO (C_s), (d) *planar*-CH_2SO (C_s), and (e) *cyclic*-CH_2SO (C_s) optimizing at the MP2/6-31G(d) level.

Table I. Structural parameters for $(CH_3)_2SO$, CH_3SCH_3, CH_3SO and CH_2SO calculated at the MP2(full)/6-31G(d) level.[a]

Parameters[b]	$(CH_3)_2SO$	CH_3SCH_3	CH_3SO	*planar*-CH_2SO	*cyclic*-CH_2SO
r(S-O)	1.510	—	1.488	1.493	1.777
r[C(1)-S]	1.806	1.804	1.801	1.625	1.779
r[C(1)-H(1)]	1.093	1.091	1.092	1.085	1.089
r[C(1)-H(2)]	1.091	1.093	1.092	1.085	1.089
r[C(1)-H(3)]	1.093	1.093	1.092	—	—
∠[OSC(1)]	107.4	—	107.0	115.4	46.5
∠[C(1)SC(2)]	95.8	98.5	—	—	—
∠[SC(1)H(1)]	109.3	107.7	109.4	122.7	116.8
∠[SC(1)H(2)]	107.4	111.3	109.0	116.1	116.8
∠[SC(1)H(3)]	110.3	111.3	109.0	—	—
∠[C(2)SC(1)H(1)]	-59.4	180.0	—	—	—
∠[C(2)SC(1)H(2)]	-177.8	61.1	—	—	—
∠[C(2)SC(1)H(3)]	62.7	-61.1	—	—	—
∠[OSC(1)H(1)]	0.8	—	180.0	0.0	-107.7
∠[OSC(1)H(2)]	-67.6	—	-59.5	180.0	107.7
∠[OSC(1)H(3)]	172.9	—	59.5	—	—

a). Bond lengths (*r*) are in Å and bond angles (∠) are in degree.
b). See Fig. 1 for the labels of the S, C, O, and H atoms.

Table II. E_0[G2(MP2)], $D_fH°_0$[G2(MP2)], and $D_fH°_0$(expt) values for $(CH_3)_2SO$, CH_3SCH_3, CH_3SO, CH_3, SO, and CH_2SO isomers.

Species	E_0[G2(MP2)] (hartree)	$D_fH°_0$[G2(MP2)][a] (kcal/mol)	$D_fH°_0$(expt)[b] (kcal/mol)
$(CH_3)_2SO$	-552.47881	-32.2	-31.4
CH_3SCH_3	-477.36393	-5.7	-5.1
CH_3SO	-512.65102	-15.8	-14.8±2[c]
planar-CH_2SO	-512.05506	-7.2	---
cyclic-CH_2SO	-512.03032	8.3	---
CH_3	-39.74390	36.2	35.6
SO	-472.81931	3.1	1.2±0.3

a). Calculated using the $D_fH°_0$(expt) values of C (170.0 kcal/mol), O(^{3}P) (59.0 kcal/mol), S (65.6 kcal/mol), and H (51.63 kcal/mol) from Ref. 9; E_0[G2(MP2)] values of C (-37.76390 hartree), O(^{3}P) (-74.97868 hartree), S (-397.64699 hartree), and H (-0.50000 hartree). See Ref. 20.

b). Values are from Ref. 9.

c). This work.

these species, CH_3, and SO are listed in Table II. The $D_fH°_0$[G2(MP2)] values are obtained using the $D_fH°_0$(expt) values of H (51.6 kcal/mol), C (170 kcal/mol), O (59.0 kcal/mol), and S (65.6 kcal/mol), E_0[G2(MP2)] values of the molecular species given in Table II, and E_0[G2(MP2)] values of H (-0.50000 hartree), C (-37.76390 hartree), $O(^3P)$ (-74.97868 hartree), and S (-397.64699 hartree).[20] The known $D_fH°_0$(expt) values for $(CH_3)_2SO$, CH_3, and SO are in good agreement with the corresponding $D_fH°_0$[G2(MP2)] predictions. Despite the similarity in atom connectivities for $(CH_3)_2CO$ and $(CH_3)_2SO$, the bonding structures for these two molecules are quite different. In the case of $(CH_3)_2CO$, the bonding around C is best described by sp^2 hybridization with the four heavy atoms lie on the same plane. The bonding between C and O is characterized by a full double bond. The angle between the two O-S-C planes in $(CH_3)_2SO$ is 102.0°, indicating that the bonding around the S atom can be considered as sp^3 hybridization. To fulfill the octet shell rule for the S atom, the most stable structure for dimethylsulfoxide has the zwitterion form $(CH_3)_2S^+$-O^-. Here, the S atom is surrounded by three s-bonds and one lone pair. The stability of the latter structure is achieved due to the greater electronegativity of the O atom compared to that of the S atom. The zwitterion structure is consistent with a significant single bond character for the S-O bond. Finite *p*-bonding between S and O atoms can be rationalized by the hypervalent nature of the S atom, a concept of which invokes the bonding participation of the sulfur *d*-orbitals. Including the *p*-bond, the S atom is surrounded by ten electrons with the structure $(CH_3)_2S{=}O$. However, the high energy and diffuse characters of the sulfur *d*- orbitals make them inefficient for bonding. According to this bonding picture, the S-O bond energy in

$(CH_3)_2SO$ is expected to be significantly lower than that of a double bond. As pointed out above, the energy of a 193.3 nm photon is more than sufficient to break the C-S bond or the S-O bond yielding $CH_3SO + CH_3$ or $CH_3SCH_3 + O$, respectively. The five highest occupied orbitals for a dialkylsulfoxide, such as $(CH_3)_2SO$, have been characterized as n(S), p(SO), s(SO), s(CSC), and n(O), where n(S) and n(O) represent nonbonding orbital localized at the S and O atoms, respectively.[21]

As shown in Table I, the structural parameters in CH_3SCH_3 and CH_3SO are similar to the corresponding values in $(CH_3)_2SO$. The bonding picture used to describe the bonding between S and O in $(CH_3)_2SO$ is mostly applicable to that in CH_3SO and *planar*-CH_2SO. The CH_2S^+-O^- structure allows S to fulfill the octet rule, whereas the hypervalent form, CH_2=S=O, emphasizes a finite double bond character for the bonding between S and O. The *cyclic*-CH_2SO isomer is a typical molecule fulfilling the octet rule. Although a three-member ring is not a structure for favorable bonding interactions, it is interesting to note that the cyclic isomer is predicted to be less stable than the planar one by only 15.5 kcal/mol at the G2(MP2) level.

Results and Discussion

Table III compares the theoretical and experimental values for selected bond dissociation energies at 0 K (D_0) for $(CH_3)_2SO$ and CH_3SO. The D_0[G2(MP2)] value for the first C-S bond in $(CH_3)_2SO$ is 52.6 kcal/mol. An experimental value identical to this prediction was cited [as unpublished results] in Ref. 7 for the C-S bond dissociation energy in $(CH_3)_2SO$. However, the temperature associated with this experimental value was not

given. An estimate of 55±2 kcal/mol was given for the CH_3-$SOCH_3$ bond dissociation energy at 298 K by Benson.[12]

Using 52.6 kcal/mol for $D_0(CH_3\text{-}SOCH_3)$, we have constructed the Newton diagram in Fig. 2 for process (1) at hn = 193.3 nm. As shown in the figure, $v_o = 1.64 \times 10^5$ cm/s, v_{lab} and $v_{c.m.}$ are the laboratory and c.m. velocities for the photofragments, $\theta_{c.m.}$ is the c.m. angle, defined by the angle between $v_{c.m.}$ and the detector axis. The circles defined by $v_{c.m.}(CH_3)$ and $v_{c.m.}(CH_3SO)$ represent the maximum $v_{c.m.}$'s for CH_3 and CH_3SO. Also shown in Fig. 2 are γ and ε, which are defined as the angles between the laser electric field **E** and $v_{c.m.}$ and between **E** and the detector axis, respectively.

Throughout the discussion below, we refer to processes (1)-(3) as at hν= 193.3 nm. The TOF spectra for CH_3SO, CH_2SO, and CH_2S obtained at θ_{lab}= 15° are depicted in Figs. 3(a), 3(b), and 3(c), respectively. Figures 4(a) and 4(b) show the respective TOF spectra for CH_3 observed at θ_{lab} = 15° and 30°. Shown in Figs. 5(a), 5(b), 5(c), and 5(d) are the TOF spectra for SO observed at θ_{lab} = 15°, 30°, 40°, and 45°, respectively.

The observation of CH_3SO here unambiguously shows that process (1) is an important photo-dissociation channel. The goal of the data analysis is to derive the $E_{c.m.}$ distributions [$P(E_{c.m.})$] for processes (1) as shown in Fig. 6, which fit all the TOF spectra of CH_3SO, CH_3, and SO of Figs. 3-5. The detailed procedure involves tedious adjustments starting from a trial $P(E_{c.m.})$. The reasoning in arriving the $P(E_{c.m.})$ for process (1) is described below. The $P(E_{c.m.})$ at $E_{c.m.} \approx$ 6-50 kcal/mol shown by solid circles in Fig. 6 is obtained by fitting the TOF spectrum of CH_3SO. This can be viewed as a trial $P(E_{c.m.})$ for process (1). The $P(E_{c.m.})$ thus

Table III. Theoretical and experimental values for selected bond dissociation energies at 0 K (D_0) for $(CH_3)_2SO$ and CH_3SO.

Reactions	D_0[G2(MP2)][a] (kcal/mol)	D_0(expt)[b] (kcal/mol)
$(CH_3)_2SO \rightarrow CH_3SO + CH_3$	52.6	—[c]
$(CH_3)_2SO \rightarrow CH_3SCH_3 + O(^3P)$	85.5	85.3
$(CH_3)_2SO \rightarrow CH_3SCH_3 + O(^1D)$	—	130.7[d]
$(CH_3)_2SO \rightarrow 2CH_3 + SO$	107.7	103.8
$CH_3SO \rightarrow CH_3 + SO$	55.1	—
$CH_3SO \rightarrow$ *planar*-$CH_2SO + H$	60.2	—
$CH_3SO \rightarrow$ *cyclic*-$CH_2SO + H$	75.7	—

a). Calculated using the E_0 values given in Table II.

b). Calculated using the $D_fH°_0$(expt) values given in Table II.

c). A value of 52.6 kcal/mol for the C-S bond dissociation energy in $(CH_3)_2SO$ was cited as unpublished results in Ref. 6. However, the temperature associated with this value is unknown.

d). The excited $O(^1D)$ state is higher than the ground $O(^3P)$ state by 45.4 kcal/mol (Ref. 23).

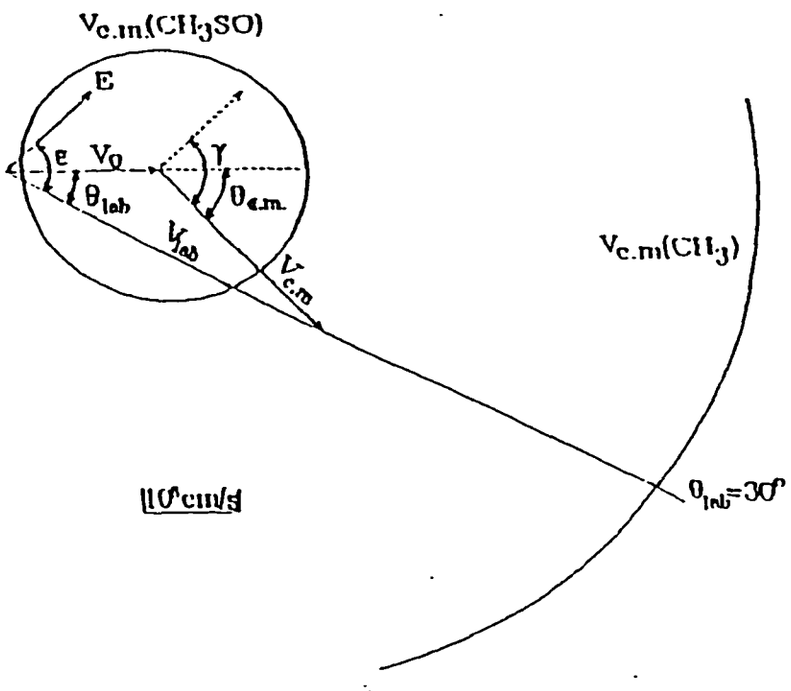

Figure 2. Kinematics for the formation of $CH_3SO + CH_3$ by 193.3 nm photodissociation of $(CH_3)_2SO$. v_o (=1.64x10^5 cm/s) is the laboratory velocity for the $(CH_3)_2SO$ beam. $v_{c.m.}(CH_3SO)$ and $v_{c.m.}(CH_3)$ are the maximum c.m. velocities for CH_3SO and CH_3, respectively. The diagram shows the relationship $\gamma = \theta_{c.m.} + \varepsilon - \theta_{lab}$ where γ is the angle between the laser electric field (**E**) and the c.m. velocity for the photofragment ($v_{c.m.}$), $\theta_{c.m.}$ is the angle between v_o and $v_{c.m.}$, ε is the angle between **E** and the detector axis, and θ is the laboratory angle between v_o and the detector axis.

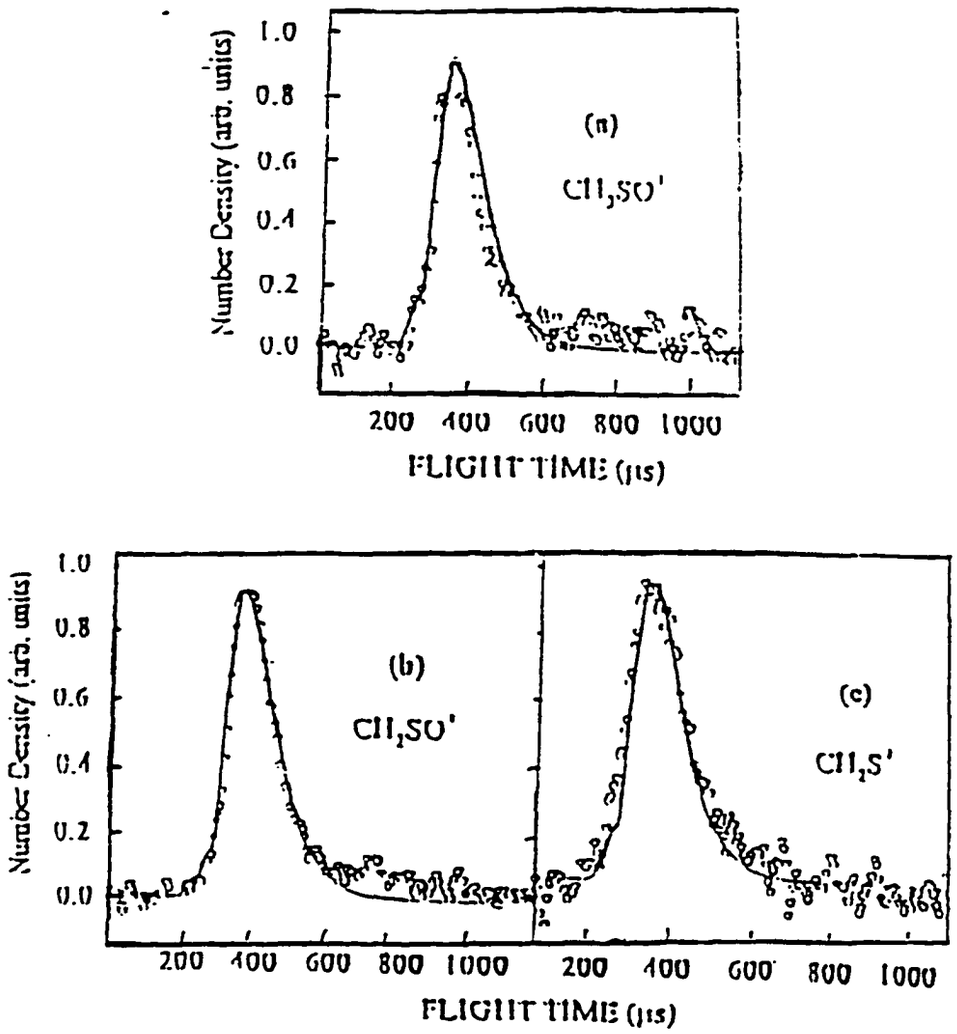

Figure 3. TOF spectra for (a) CH_3SO, (b) CH_2SO, (c) CH_2S obtained at $\theta_{lab} = 15°$. The solid line represents the best fit of the data using the $P(E_{cm})$ for process (1) shown in Fig. 6 (see the text). $v_o = 1.64 \times 10^5$ cm/s; $\alpha = 5.5 \times 10^3$ cm/s.

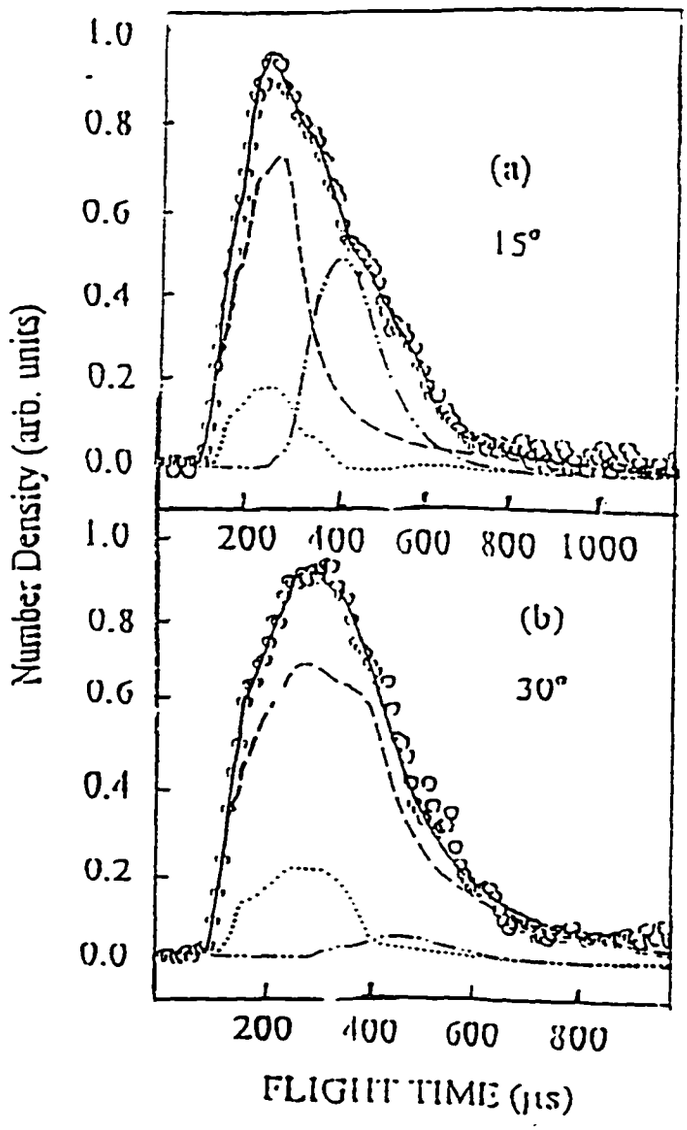

Figure 4. TOF spectra for CH_3 obtained at (a) $\theta_{Lab} = 15°$ and (b) 30°. Circles represent experimental data. Contributions are shown for CH_3 (- -) from process (1), CH_3SO (- ···-) from process (1), and CH_3 (···) from process (3). The sum of these contributions are shown as the solid line. $v_o = 1.56 \times 10^5$ cm/s. $\alpha = 5.2 \times 10^3$ cm/s.

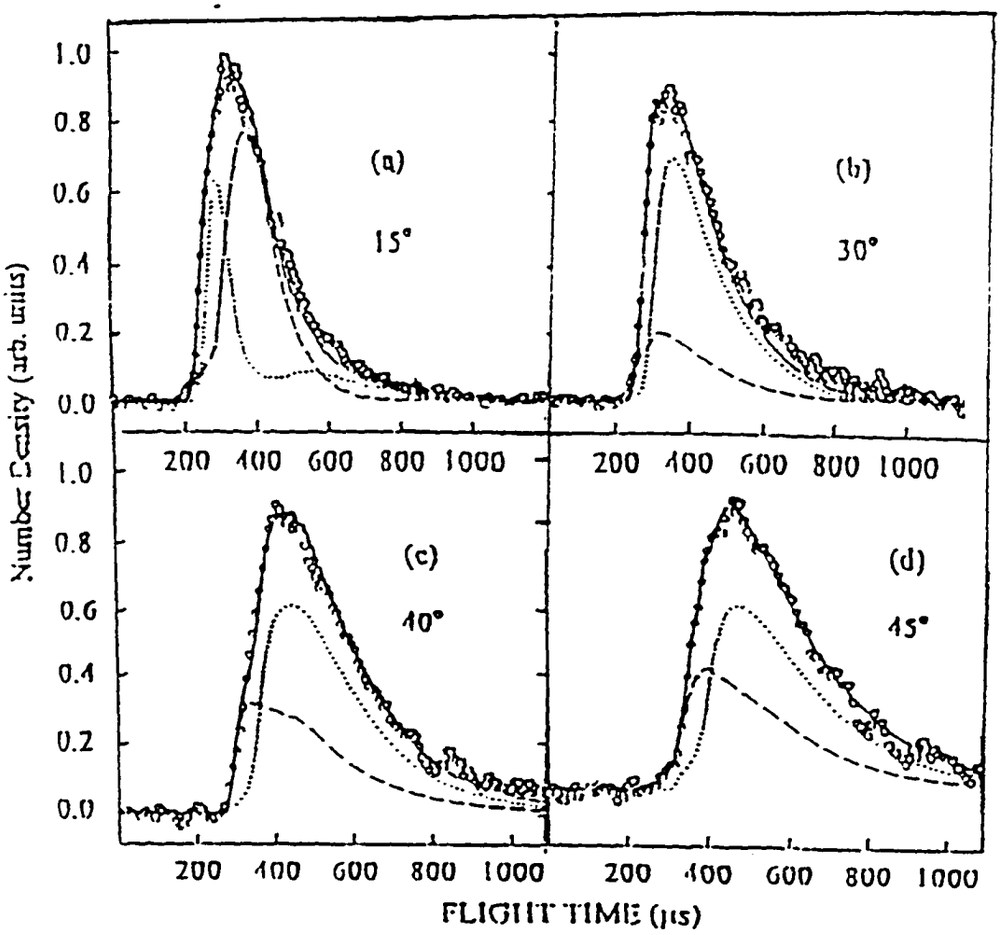

Figure 5. TOF spectra for SO obtained at θ_{lab}= (a) 15°, (b) 30°, (c) 40°, and (d) 45°. Contributions are shown for CH_3SO (- -) from process (1) and SO (···) from process (3). The sum of these contributions are shown as the solid line. $v_o = 1.64 \times 10^5$ cm/s. a $= 5.5 \times 10^3$ cm/s.

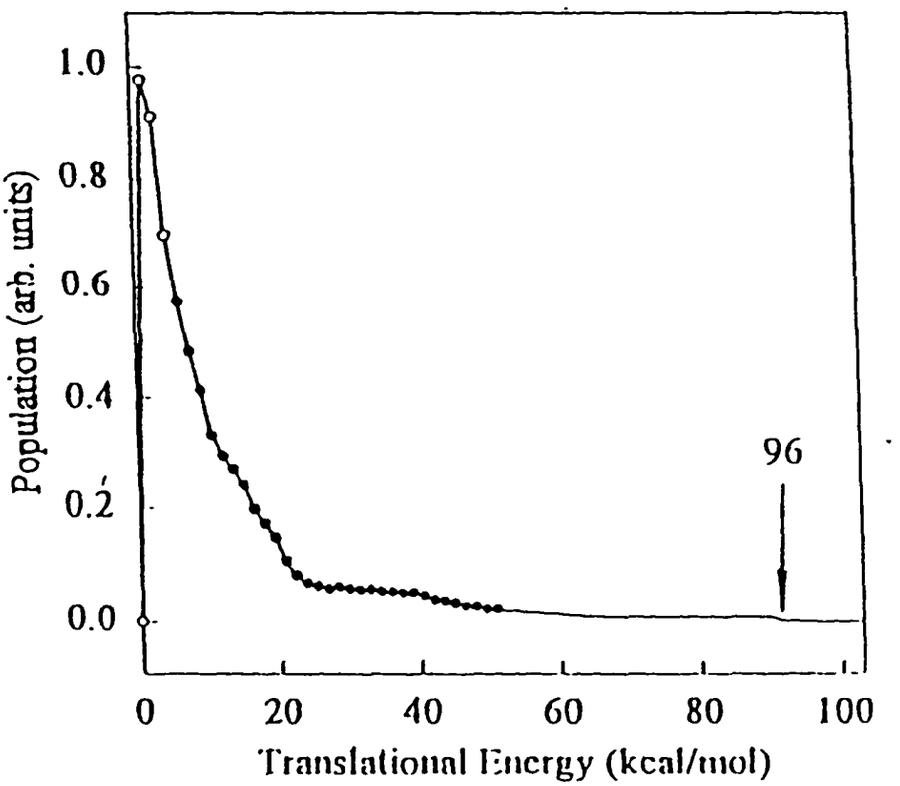

Figure 6. $E_{c.m.}$ distribution [$P(E_{c.m.})$] for process (1) (solid line) derived by fitting the TOF spectra for CH_3SO, CH_3, and SO. The $P(E_{c.m.})$ derived from fitting the TOF spectrum of CH_3SO is given in solid circles and the $P(E_{c.m.})$ derived by fitting the TOF spectra for CH_3 is shown in open circles.

obtained decreases rapidly from $E_{c.m.} \approx 6$ kcal/mol toward higher $E_{c.m.}$, and appears to have small populations at $E_{c.m.} > 60$ kcal/mol. We find that the fit to the CH_3SO spectrum is not very sensitive for determining the $P(E_{c.m.})$ at $E_{c.m.}$ greater than ≈ 50 kcal/mol. This can be understood by the fact that CH_3SO is the heavy moiety formed in process (1). The $P(E_{c.m.})$ for process (1) near its $E_{c.m.}$ threshold can be more reliably determined using the TOF spectrum for CH_3, the lighter moiety formed in process (1). The fact that the early parts of the TOF spectra for CH_3 are contributed solely by CH_3 formed in process (1) allows the derivation of the $P(E_{c.m.})$ at $E_{c.m.} > 60$ kcal/mol of Fig. 6 (solid line) by fitting or direct transformation of the early part of the TOF spectra for CH_3. We note that since the $E_{c.m.}$ distribution for the excited CH_3SO radicals, which have undergone further dissociation in the time scale of this experiment, has not been taken into account, the $P(E_{c.m.})$ obtained by fitting the TOF spectrum of CH_3SO can only be considered as an estimate for the $P(E_{c.m.})$ for process (1). Further modification of the $P(E_{c.m.})$ derived from the CH_3SO TOF spectrum is needed, especially at low $E_{c.m.}$ where the population may have to be raised to obtain the correct $P(E_{c.m.})$ for process (1). This is due to the fact that primary CH_3SO radicals with high internal energies (E_{int}), which decompose and thus are not detected as CH_3SO^+ in this experiment, correspond to the population at low $E_{c.m.}$. Nevertheless, the $P(E_{c.m.})$ for process (1) seems to peak at low $E_{c.m.}$'s, consistent with the conclusion that the CH_3SO and CH_3 radicals formed by process (1) contain a significant amount of internal energies. Thus, the further dissociation of a portion of the internally excited CH_3SO initially formed by process (1) is to be expected.

The direct transformation of TOF data near the onset of the TOF spectra for CH_3 reveals a weak, but distinct, onset at $E_{c.m.}$ = 96±2 kcal/mol for the $P(E_{c.m.})$ of process (1). By energy conservation, we have the relationship

$$E(h\nu) + E_{int}[(CH_3)_2SO] = D_0(CH_3\text{-}SOCH_3) + E_{c.m.} + E_{int}(CH_3SO) + E_{int}(CH_3) \qquad (4)$$

where E(hν= 193.3 nm) = 147.9 kcal/mol and $E_{int}[(CH_3)_2SO]$, $E_{int}(CH_3SO)$, and $E_{int}(CH_3)$ represent the respective E_{int} values for $(CH_3)_2SO$, CH_3SO, and CH_3. Assuming that $E_{int}[(CH_3)_2SO]$ is negligible because of supersonic expansion, and that photofragments ($CH_3SO + CH_3$) formed at the threshold $E_{c.m.}$ = 96 kcal/mol contain no E_{int}, we calculate a value of 52±2 kcal/mol for $D_0(CH_3\text{-}SOCH_3)$. Under the supersonic expansion conditions used in this experiment, the rotational relaxation for $(CH_3)_2SO$ is expected to be efficient. However, the vibrational relaxation for $(CH_3)_2SO$ is most likely incomplete. Using the calculated vibrational frequencies for $(CH_3)_2SO$, we estimate that the vibrational energy for $(CH_3)_2SO$ is ≈ 2.1 kcal/mol at 323 K. If we assume that $(CH_3)_2SO$ is cooled to a vibrational temperature of ≈ 150 K after the supersonic expansion, a value of 53±2 kcal/mol is obtained for $D_0(CH_3\text{-}SOCH_3)$, which is in agreement with the G2(MP2) prediction of 52.6 kcal/mol. Combining the $D_0(CH_3\text{-}SOCH_3)$ value determined here and the known $D_fH°_0$ values for $(CH_3)_2SO$ and CH_3,[9] we calculate a value of 14.8±2.0 kcal/mol for $D_fH°_0(CH_3SO)$, which is also consistent with the G2(MP2) prediction of 15.8 kcal/mol (see Table II).

The SO^+ ions can be formed by the dissociative ionization of CH_3SO. We note that the TOF spectrum for CH_3SO [Fig. 3(a)] peaks at ≈ 370 μs, which is significantly later than the peak position of ≈ 320 μs for the SO TOF spectrum [Fig. 5(a)] at θ_{lab} = 15°. This

observation indicates that the SO TOF spectrum is also contributed by other processes, such as process (2). This conclusion is consistent with previous 193.3 nm photodissociation studies of $(CH_3)_2SO$,[10,11] in which SO was identified as a nascent photoproduct and its rovibrational state distributions was measured using LIF techniques. The $P(E_{c.m.})$ for the concerted three-body photodissociation process $(CH_3)_2SO + h\nu \rightarrow 2CH_3 + SO$ cannot be determined in this experiment. However, as we show in the discussion below, all TOF data obtained here can be satisfactorily fitted by assuming a stepwise mechanism for the formation of SO. The rough fitting of the SO spectrum at $\theta_{lab} = 15°$ [Fig. 5(a)] shows that the majority of SO products formed by the secondary dissociation process (2) are faster than CH_3SO produced by process (1). By introducing the secondary $P(E_{c.m.})$ (Fig. 7) for the formation of $SO + CH_3$ by process (2), together with the estimated $P(E_{c.m.})$ for process (1), we have obtained satisfactory fits all the TOF spectra of SO as shown in Figs. 5(a)-5(d). The angular distribution of the secondary $P(E_{c.m.})$ used in the fitting is isotropic. We note that the data fitting does not provide information about the secondary $P(E_{c.m.})$ at $E_{c.m.} < 4$ kcal/mol. As shown in Fig. 7, the $P(E_{c.m.})$ for the secondary dissociation process (2) obtained here decreases rapidly from $E_{c.m.} \approx 4$ kcal/mol and has a $E_{c.m.}$ threshold at ≈ 16 kcal/mol.

The CH_3^+ signals can be contributed by direct ionization of CH_3 formed in processes (1) and (2) and the dissociative electron ionization of stable CH_3SO formed in process (1). The estimated $P(E_{c.m.})$ for process (1) (solid circles in Fig. 6) and the isotropic $P(E_{c.m.})$ for the secondary dissociation process (2) (Fig. 7) are used to fit the TOF spectra for CH_3. Due to

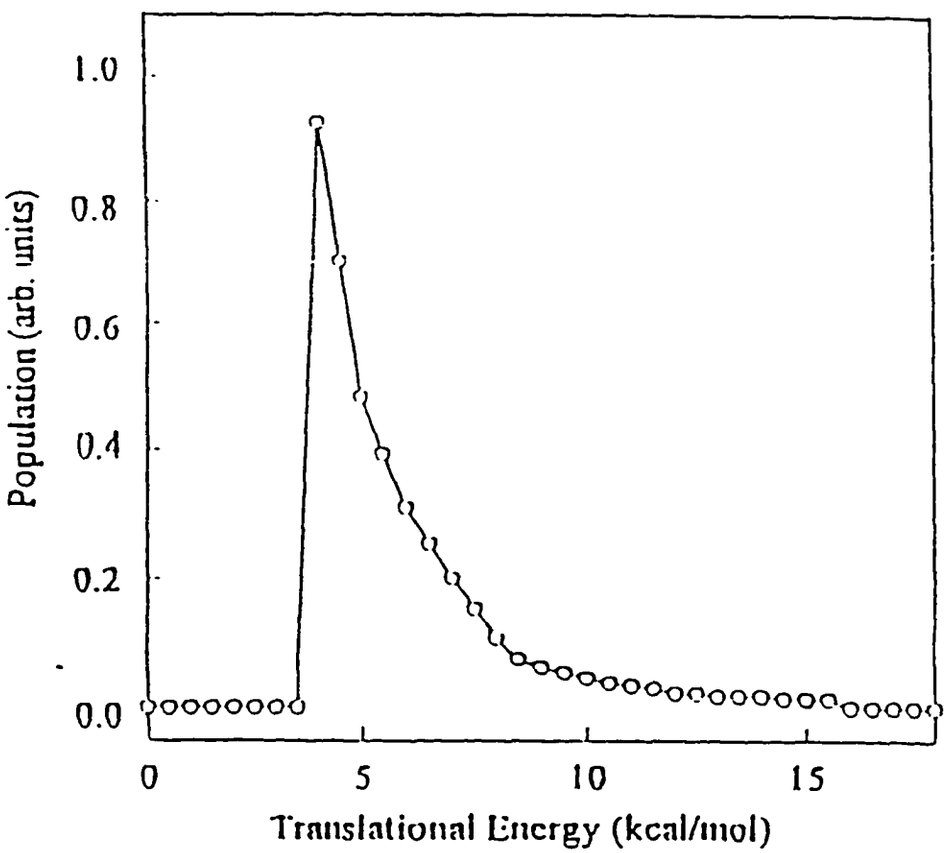

Figure 7. $P(E_{cm})$ for the secondary dissociation process (3). The angular distribution for this $P(E_{cm})$ is assumed to be isotropic. We note that the fitting is not sensitive to $P(E_{cm})$ at $E_{cm} < 4$ kcal/mol.

the momentum balance requirement, the TOF distribution of CH_3 radicals which correlate with the stable CH_3SO fragments can be predicted using the known TOF spectrum for CH_3SO. Here, the CH_3 radicals formed in process (1) contain the contribution from CH_3 radicals that are correlated with the excited CH_3SO radicals (which have undergone further dissociation). The fitting of the TOF data for CH_3 is expected to provide the correction needed for the estimated $P(E_{c.m.})$ (solid circles in Fig. 6) at low $E_{c.m.}$. The open circles at $E_{c.m.} < 6$ kcal/mol shown in Fig. 6 are derived from fitting the TOF spectra for CH_3. The careful fitting of the TOF spectra for CH_3, SO, and CH_3SO leads to the $P(E_{c.m.})$ (solid line in Fig. 6) for process (1).

The fast peaks (dash-curves) shown in Figs. 4(a) and 4(b) account for the contribution by CH_3 formed by process (1), while the slow peaks (dash-dot-curves) of the figures represent the contribution by stable CH_3SO. The dotted peaks shown in the TOF spectra for CH_3 account for the contribution of CH_3 formed in the secondary dissociation process (2). The fitting of the spectra of Fig. 4(a) and 4(b) also shows that the CH_3^+ signals due to dissociative ionization of CH_3SO become less important compared to that from CH_3 formed by process (1) as θ_{lab} is increased. The fitting of the TOF data described above provides an estimate that 53% of CH_3SO initially formed by process (1) undergoes further dissociation to produce CH_3 + SO. That is, the quantum yield for CH_3 formed in the 193 nm photodissociation of $(CH_3)_2SO$ is 1.53. The latter value is arrived based on the assumption that CH_3 radicals formed in different internal states have the same electron impact ionization cross sections.

As shown in Table III, the G2(MP2) prediction of 55.1 kcal/mol for $D_0(CH_3\text{-}SO)$ is only lower than the predicted value of 60.2 kcal/mol for $D_0(H\text{-}CH_2SO)$ by 5 kcal/mol. Thus, it is energetically possible that excited CH_3SO initially formed by process (1) might also dissociate to form *planar*-CH_2SO + H. The TOF spectrum for CH_2SO observed at $\theta = 15°$ is shown in Fig. 3(b). We find that this spectrum can be fitted by the $P(E_{c.m.})$ for process (1), indicating that the CH_2SO^+ signals observed are due to dissociative electron ionization of CH_3SO. This, together with the failure to observe the TOF spectrum for H, suggests that the further dissociation of internally excited CH_3SO to form *planar*-CH_2SO + H is not a significant process.

Within the sensitivity of this experiment, no TOF signals for O atoms were observed. The mass for CH_3SCH_3 is identical to that of CH_2SO. Effort was made to observe the TOF signals for CH_3S^+ and CH_2S^+, which are possible fragment ions formed in the dissociative electron ionization of CH_3SCH_3. Since the weak CH_3S^+ (mass 47) signal is only one mass away from the strong SO^+ (mass 48) signal, the TOF spectrum for CH_3S is affected and found to be similar to the SO TOF spectrum. We show in Fig. 3(c) the TOF spectrum for CH_2S^+ observed at $\theta_{lab} = 15°$. This spectrum is also found to stem from dissociative electron ionization of CH_3SO because the spectrum can be fitted by the $P(E_{c.m.})$ for process (1). On the basis of this experiment, we conclude that process (3) is not important at 193.3 nm.[22] We note that both $(CH_3)_2SO$ and CH_3SCH_3 are closed shell molecules. The low probability for the formation of $CH_3SCH_3 + O(^3P)$ by process (3) may be rationalized by its violation of the spin conservation rule. In order to conserve the total electron spin, the O atoms may be

formed in the $O(^1D)$ state. However, such a process requires 45.4 kcal/mol of additional energy (see Table III),[23] making the formation of $O(^1D)$ energetically less favorable.

The angular distribution of the photofragments has the form: $P(\gamma) = 1/4\pi[1 + \beta P_2(\cos\gamma)]$, where $P_2(\cos\gamma)$ is the second Legendre polynomial and β is the anisotropy parameter. The TOF spectra for SO observed at $\theta_{lab} = 15°$ and $\varepsilon = 30°$, 70°, 90°, 130°, and 170° are shown in Fig. 8(b), while the SO spectra measured at $\theta = 30°$ and $\varepsilon = 30°$, 70°, 90°, 130°, and 170° are depicted in Fig. 8(c). We have also obtained the TOF spectra for CH_3SO at $\theta_{lab} = 15°$ and $\varepsilon = 0°$ and 90° [Fig. 8(a)]. Within the error limits of the experiment, no difference in the SO and CH_3SO TOF spectra was observed, indicative of an isotropic distribution, i.e.,$\beta = 0$. We note that the data analysis of the SO TOF spectra suggests that both processes (1) and (2) contribute to the spectra at $\theta = 15°$ and 30°. The results of the measurements obtained here Contributions to the involves a $p \rightarrow p^*$ transition associated with the S-O bond, the breaking of the C-S bond likely proceeds via a predissociation mechanism. The observation of an isotropic distribution for the formation of $CH_3SO + CH_3$ indicates that the predissociation lifetime is longer than the rotational period of the excited $(CH_3)_2SO$ precursor molecule. The observed $P(E_{c.m.})$ for process (1) is close to that expected of a statistical unimolecular dissociation process, which likely involves a significant change in molecular geometry prior to dissociation. We note are consistent with the conclusion that the angular distribution for photoproducts of process (1) is isotropic. If the 193.3 nm excitation of $(CH_3)_2SO$ that the photofragments resulting from the 193.3 nm photodissociation of $(CH_3)_2CO$ are also found to have an isotropic distribution.[24,25]

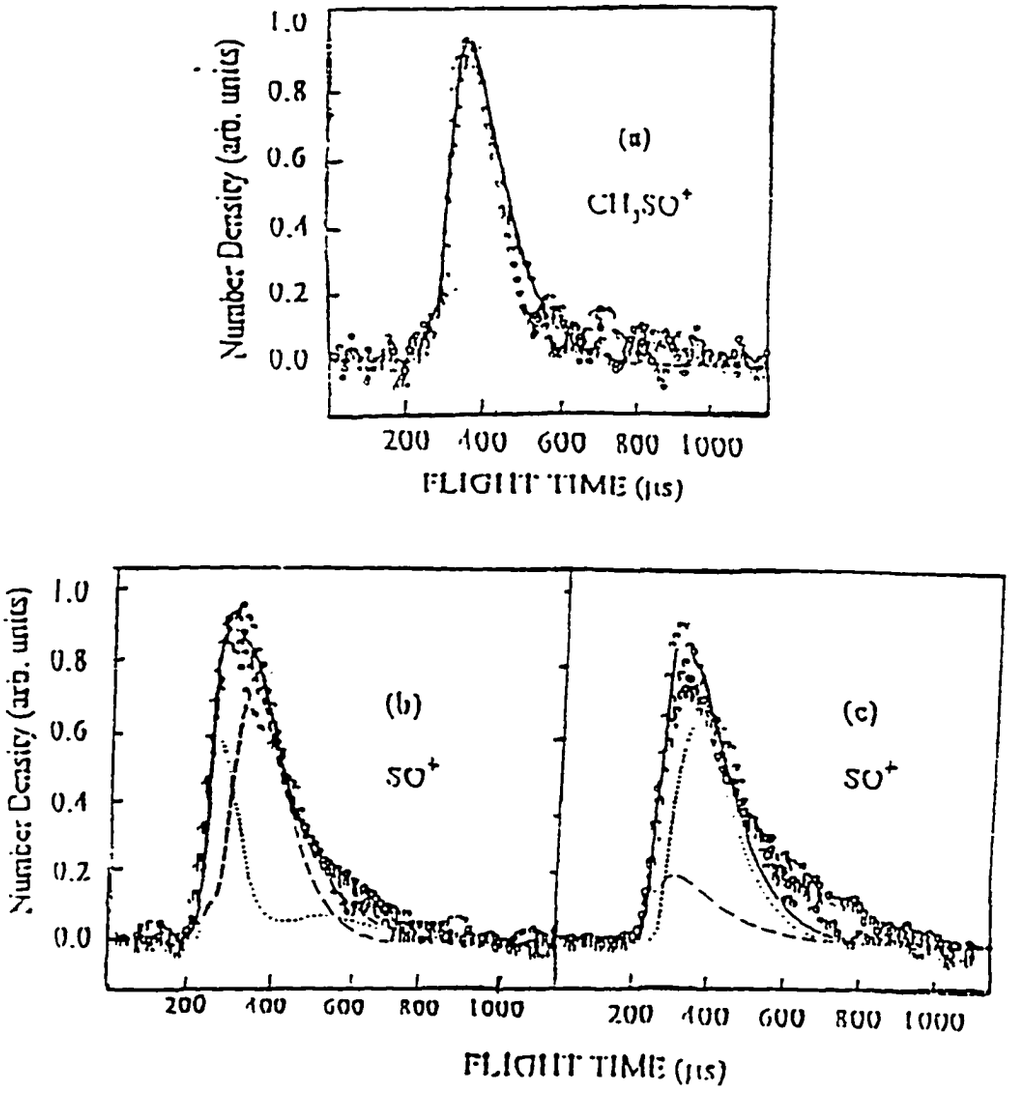

Figure 8. (a) The TOF spectra for CH_3SO (a) observed at θ_{lab}= 15° and ε = 0° and 90°. (b) The TOF spectra for SO observed at θ_{lab} = 15° and ε = 30°, 70°, 90°, 130°, and 170°. (c) The TOF spectra for SO observed at θ_{lab} = 30° and ε = 30°, 70°, 90°, 130°, and 170°. SO TOF spectra are shown for CH_3SO (- -) from process (1) and SO (···) from process (3). The sum of these contributions are shown as the solid line. v_o = 1.64×10^5 cm/s. α= 5.5×10^3 cm/s.

Conclusion

The product channels resulting from the 193.3 nm photofragmentation of $(CH_3)_2SO$ have been investigated by the molecular beam TOF mass spectrometric technique. The results of this experiment show that CH_3SO, CH_3 and SO are the dominant photoproducts. The $E_{c.m.}$ energy distribution for photofragments of process (1) is found to peak at $E_{c.m.} \approx 3$ kcal/mol, indicating that the CH_3SO and CH_3 are formed with considerable internal energies. The data analysis suggests that $\approx$ 53% of the CH_3SO radicals initially formed by process (1) undergo spontaneous dissociation to form CH_3 + SO, yielding a quantum yield of $\approx$ 1.53 for CH_3 formed in the 193 nm photodissociation of $(CH_3)_2SO$. Within the sensitivity of this experiment, photodissociation leading to the formation of CH_3SCH_3 + O is not found. The unfavorable production of $CH_3SCH_3 + O(^3P)$ is attributed to the violation of the spin conservation rule.

On the basis of the $E_{c.m.}$ threshold determined by the TOF spectrum of CH_3, we obtain a value of 53±2 kcal/mol for $D_o(CH_3SO\text{-}CH_3)$, in excellent agreement with the prediction at the G2(MP2) level of theory. This measurement yields a value of -14.8±2.0 kcal/mol for $D_fH°_0(CH_3SO)$.

The angular distribution measurements indicate that the photofragments of processes (1) have an isotropic distribution. This observation is consistent with a predissociation mechanism for photoexcited $(CH_3)_2SO$ with a lifetime longer than its rotation period.

References

(1) C.-W. Hsu, C.-L. Liao, Z.-X. Ma, and C. Y. Ng, *J. Phys. Chem.* **99**, 1760 (1995).

(2) C. E. M. Strauss and P. L. Houston, *J. Phys. Chem.* **94**, 8751 (1990).

(3) K. A. Trentelman, S. H. Kable, D. B. Moss, and P. L. Houston, *J. Chem. Phys.* **91**, 7498 (1989)

(4) S. W. North, D. A. Blank, J. D. Gezelter, C. A. Longfellow, and Y. T. Lee, *J. Chem. Phys.* **102**, 4447 (1995).

(5) S. K. Kim, S. Pederson, and A. H. Zewail, *J. Chem. Phys.* **103**, 477 (1995). We note that the experiments of Refs. 4 and 5 were conducted at different photodissociation energies. Thus, the excited dissociation states involved in the two experiments are also different.

(6) K. Gollnick and H. U. Stracke, *Pure Appl. Chem.* **33**, 217 (1973).

(7) K. Gollnick and H. U. Stracke, *Tetrahedron Lett.* 203 (1971).

(8) K. Gollnick and H. U. stracke, *Tetrahedron Lett.* 207 (1971).

(9) S. G. Lias, J. E. Bartmess, J. F. Liebman, J. L. Holmes, R. D. Levin, and W. G. Mallard, *J. Phys. Chem. Ref. Data*, **17** (1988), suppl. No. 1.

(10) X. Chen, F. Asmar, H. Wang, and B. R. Weiner, *J. Phys. Chem.* **95**,6415 (1991).

(11) X. Chen, H. wang, B. R. Weiner, M. Hawley, and H. H. Nelson, *J. Phys. Chem.* **97**, 12269 (1993).

(12) S. W. Benson, *Chem. Rev.* **78**, 23 (1978).

(13) L. A. Curtiss, K. Raghavachari, G. W. Trucks and J. A. Pople, *J. Chem. Phys.* **94**, 7221 (1991).

(14) L. A. Curtiss, K. Raghavachari and J. A. Pople, *J. Chem. Phys.* **98**, 1293 (1993).

(15) W.-B. Tzeng, H.-M. Yin, W.-Y. Leung, J.-Y. Luo, S. Nourbakhsh, G. D. Flesch, and C. Y. Ng, *J. Chem. Phys.* **88**, 1658 (1988)

(16) T. K. Minton, G. M. Nathanson, and Y. T. Lee, *J. Chem. Phys.* **86**, 1991 (1987).

(17) E. J. Hintsa, X. Zhao, and Y. T. Lee, *J. Chem. Phys.* **92**, 2280 (1990).

(18) X. Zhao, Ph.D. thesis, University of California, Berkeley, CA, 1988.

(19) M. J. Frisch *et al.*, *Gaussian 94* (Gaussian, Pittsburgh, PA 1994).

(20) S.-W. Chiu, W.-K. Li, W.-B. Tzeng, and C. Y. Ng, J. Chem. Phys. **97**, 6557 (1992).

(21) H. Bock and B. Solouki, *Angew. Chem.* **72**, 618 (1960).

(22) We found that when the temperature for the container of the dimethylsulfoxide sample was increased to ^{3} 350 K, a fast peak was observed in the TOF for CH_3. This fast peak is attributed to CH_3 formed by the 193 nm photodissociation of CH_3SCH_3, which is produced by pyrolytic processes in the sample container.

(23) H. Okabe, *Photochemistry of Small Molecules* (Wiley, New York, 1978).

(24) G. Hancock and K. R. Wilson, in Proceedings, *IVth International Symposium on Molecular Beams*, Cannes, France, 1973.

(25) L. D. Waits, R. J. Horwitz, and J. A. Guest, *Chem. Phys.* **155**, 149 (1991).

193 NM LASER PHOTOFRAGMENTATION TIME-OF-FLIGHT MASS SPECTROMETRIC STUDY OF $HSCH_2CH_2SH$

A paper submitted to the Journal of Chemical Physics

H.-Q. Zhao, Y.-S. Cheung, C.-X. Liao, and C. Y. Ng

Abstract

The kinetic energy release spectra for SH resulting from the 193 nm laser photofragmentation of $HSCH_2CH_2SH$ have been measured. On the basis of the observed maximum kinetic energy for the formation of HS + CH_2CH_2SH, a value of 74 ± 2 kcal/mol is derived for the bond dissociation energy of HS–CH_2CH_2SH at 0 K [D_0(HS–CH_2CH_2SH]. Angular distribution measurements for SH yield an anisotropic parameter β=-0.4 ± 0.1 for the HS + CH_2CH_2SH channel, indicating that the C–S bond fission is fast with respect to molecular rotation. The energetics for the formation of HS + CH_2CH_2SH from $HSCH_2CH_2SH$ have been investigated using the Gaussian–2 (G2) and G2(MP3) *ab initio* quantum chemical procedures. The G2/G2(MP3) calculations give a prediction of 72.5 kcal/mol for D_0(HS–CH_2CH_2SH), in excelient agreement with the experimental value. *Ab initio* first-order configuration interaction calculations have also been made to examine the possible excited state of $HSCH_2CH_2SH$ involved in the photodissociation process and to rationalize the observed angular distribution for the HS + CH_2CH_2SH channel.

Introduction

Volatile organosulfur molecules are produced as atmospheric pollutants by combustion of fossil fuels as well as by natural sources. [1-4] Radicals formed in the

atmospheric ultraviolet (UV) breakdown of organosulfur pollutants are intermediates in the atmospheric sulfur cycles and have the effect of accelerating the oxidation of organosulfur pollutants, leading to the formation of SO_2. [5-7] Acid rain results when sulfur–containing compounds, including SO_2, are removed from the atmosphere by rain or snow. Thus, laboratory UV laser photodissociation of volatile organosulfur species is relevant to the modeling of atmospheric sulfur chemistry cycles. In an effort to obtain energetic information and to identify the primary product channels resulting from the UV photolysis of organosulfur pollutants, we have performed UV laser photodissociation and photoionization studies of a series of volatile sulfur-containing species in recent years. [8-22]

These experimental studies indicate that the 193 (or 248) nm laser photodissociation of sulfur–containing hydrocarbons often involves prompt breakage of C–S and S–H bonds with little structural rearrangement. For example, CH_3S (CH_3CH_2S) is found to be the primary isomer formed in the 193 nm photodissociation of CH_3SH (CH_3CH_2SH) and CH_3SCH_3 ($CH_3CH_2SCH_2CH_3$). [10–13, 18, 21, 23–28] This observation is consistent with the interpretation that a repulsive excited electronic potential surface along the C–S (or S–H) coordinate is formed by direct photoexcitation and/or by rapid intramolecular access following photoexcitation, resulting in the prompt C–S (or S–H) bond scission. [23–26] On the basis of this understanding, along with the high dissociation cross sections, organosulfur compounds are excellent molecular precursors for the preparation of polyatomic radicals with a specific isomeric structure using the UV excimer laser photodissociation method.

In recent experiments, the energetics, such as ionization energies and heats of formation at 0 K ($\Delta_f H_0^\circ$'s), for two of the C_2H_5S isomers CH_3CH_2S and CH_3SCH_2, have been characterized. [18, 29] *Ab initio* calculations indicate that CH_2CH_2SH is also a stable isomer for C_2H_5S. The 193 nm laser photofragment time–of–flight (TOF) mass spectrometric experiment reported here is designed in part to measure the energetics of the CH_2CH_2SH radical, which is expected to be the primary product resulting from the C–S bond scission process,

$$HSCH_2CH_2SH + h\nu(193\ nm) \rightarrow HS + CH_2CH_2SH \qquad (1)$$

In addition to determining the bond dissociation energy at 0 K (D_0) for $HS–CH_2CH_2SH$, the kinetic energy release and the angular distribution of process (1) are obtained.

Since the $\Delta_f H_0^\circ$ values for CH_2CH_2SH and $HSCH_2CH_2SH$ are not known, we have performed *ab initio* quantum chemical calculations on these species at the Gaussian–2 (G2) level of theory. [30, 31] These calculations provide the important energetic information needed for the analysis of the TOF data obtained in this study. *Ab initio* first–order configuration interaction (FOCI) calculations [32] for several low lying excited electronic states of $HSCH_2CH_2SH$ also shed light on the mechanism of process (1).

Experimental and Theoretical Methods

A. Experiment

The rotatable beam source laser photofragmentation apparatus used in this study has been described in detail previously. [8-14] The apparatus consists of three main components; an ArF excimer laser, a photodissociation chamber in which a rotatable supersonic molecular beam intersects with the laser beam, and a linearly movable ultrahigh vacuum electron ionization quadrupole mass spectrometer.

A molecular beam of $HSCH_2CH_2SH$ was produced by supersonic expansion through a nozzle with a diameter of 0.125 nm. The beam has an angular divergence of $\approx 3°$, which is defined by the opening of the conical skimmer and by the circular aperture between the differential pumping chamber and the photodissociation chamber. The 3° angular spread of the beam gives a beamwidth of 3 mm in the photodissociation region. For the measurements at the laboratory angles (θ_{lab}) (defined by the direction of molecular beam with respect to the detector axis) of 30° and 45°, the ratio of the pressure of $HSCH_2CH_2SH$ to that of He was about 2%. The nozzle temperature (T_0) and the total stagnation pressure (P_0) were maintained at 333 K and 560 Torr, respectively. For the measurements at θ_{lab}=70° and 90°, the pressure ratio and T_0 were increased to 12% and 403K, respectively. We also obtained TOF spectra at θ_{lab}=70° and 5°(not shown here). At these θ values, the influence of clusters and dimmers cannot be avoided, even though P_0 was reduced to 150 Torr and T_0 was increased to 453K.

All TOF spectra were taken at a flight path of 65.5 cm, the distance between the photodissociation region and the electron impact ionizer. The ionization electron energy was 75 eV.

The energy of the excimer laser (Questek model 2460) used was varied in the range of 30-55 mJ. This energy range was used to minimize two-photon dissociation processes. The laser beam enters the photodissociation chamber through a MgF_2 focusing lens and is perpendicular to the seeded $HSCH_2CH_2SH$ beam.

The TOF spectra presented here were recorded on a multichannel scaler (Stanford Research model SRT430) with a channel width of 1.28 μs. The ion drift times though the quadrupole mass filter were determined to be 4.114 $m^{1/2}$, where m is the ion mass. The actual flight times of photofragments were corrected for the corresponding ion drift times. The velocity distribution of the parent $HSCH_2CH_2SH$ beam was determined by taking the laser hole burning spectra of $HSCH_2CH_2SH^+$ at $\theta=0^0$. The measured speed profile of species was then fitted to an assumed functional form, [8,33] $f(v)\sim v^2 \exp[-(v-v_0)^2/\alpha^2]$, where v_0 is the most probable speed and α is a measure of the width of the speed profile. For the $HSCH_2CH_2SH$ to He seeding ratio of 2%, T_0=333 K, and P_0=560 Torr, we found that $v_0=1.65 \times 10^5$ cm/s and $\alpha=0.65 \times 10^4$ cm/s, while $v_0=1.31 \times 10^5$ cm/s and $\alpha=0.65 \times 10^4$ cm/s for the $HSCH_2CH_2SH$ to He seeding ratio of 12%, T_0=403K, and P_0=560 Torr.

The analysis of the TOF data was performed by a forward simulation method.[34-36]. Briefly, the procedure began with a trial kinetic energy distribution $P(E_{c.m.})$, which was transformed to a TOF spectrum for comparison with the experimental TOF spectrum. Here, $E_{c.m.}$ represents the center-of-mass kinetic energy of the photofragments. The $p(E_{c.m.})$ distribution was adjusted until satisfactory agreement between the experimental and calculated TOF data was obtained. For the determination of the kinetic energy threshold for

process (1), the $P(E_{c.m.})$ distribution near the $E_{c.m.}$ onset was obtained by direct transformation [8] of the TOF data.

In the measurements of the angular distribution, the laser light was polarized by a stack of ten quartz plates set at the Brewster angle. The electric vector **E** of the polarized laser beam was set perpendicular to the detector and then rotated into the desired direction with a half-wave retarder. The laser energy was measured by a pyroelectric detector, and was kept at 10 mJ/pulse. The θ_{lab} value was set at 45° with respect to the detector axis, and the $HSCH_2CH_2SH$ to He seeding ratio was 9%, T_0=403 K, and P_0=360 Torr. In order to determine the angular distribution for process (1), the TOF spectrum for SH was recorded in the interval of $\varepsilon \approx 50°$ with each spectrum accumulated for a fixed number of laser shots. Here, ε is the angle between **E** and the direction of the molecular beam. The detector axis, the molecular beam axis, and **E** are in the same plane, which is perpendicular to the laser propagation direction.

B. *Ab initio* Calculations

The Gaussian-2 (G2) *ab initio* theoretical procedure has been described in detail by Curtiss et al. [30] Briefly, at the G2 level of theory, molecular structures are optimized with the Hartree–Fock (HF) approach and the second-order Møller-Plesset perturbation theory (MP2) with all electrons included using the 6-31G(d) basis set [i.e., at the HF/6-31G(d) and MP2(full)/6-31G(d) levels]. Harmonic vibrational frequencies are calculated at the HF/6-31G(d) geometry for stationary point characterization. All subsequent single-point calculations at higher levels involved are based on the MP2/6-31G(d) optimized structures.

Approximations of QCISD(T)/6-311 + G(3df, 2p) energies are obtained with frozen-core single-point calculations at the QCISD(T)/6-311G(d, p), MP4/6-311G(d, p), MP4/6-311 + G(d, p), MP4/6-311G(2df, p), and MP2/6-311 + G(3df, 2p) levels. A small semiempirical correction is applied to account for high level correction effects to obtain the total electronic energy (E_e). The HF/6-31G(d) harmonic vibrational frequencies, scaled by 0.8929, are used for zero-point vibrational energy (ZPVE) correction. The total energy at 0 K (E_0) is equal to E_e + ZPVE.

The G2(MP3) theory [31] is a variation of the G2 procedure in which all the MP4 single-point energies are replaced by the corresponding MP3 energies. The correction for high level correlation effects in the G2(MP3) theory is also slightly different from that in the G2 procedure. The G2(MP3) theory, which provides substantial savings in computational time and disk storage, has been tested on the same set of 125 systems used for validation of the G2 theory. The average absolute deviations of G2(MP3) theory from experiment are only ≤0.4 kcal/mol. In view of the large size of $HSCH_2CH_2SH$, the G2(MP3) method was used for this molecule and the G2 theory was used for the smaller CH_2CH_2SH molecule. All calculations were carried out on IBM RS6000-320h and RS6000/340 workstations or CRAY-YMP and CRAY-2 using the GAUSSIAN 90 and GAUSSIAN 92 package programs. [17]

For $HSCH_2CH_2SH$, a number of rotational isomers with different conformations were obtained. The most stable isomer of $HSCH_2CH_2SH$ at the MP2/6-31G(d) level has C_{2h} symmetry (Fig. 1). In order to study the HS-CH_2CH_2SH bond cleavage process, we also performed calculations on CH_2CH_2SH. At the MP2/6-31G(d) level, two isomers were

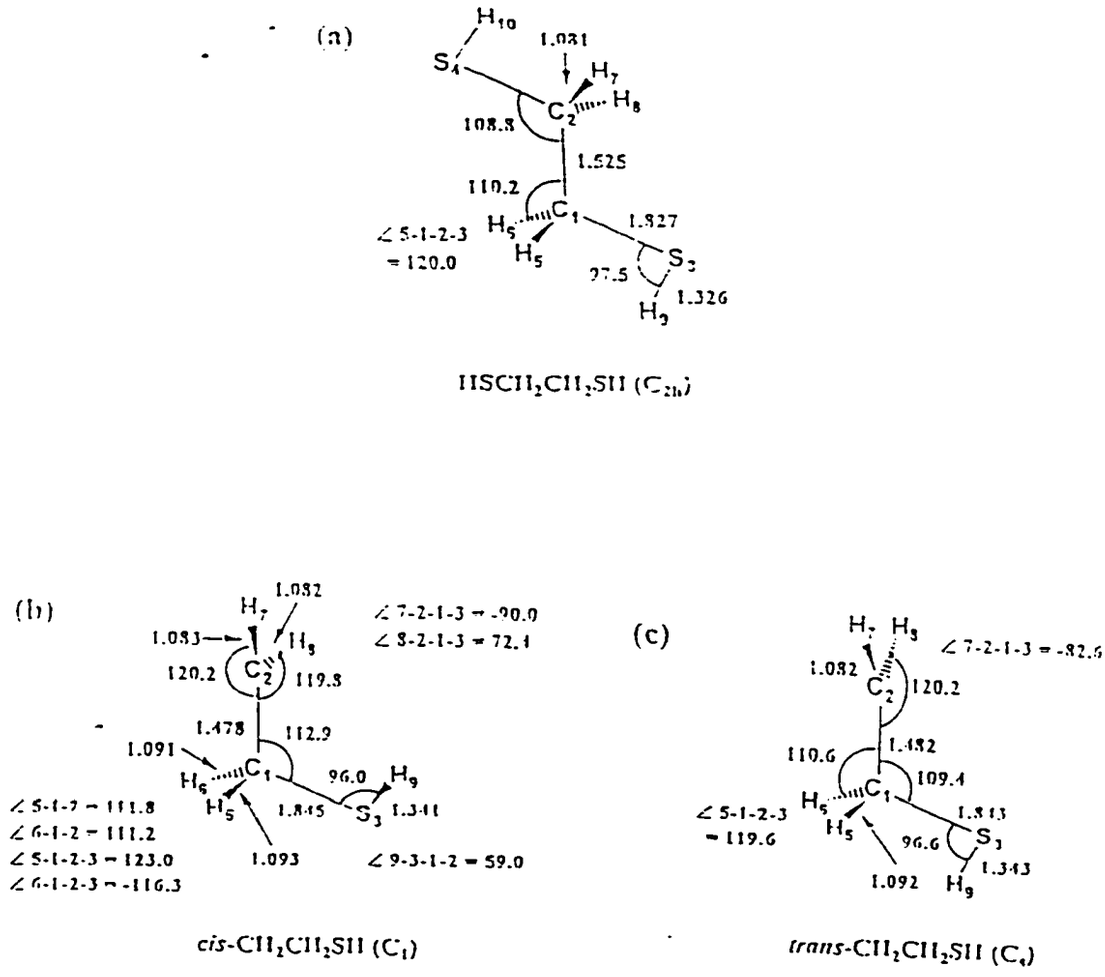

Figure 1. The structures of (a) $HSCH_2CH_2SH$ (C_{2h}), (b) *cis*-CH_2CH_2SH(C_1), and (c) *trans*-CH_2CH_2SH (C_s) optimized at the MP2/6-31G(d) level.

obtained for CH_2CH_2SH with Cs and C1 symmetries (Fig. 1). The $CH_2CH_2SH(C_1)$ structure is a *cis*-isomer with the H attached to S and the terminal CH_2 group in the *cis* positions, whereas the $CH_2CH_2SH(C_s)$ structure is the *trans*-isomer with the terminal H and CH_2 group in the *trans* positions [i.e. $\angle$H(9)-S(3)-C(1)-C(2)=180°]. We note that the structure for the -CH_2SH entity in $CH_2CH_2SH(C_s)$ and $HSCH_2CH_2SH$ are similar. The -CH_2SH entity in $CH_2CH_2SH(C_1)$ is also similar in geometry to that in the parent molecule $HCH_2CH_2SH(C_{2h})$ other than the difference in conformation. The $CH_2CH_2SH(C_1)$ isomer is more stable than the $CH_2CH_2SH(C_s)$ isomer by only 1.2 kcal/mol at the G2 level. Although the structure of -CH_2SH in *cis*- and *trans*-CH_2CH_2SH are similar to that in $HSCH_2CH_2SH(C_{2h})$, significant changes in geometry of the terminal methylene group in CH_2CH_2SH are observed . The $\angle$C(1)-C(2)-H(7) and $\angle$C(1)-C(2)-H(8) changes from 110.2° in $HSCH_2CH_2SH(C_{2h})$ to 120.2° and 119.8° in $CH_2CH_2SH(C_1)$, respectively. The $\angle$H(7)-C(2)-C(1)-S(8) in $HSCH_2CH_2SH(C_{2h})$ is 120.0° and becomes 162.4° in $CH_2CH_2SH(C_s)$. That is, the atoms C(1), C(2), H(7), and H(8) are almost coplanar, indicating that the hybridization of C(2) changes from sp^3 in $HSCH_2CH_2SH$ to sp^2 in CH_2CH_2SH, as expected for an alkyl radical.

The E_0 [G2(MP3)] and $\Delta_fH_0°$[G2(MP3)] values for $HSCH_2CH_2SH$ and E_0(G2) and $\Delta_fH_0°$(G2) values for SH, [30] CH_2CH_2, [30] CH_2SH, [38] and *cis*- and *trans*-CH_2CH_2SH are listed in Table I. The $\Delta_fH_0°$(G2) values are obtained using the experimental [39] $\Delta_fH_0°$ values of C (170 kcal/mol), H (51.6 kcal/mol), and S(65.6 kcal/mol) and E_0 (G2) (Ref. 24) values of C (-37.78432 hartree), H(-0.50000 hartree), and S (-397.65495 hartree). The

TABLE I. G2[or G2(MP3)] total energies(E_0) and $\Delta_fH_0°$ values for SH, C_2H_4, CH_2SH, C_2H_5S isomers, and $HSCH_2CH_2SH$.

Species	E_0[G2 or G2(MP3)][a]	$\Delta_fH_0°$[G2 or G2(MP3)][a, b] (kcal/mol)	$\Delta_fH_0°$(expt)[c] (kcal/mol)
$HSCH_2CH_2SH(C_{2h})$	-875.11395	3.4	...
cis-$CH_2CH_2SH(C_1)$	-476.71323	41.5	...
trans-$CH_2CH_2SH(C_s)$	-476.71304[d]	42.7	...
$CH_3CH_2S(C_s)$	-476.73761[d]	27.5[d]	31.4±2[e]
cis-$CH_3CHSH(C_1)$	-476.72512[d]	35.3[d]	...
trans-$CH_3CHSH(C_1)$	-476.72459[d]	35.6[d]	...
$CH_3SCH_2(C_1)$	-476.72189[d]	37.3d	34.8±2.5[f]
			35.2±1.6[g]
CH_2SH	-437.49655[h]	40.8[h]	37.7±2.0
CH_2CH_2	-78.41593[i]	14.7[i]	14.5±0.2
SH	-398.286[h]	34.4[h]	32.6±1.2

[a]All are G2 values except those for $HSCH_2CH_2SH$ are G2(MP3) values.
[b]Calculated using the experimental $\Delta_fH_0°$ values of C (170.0 kcal/mol), H(51.63 kcal/mol), and S(65.6±0.1 kcal/mol) from Ref. 39; E_0(G2) values of C(-37.78432 hartree), H(-0.50000 hartree) and S(-397.65495 hartree) from Ref. 30; and E_0[G2(MP3)] values of C(-37.78432 hartree), H(-0.50000 hartree) and S (-397.65326 hartree) from Ref. 31.
[c]Experimental $\Delta_fH_0°$ values. Unless specified, values are from Ref. 39.
[d]Reference 18.
[e]Reference 12.
[f]Reference 10.
[g]Reference 42.
[h]Reference 38.
[i]Reference 30.

$\Delta_f H_0°$[G2(MP3)] for $HSCH_2CH_2SH$ is calculated using the same experimental $\Delta_f H_0°$ for C, S, and H, the E_0[G2(MP3)] values for C, S, and H from Ref. 40 and for $HSCH_2CH_2SH$ obtained in this study. The theoretical and experimental results [10, 12, 18, 41] obtained recently for the energetics of other C_2H_5S isomers (CH_3CH_2S, CH_3SCH_2, and *cis/trans*-CH_3CHSH) are also included in the table.

To shed light on the excited potential energy surfaces responsible for process (1), we also calculated the vertical excitation energies for several low lying excited states of $HSCH_2CH_2SH$ based on the FOCI method. The 1s, 2s, and 2p orbitals for sulfur atoms and the 1s orbitals for carbon atoms were treated as core orbitals and were kept frozen in the FOCI calculations. In order to properly describe the possible diffuse nature of the excited orbitals of $HSCH_2CH_2SH$, we used for each of the sulfur and carbon atoms. All calculations on the excited states of $HSCH_2CH_2SH$ were performed on an IBM RS6000/340 workstation using the GAMESS program.[32]

The electronic configuration for the ground $HSCH_2CH_2SH$ (C_{2h}, $X\ ^1A_g$) state is $...(9b_u10a_g3b_g3a_u)^2(11a_g)^0$. The occupied molecular orbitals $9b_u$, $10a_g$, $3b_g$, and $3a_u$ are mainly contributed by the four lone-pairs(nonbonding orbitals) of the sulfur atoms, while the 6-31 + G(d, p) basis set, which includes a set of diffuse atomic orbitals the virtual molecular orbital $11a_g$ has appreciable antibonding character for the C-S bonds. The FOCI calculations indicate that the excited states with vertical excitation energies <8.5 eV are: 1 ^1A_u(5.9 eV), 1 ^1B_g(6.0 eV), 2 ^1B_g (6.8 eV), 2 ^1A_u(6.9 eV), 3 ^1B_g(8.1 eV), 3 ^1A_u(8.2 eV). 2

^1A_g(8.3 eV), and 1 ^1B_u(8.5 eV), where the values in parentheses are the corresponding vertical excitations from the ground X ^1A_g state.

Results and Discussion

On the basis of the previous 193 nm photodissociation study of CH_3CH_2SH,[12] the absorption of a 193 nm laser photon by $HSCH_2CH_2SH$ may induce the production of HS + CH_2CH_2SH [process (1)], H + SCH_2CH_2SH, and/or $2CH_2SH$. Other than the TOF signal for SH, we have also searched carefully the TOF spectra for CH_2CH_2SH, CH_2SH, CH_2, CH_2CH_2, and H at beam angles of 10°, 15°, 20°, and 30°. Within the sensitivity of this experiment, the spectra for these species are not observed. Thus, we conclude that HS + CH_2CH_2SH is overwhelmingly the major product channel. We note that the CH_3CH_2 + SH channel, which involves the C-S bond scission, is also the major product channel in the 193 nm photodissociation of CH_3CH_2SH. As is evidenced in the analysis given below, the electron impact ionization of CH_2CH_2SH produced in process (1) yields predominantly SH^+,

$$CH_2CH_2SH + e^- \rightarrow CH_2CH_2 + SH^+ + 2e^- \qquad (2)$$

Since the experimental $\Delta fH_0°$ values for both $HSCH_2CH_2SH$ and CH_2CH_2SH are not available, the D_0(HS-CH_2CH_2SH) is unknown. Table II compares the experimental 11, 12 and G2[or G2(MP3)] theoretical [38] D_0 values for the CH_3-SH, CH_3CH_2-SH, and HS-CH_2CH_2SH. The theoretical value for D_0(HS-CH_2CH_2SH) is calculated using the G2 values for $\Delta_fH_0°$(*cis*- and *trans*-CH_2CH_2SH) and $\Delta_fH_0°$(SH) and the G2(MP3) value for

TABLE II. Bond dissociation energies at 0 K (D_0) and the most probable c.m. kinetic [$(E_{c.m.})_{mp}$] and internal [$(E_{int})_{mp}$] energies of fragments formed in the 193 nm photolysis of CH_3SH, CH_3CH_2SH, and $HSCH_2CH_2SH$.

Process	D_0(theor)[a] (kcal/mol)	D_0(expt) (kcal/mol)	$\%(E_{c.m})_{mp}$	$\%(E_{int})_{mp}$
$CH_3SH + h\nu$ (193 nm) $\rightarrow CH_3 + SH$	73.0[b]	72.4±1.5[c]	70[c]	30[c]
			79d	21[d]
$CH_3CH_2SH+h\nu$(193 nm)$\rightarrow CH_3CH_2+SH$	...	72.3±1.5[e]	46[e]	54[e]
$HSCH_2CH_2SH+h\nu$(193 nm)$\rightarrow HS+CH_2CH_2SH$	72.5[f]	74±2	40	60
		73.7[g]		
$HSCH_2CH_2SH \rightarrow 2CH_2SH$	77.3	...	...	...
$CH_2CH_2SH \rightarrow CH_2CH_2 + SH$	7.6	...	...	...

[a]Values calculated using $\Delta_fH_0^\circ$(G2) and $\Delta_fH_0^\circ$[G2(MP3)] predictions given in Table I.
[b]Reference 38, [c]Reference 11, [d]Reference 23, [e]Reference 12.
[f]Value corresponds to the formation of *cis*-CH_2CH_2SH.
[g]Value corresponds to the formation of *trans*-CH_2CH_2SH.

$HSCH_2CH_2SH$. The G2 $D_0(HS\text{-}CH_2CH_2SH)$ values for the formation HS + *cis*-CH_2CH_2SH and HS + *trans*-CH_2CH_2SH are 72.5 and 73.7 kcal/mol, respectively. In view of the fact that $D_0(CH_3\text{-}SH)$=72.4±1.5 kcal/mol (Ref. 11) is essentially identical to $D_0(CH_3CH_2\text{-}SH)$=72.3±1.5 kcal/mol,[12] we expect that $D_0(HS\text{-}CH_2CH_2SH)$ has a value similar to those for $D_0(CH_3\text{-}SH)$ and $D_0(CH_3CH_2\text{-}SH)$, i.e., ≈72-73 kcal/mol. This, together with the excellent agreement observed between the experimental $D_0(CH_3\text{-}SH)$ and the G2 prediction lends support to the G2/G2(MP3) prediction of 72.5/73.7 kcal/mol for $D_0(HS\text{-}CH_2CH_2SH)$. Using the latter value, we have constructed the Newton diagram for process (1) as shown in Fig. 2, where v_0=1.65X10^5 cm/s, v_{lab} and $v_{c.m.}$ are the laboratory and center-of-mass velocities for the photofragments, and θ and $\theta_{c.m.}$ are the laboratory and center-of-mass angles, defined by the angles between the detector and molecular beam axis and between $v_{c.m.}$ and the detector axis, respectively. The circles defined by $v_{c.m.}$(SH) and $v_{c.m.}(CH_2CH_2SH)$ are the maximum $v_{c.m.}$'s for SH and CH_2CH_2SH produced by process (1). Also shown in Fig. 2 are γ and ε, which are defined as the angles between the laser electric field **E** and $v_{c.m.}$ and between **E** and the detector axis, respectively.

The TOF spectra for HS obtained at θ_{lab}=30°, 45°, 70°, and 90° are depicted in Figs. 3(a), 3(b), 3(c), and 3(d), respectively. Although we conclude that the production of $2CH_2SH$ and H + SCH_2CH_2SH from the 193 nm photodissociation of $HSCH_2CH_2SH$ is negligible, we cannot completely exclude the formation of these channels. The D_0 value for a S-H bond (≈86 kcal/mol) (Refs. 12, 26, 28, 41) is significantly higher than that for a C-S

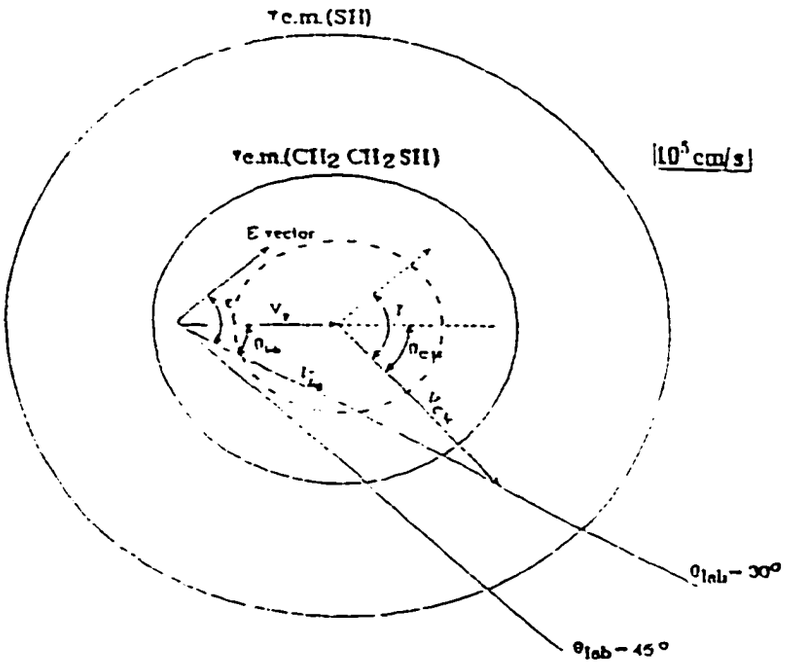

Figure 2. Kinematics for the formation of $HSCH_2CH_2$ + SH by the 193 nm photodissociation of $HSCH_2CH_2SH$. v_0(=1.65 X 10^5 cm/s) is the laboratory velocity for $HSCH_2CH_2SH$. $v_{c.m}$(SH) and $v_{c.m}$(CH_2CH_2SH) are the maximum c.m. velocities for SH and CH_2CH_2SH, respectively. The dashed circle define the maximum velocity for SH formed in the secondary dissociation of excited CH_2CH_2SH formed originally by process (1). The diagram shows the relationship $\gamma=\theta_{c.m} + \varepsilon - \theta_{lab}$, where γ is the angle between the laser electric field (E) and the c.m. photofragment velocity; $\theta_{c.m}$ is the angle between the molecular beam velocity and the fragment recoil c.m. velocity; ε is the angle between E and detector axis; and θ is the laboratory angle between the molecular beam and the detector axis.

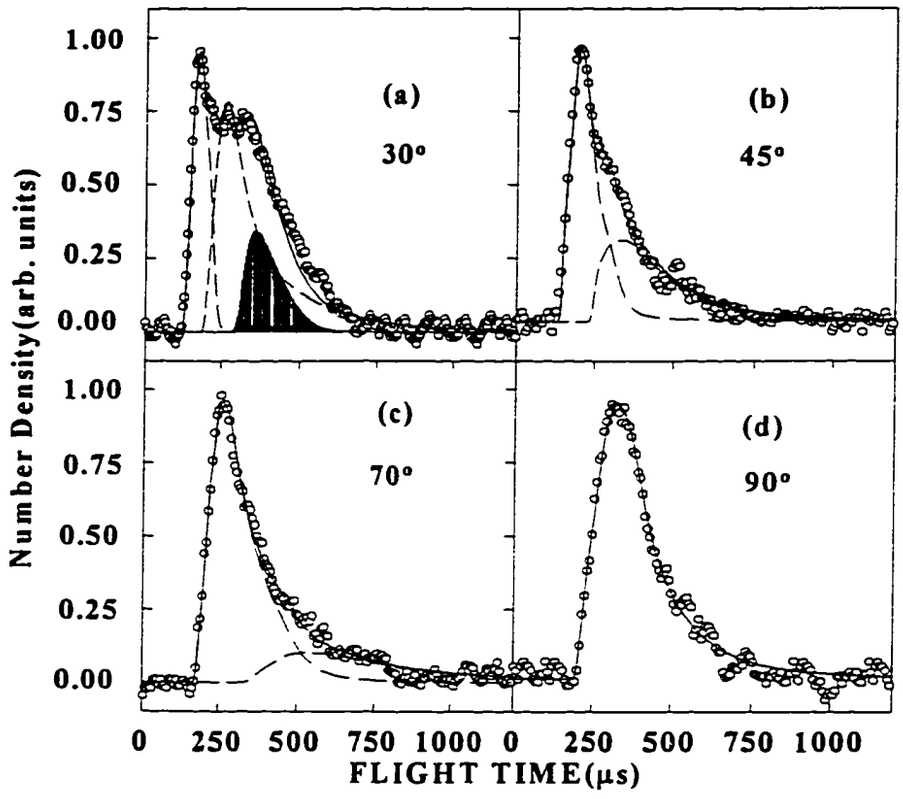

Figure 3. TOF spectra for SH measured at θ_{lab}=(a) 30°, (b)45°, (c)70°, and (d) 90°. The dashed and dotted lines show the best fits due to SH and CH_2CH_2SH, respectively, formed by process(1). The shaded peak is attributed to the secondary dissociation of internally excited $CH_2CH_2SH \rightarrow CH_2CH_2 + SH$. The solid line is the sum of all these contributions.

bond. The G2 calculations show that $D_0(HSCH_2\text{-}CH_2SH)$=77.3 kcal/mol is also higher than $D_0(HS\text{-}CH_2CH_2SH)$ by 4 kcal/mol. Even if the formation of the 2 CH_2SH and H + SCH_2CH_2SH channels is finite, the SH^+ signals due to electron impact ionization of CH_2SH and SCH_2CH_2SH would not affect the onset of process (1). Thus, the $E_{c.m.}$ threshold for process (1) can be determined by direct transformation of TOF data near the onset of the spectra shown in Figs. 3(a)-3(d) into $E_{c.m.}$ distributions, i.e., $P(E_{c.m.})$. This transformation reveals a relatively sharp onset at $E_{c.m}$=75 ± 1.5 kcal/mol for process (1). By energy conservation, we have the relationship

$$E(h\nu) + E_{int}(HSCH_2CH_2SH) = D_0(HS\text{-}CH_2CH_2SH) + E_{c.m.} + E_{int}(SH) + E_{int}(CH_2CH_2SH) \quad (3)$$

where E(hν=193.3 nm)= 147.9 kcal is the photon energy and $E_{int}(HSCH_2CH_2SH)$, $E_{int}(SH)$, and $E_{int}(CH_2CH_2SH)$ represent the respective internal energies for $HSCH_2CH_2SH$, SH, and CH_2CH_2SH. Assuming that $E_{int}(HSCH_2CH_2SH)$ is negligible because of the supersonic expansion, and that photofragments (HS + CH_2CH_2SH) formed at $E_{c.m.}$ threshold of 75 kcal/mol contain no internal energies, $D_0(HS\text{-}CH_2CH_2SH)$ is calculated to be 72.9 ± 1.5 kcal/mol. Under the supersonic expansion conditions used in this experiment, the rotational relaxation for $HSCH_2CH_2SH$ is expected to be efficient. However, the vibrational relaxation for $HSCH_2CH_2SH$ is most likely incomplete. Using the calculated HF/6-31G(d) vibrational frequencies for $HSCH_2CH_2SH$, we estimate that the vibrational energy for $HSCH_2CH_2SH$ is ≈2.8 kcal/mol at 330 K. The vibrational excitation

of $HSCH_2CH_2SH$ has the effect of shifting the onset to higher $E_{c.m.}$, which in turn yields a lower value for $D_0(HS\text{-}CH_2CH_2SH)$. Without detailed experimental characterization of the $HSCH_2CH_2SH$ beam, we assume that $HSCH_2CH_2SH$ is cooled to a vibrational temperature of ≈150 K after the supersonic expansion. To take into account this possible vibrational hot band effect, we recommend a value of 74 ± 2 kcal/mol for $D_0(HS\text{-}CH_2CH_2SH)$. As expected, this latter value is close to the experimental D_0 values for CH_3-SH and CH_3CH_2-SH and is in good agreement with the theoretical prediction of 72.5 kcal/mol (see Table II).

In a previous G2 study of the C_2H_5S isomers, CH_3CH_2S, *cis*-CH_3CHSH, *trans*-CH_3CHSH, and CH_3SCH_2 were found to be stable with Δ_fH_0 values of 27.5, 35.3, 35.6, and 37.3 kcal/mol, respectively.[18] The G2 calculations indicates that these isomers are more stable than *cis*- and *trans*-CH_2CH_2SH, which have the respective $\Delta_fH_0°$(G2) values for CH_3CH_2S (31.4±2 kcal/mol) (Ref. 12) and CH_3SCH_2 (34.8±2.5 kcal/mol) (Ref. 10) determined in 193 nm laser photofragmentation TOF mass spectrometric experiments are in reasonable agreement with the corresponding G2 predictions. A value of 35.2 ±1.6 kcal/mol for $\Delta_fH_0°(CH_3SCH_2)$ has also been obtained in a recent kinetic study. [42] These values are included in Table II for comparison with the G2 $\Delta_fH_0°(CH_2CH_2SH)$ value. However, an experimental value for $\Delta_fH_0°(CH_2CH_2SH)$ cannot be obtained because the experimental $\Delta_fH_0°(HSCH_2CH_2SH)$ is unknown. The fact that the experimental and G2/G2(MP3) theoretical $D_0(HS\text{-}CH_2CH_2SH)$ are in agreement supports the conclusion that the C_2H_5S radical formed in the 193 nm photodissociation of $HSCH_2CH_2SH$ has the

CH_2CH_2SH structure. This conclusion is consistent with the previous observation that breakage of the C–S bonds in CH_3SCH_3,[12] $CH_3CH_2SCH_2CH_3$,[18] and CH_3SSCH_3 (Ref. 9) induced by the absorption of a 193 nm photon are prompt, yielding the photoproduct without atomic rearrangement, i.e., forming $CH_3S + CH_3$, $CH_3CH_2S + CH_2CH_3$, and $CH_3 + SSCH_3$, respectively.

The TOF spectrum for SH observed at 30° reveals three peaks[Fig. 3(a)]. The fastest and most intense peak is attributable to SH formed by process (1) (dashed curve), while the second peak can be fitted by the corresponding fragment CH_2CH_2SH (dotted curve). That is, the SH^+ signal observed for the second peak is formed by the electron impact dissociative ionization process (2). The shaded peak can accounted for by the secondary dissociation of internally excited CH_2CH_2SH. Using the G2 values of $\Delta_fH_0°(CH_2CH_2)$=14.7 kcal/mol and $\Delta_fH_0°(SH)$=34.4 kcal/mol and the G2(MP3) $\Delta_fH_0°$(*cis*-CH_2CH_2SH)=41.5 kcal/mol obtained here, the dissociation process,

$$CH_2CH_2SH \rightarrow CH_2CH_2 + SH \qquad (4)$$

is predicted to be endothermic by only 7.6 kcal/mol. The maximum velocity for SH formed by process (4) is also shown by the dashed circle in the Newton diagram of Fig. 2. Due to the kinematic constraints of the primary CH_2CH_2SH radicals, the TOF distribution for the secondary SH radicals is slow and broad, as shown by the shaded curve in Fig. 3(a). The $P(E_{c.m.})$ of the secondary dissociation process (4) is found to decrease nearly exponentially

toward higher $E_{c.m.}$ (low internal excitation), in accordance with that expected for a statistical unimolecular dissociation process.[33] The contributions to the TOF spectra observed at θ_{lab} =45°, 70°, and 90° due to the secondary dissociation of CH_2CH_2SH[process(3)] are negligible.

The $P(E_{c.m.})$ for process (1) shown in Fig. 4 represents the best fit of the TOF spectra for SH observed at θ_{lab}=30°, 45°, 70°, and 90°. This $P(E_{c.m.})$ of process (1) has a maximum at $E_{c.m.}$ ≈30 kcal/mol. Due to the kinematic constraint, the $P(E_{c.m.})$ at $E_{c.m.}$< 9 kcal/mol cannot be probed at θ_{lab} ≥30°. The $P(E_{c.m.})$ of Fig. 3(b) is zero at $E_{c.m.}$< 10 kcal/mol. However, this portion of the $P(E_{c.m.})$ has no effect on the fit of the TOF spectra measured at θ >30°. It is most likely that the $P(E_{c.m.})$ at $E_{c.m.}$<10 kcal/mol is small, but finite.

The formation of CH_2CH_2SH in the 193 nm photodissociation of $HSCH_2CH_2SH$ observed here is consistent with the conclusion that the dissociation involves a repulsive potential surface associated with the C-S bond, which is formed by direct photoexcitation and/or by rapid intramolecular access followed by photoexcitation. The $P(E_{c.m.})$ for process (1) is similar to that observed for the formation of CH_3CH_2 + SH in the 193 nm photodissociation of CH_3CH_2SH. The prompt dissociation from a repulsive surface would not allow atomic rearrangement of the photofragments. Since photoexcitation involves a vertical transition, the initial geometry formed on the excited surface should be similar to the $HSCH_2CH_2SH$ (C_{2h}) structure. The similarity of the structure for CH_2CH_2SH, especially for *trans*-CH_2CH_2SH, to that of $HSCH_2CH_2SH$(Fig. 1) is consistent with the prompt C-S bond cleavage mechanism. The main relaxation step to produce the stable

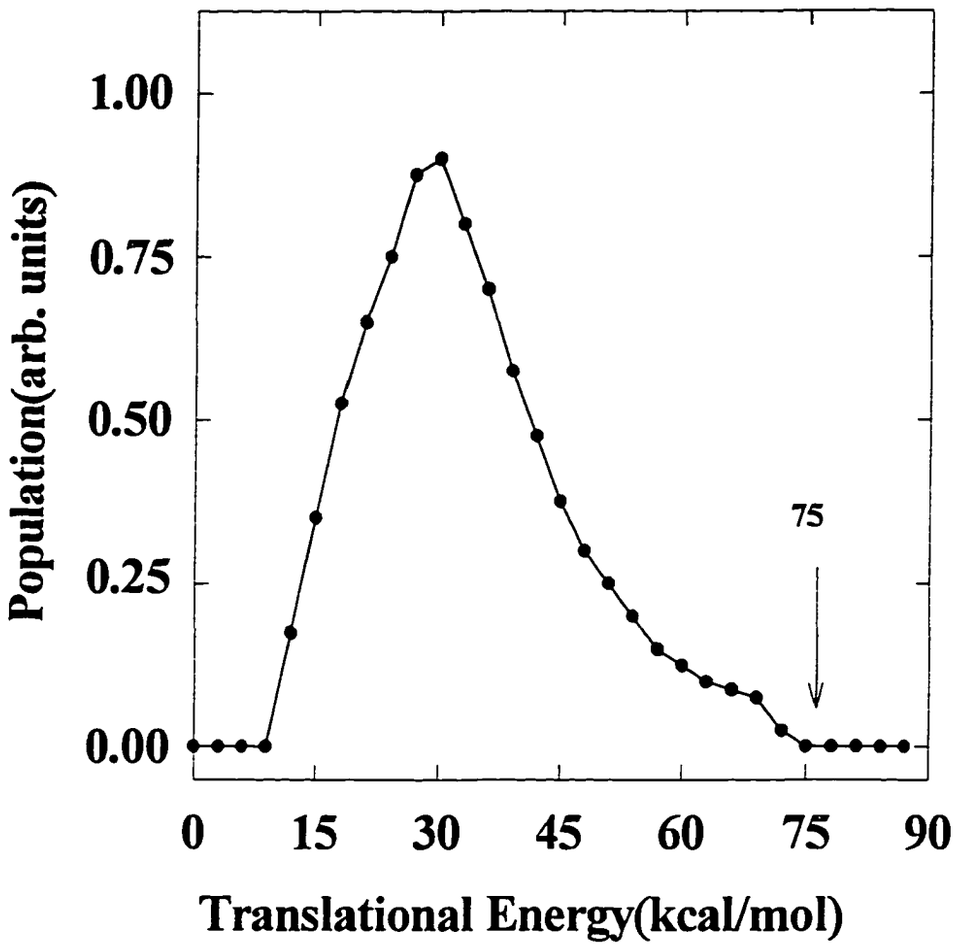

Figure 4. The $P(E_{c.m})$ distribution obtained by the forward simulation procedure, which gives the best fit for all the TOF spectra of Fig. 3.

CH_2CH_2SH radical followed by the C-S bond cleavage involves the rehybridization of the terminal carbon atom from sp^3 to sp^2.

Considering the photon energy of 6.43 eV(193 nm) used in this experiment and the accuracy (≈0.5 eV) of the FOCI calculations, the possible excited states involved in process (1) are $1\,^1A_u$, $1\,^1B_g$, and $2\,^1B_g$ with vertical excitation energies of 5.9, 6.0, and 6.8 eV, respectively. However, the transitions $X\,^1A_g \rightarrow 1\,^1B_g$ and $X\,^1A_g \rightarrow 2\,^1B_g$ are dipoleforbidden processes. Thus, the $1\,^1A_g$ state is mostly likely the excited state responsible for the 193 nm photodissociation of $HSCH_2CH_2SH$. Since the major electronic configuration for the $HSCH_2CH_2SH(1\,^1A_u)$ is $...(9b_u10a_g3b_g)^2(3a_u1a_g)^1$, the $X\,^1A_g \rightarrow 1\,^1A_u$ transition corresponds to a $n \rightarrow \sigma^*$ transition, and the potential energy surface is probably repulsive along the stretching of the C-S bond, leading to prompt C-S bond cleavage. This is consistent with the conclusion inferred from the experimental observation. We note that the $1\,^1A_u$ state may interact with other excited states with the same symmetry, such as $2\,^1A_u$, along the dissociation coordinates, Such an interaction which results in an avoided crossing has been found in the theoretical studies of other organosulfur systems. [24, 25, 43]

Since the ∠(H-S-C) in $HSCH_2CH_2SH$ is predicted to be 97.5°, the SH fragments produced by process (1) are expected to be in high rotationally excited states. The accompanying CH_2CH_2SH fragment should be excited rotationally as well as vibrationally. As shown in the $P(E_{c.m})$ of Fig. 4, the most probable $E_{c.m}$ $[(E_{c.m})_{mp}]$ for the formation of SH + CH_2CH_2SH is ≈30 kcal/mol, which is ≈40% of the available energy of 74 kcal/mol. The corresponding most probable internal excitation$[(E_{int})_{mp}]$ for the photoproducts is ≈44

kcal/mol (≈60% of the available energy). Table II compares the partitions of $(E_{c.m})_{mp}$ and $(E_{int})_{mp}$ for the C-S scission process observed in the 193 nm photodissociation of CH_3SH, [11, 23] CH_3CH_2SH, [12] and $HSCH_2CH_2SH$. The trend of increasing $(E_{int})_{mp}$ observed as the precursor molecule is changed from CH_3SH to CH_3CH_2SH to $HSCH_2CH_2SH$ can simply be attributed to the increasing complexity of the molecule with greater internal degrees of freedom.

The angular distribution of the photofragments has the form [44]

$$P(\gamma)=(1/4\pi)[1 + \beta P_2(\cos\gamma)] \quad (5)$$

where $P_2(\cos\gamma)$ is the second Legendre polynomial and β is the anisotropy parameter. Figure 5 shows the angular distribution for process (1) obtained by integration of the contribution of SH formed by process (1) to the measured TOF spectra at $\theta_{lab}=45°$. The fitting (solid curve) of the measured (solid dots) angular distribution using Eq. (5) yields $\beta=-0.4\pm0.1$ for process (1). For an instaneous photodissociation process whose kinetic energy of dissociation is very large compared to the energy of rotation, β can be expressed by the simple equation, $\beta=3\cos^2\vartheta - 1$, [44] where ϑ is the angle between the recoil velocity of the fragment and the transition dipole moment. Hence, in the case of $\beta=-0.4$, ϑ corresponds to 63.4°.

The observed β value and $P(\gamma)$ can be rationalized by symmetry arguments and results of the FOCI calculations. When the z-axis is taken as the molecular twofold axis in the C_{2h} point group, the x-, y-, and z-axes transform as the B_u, B_u, and A_u irreducible representations, respectively. Hence, the x- and y-components of the $X\ ^1A_g \rightarrow 1\ ^1A_u$

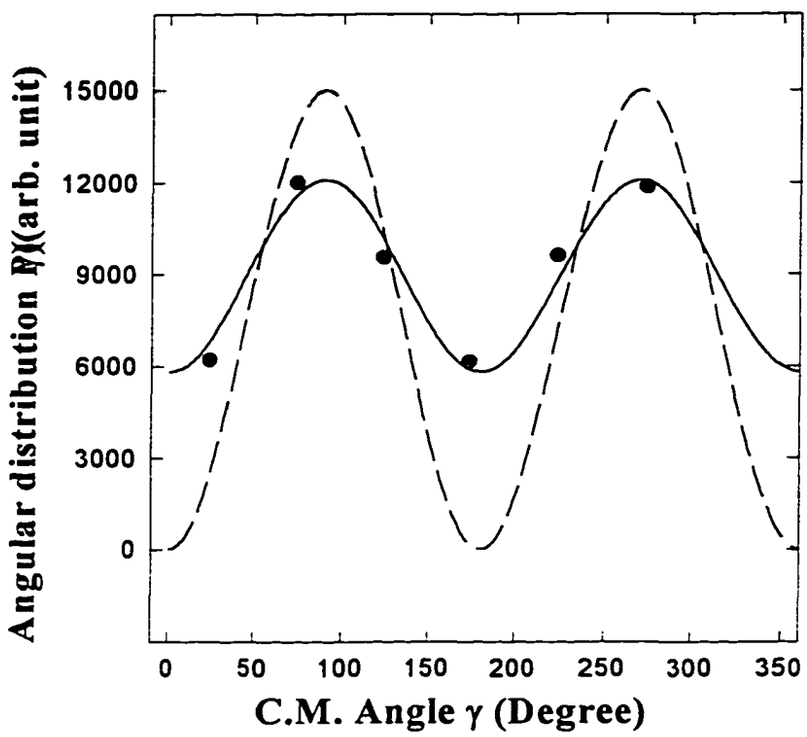

Figure 5. Angular distribution. P(γ), for channel (1) measured at θ_{lab}=45°. The solid dots are experimental results and the solid curve represents the best fit using Eq. (4) with β=-0.4±0.1. γ is the angle between the laser electric field (**E**) and the c.m. fragment velocity. The dotted curve corresponds to β=-1 for an instantaneous photodissociation process (see the text).

transition moment vanish. That is, the transition moment for the $X\ ^1A_g \rightarrow 1\ ^1A_u$ excitation must coincide with the z-axis. Since the carbon and sulfur atoms of $HSCH_2CH_2SH$ lie on the σ_h-plane, the transition moment for the $X\ ^1A_g \rightarrow 1\ ^1A_u$ excitation is perpendicular to the C-S bonds. For an instantaneous photodissociation process, we expect $\gamma=90^\circ$ and $\beta=-1$. The angular distribution for $\beta=-1$ is shown as the dotted curve in Fig. 5. The less anisotropic distribution measured experimentally could result from either moderate rotational smearing or a distortion of the molecular frame in the excited state. Furthermore, the finite involvement of less stable conformers of both $HSCH_2CH_2SH$ and CH_2CH_2SH in the photodissociation process may also contribute to the less anisotropic angular distribution for process (1) observed in this experiment. Nevertheless, we may conclude that the experimental β value of -0.4 for process (1) is in qualitative agreement with the prediction of FOCI calculations and symmetry arguments that the C-S bond scission in the 193 nm photodissociation of $HSCH_2CH_2SH$ is fast compared to molecular rotation.

Conclusion

The product channels resulting from the 193 nm photofragmentation of $HSCH_2CH_2SH$ have been investigated by the TOF mass spectrometric technique. Similar to the observation of the 193 nm photofragmentation of CH_3CH_2SH, the C-S scission to yield SH + CH_2CH_2SH constitutes the overwhelmingly dominant product channel. Within the sensitivity of the present experiment, the formation of H + SCH_2CH_2SH and $2CH_2SH$ are not found, indicating that the dissociation channels involving S-H and C-C bond cleavages are not important. On the basis of the $E_{c.m}$ threshold for the $P(E_{c.m})$ distribution

of process(1), we obtain a value of 74±2 kcal/mol for D_0(HS-CH_2CH_2SH). The translational energy distribution for photofragments of channel (1) is found to peak at $E_{c.m}$ ≈30 kcal/mol. The D_0 values for HS-CH_2CH_2SH, CH_3-SH, and CH_3CH_2-SH are identical within the experimental uncertainties. This observation is consistent with the interpretation that the σ-bonding involved in the C-S bonds of these molecules is localized. The angular distribution measurements of SH gives β=-0.4±0.1 for process (1), indicating that the C-S bond fission is fast with respect to molecular rotation.

The structure and energetics for CH_2CH_2SH and $HSCH_2CH_2SH$ have been investigated at G2/G2(MP3) level of theory. The predictions for D_0(HS-CH_2CH_2SH)=72.5/73.7 kcal/mol are in excellent agreement with the experimental result. This observation supports that the C_2H_5S isomer formed in the 193 nm photodissociation of $HSCH_2CH_2SH$ has the CH_2CH_2SH structure.

The FOCI calculations suggest that an $n \rightarrow \sigma^*$ transition is involved for process (1), resulting in a repulsive surface ($1\ ^1A_u$) with mostly antibonding character for the C-S bonds. Furthermore, the transition moment for the $X\ ^1A_g \rightarrow 1\ ^1A_u$ excitation is perpendicular to the C-S bonds, resulting in anisotropic angular distribution in qualitative agreement with experimental observation.

References

(1) T. E. Graedel, Rev. Geophys., *Space Phys.* **15**, 421(1977).

(2) S. W. Benson, *Chem. Rev.* **78**, 23(1978).

(3) W. E. Burnett, Environ. *Sci. Technol.* **8**, 744(1969).

(4) M. D. Bentley, I. B. Douglass, J. A. Lacadie, and D. R. Whittier, J. *Air Pollution Control Assoc.* **22**, 744(1969).

(5) J. G. Calvert and J. N. Pitts, Jr. Photochemistry (Wiley, New York, 1966).

(6) S. D. Thompson, D. G. Carroll, F. Watson, M. O'Donnell, and S.P.McGlynn, *J. Chem. Phys.* **45**, 1367(1966).

(7) P. M. Rao and A. R. Knight, *Can. J. Chem.* **46**, 2462 (1968).

(8) W.-B. Tzeng, H.-M. Yin, W.-Y Leung, J.-Y. Luo, S.Nourbakhsh, G. D. Flesch, and C. Y. Ng, *J. Chem. Phys.* **88**, 1658(1988).

(9) S. Nourbakhsh, C.-L. Liao, and C. Y. Ng, *J. Chem. Phys.* **92**, 6587(1990).

(10) S. Nourbakhsh, K. Norwood, H.-M. Yin, C.-L Liao, and C.Y. Ng, *J. Chem. Phys.* **95**, 5014(1991).

(11) S. Nourbakhsh, K. Norwood, H.-M. Yin, C.-L. Liao, and C. Y. Ng, *J. Chem. Phys.* **95**, 946(1991).

(12) S. Nourbakhsh, H.-M. Yin, C.-L. Liao, and C. Y. Ng, *Chem. Phys. Lett.* **183**, 348(1991).

(13) S. Nourbakhsh, K. Norwood, G.-Z. He, and C. Y. Ng, *J. Am. Chem. Soc.* **113**, 6311(1991).

(14) S. Nourbakhsh, H.-M. Yin, C.-L. Liao, and C. Y. Ng, *Chem. Phys. Lett.* **190**, 469(1992).

(15) K. Norwood, S. Nourbakhsh, G.-Z. He, and C. Y. Ng, *Chem. Phys. Lett.* **184**, 147(1991).

(16) C.-W Hsu, C.-L Liao, Z.-X. Ma, P. J. H. Tjossem, and C. Y. Ng, *J. Chem. Phys.* **97**, 6283(1992).

(17) C.-W. Hsu, C.-L. Liao, Z.-X. Ma, P. J. H. Tjossem, and C. Y. Ng, *Chem. Phys. Lett.* **199**, 78(1992).

(18) Z.-X. Ma, C.-L. Liao, H.-M. Yin, C. Y. Ng, S.-W. Chiu, I. Ma, and W.-K. Li, *Chem. Phys. Lett.* **213**, 250(1993).

(19) Z.-X. Ma, C.-L. Liao, C. Y. Ng, Y.-S. Cheung, W.-K. Li, and T. Baer, *J. Chem. Phys.* **100**, 4780(1994).

(20) C.-W. Hsu, D.P. Baldwin, C.-L. Liao, and C.Y. Ng, *J. Chem. Phys.* **100**, 8047(1994).

(21) C.W. Hsu and C. Y. Ng, *J. Chem. Phys.* **101**, 5596(1994).

(22) C.-W. Hsu, C.-L. Liao, Z.-X. Ma, and C.Y. Ng, *J. Phys. Chem.* **99**, 1760(1995).

(23) J.S.Keller, P. W. Kash, E. Jensen, and J. L. Butler, *J. Chem. Phys.* **96**, 4324(1992).

(24) E. Jensen, J. S. Keller, G.C.G. Waschewsky, J. E. Stevens, R. L. Graham, K. F. Freed, and L. J. Butler, *J. Chem. Phys.* **98**, 2882(1993).

(25) J. E. Steven, H. W. Jang, L. J. Butler, and J. C. Light, *J. Chem. Phys.* **102**, 7059(1995).

(26) J. Segall, Y. Wen, R. Singer, M. Dulligan, and C. Wittig, *J. Chem. Phys.* **99**, 6600(1993).

(27) S. H. S. Wilson, M. N. R. Ashfold, and R. N. Dixson, *Chem. Phys. Lett.* **222**, 457(1994).

(28) S. H. S. Wilson, M. N. R. Ashold, and R. N. Dixon, *J. Chem. Phys.* **101**, 7538(1994).

(29) J. Baker and J. M. Dyke, *Chem. Phys. Lett.* **213**, 257(1993).

(30) L. A. Curtiss, K. Raghavachari, G. W. Trucks, and J. A. Pople, *J. Chem. Phys.* **94**, 7221(1991).

(31) L. A. Curtiss, K. Raghavachari, and J. A. Pople, *J. Chem. Phys.* **98**, 1293(1993).

(32) M. W. Schmidt, K. K. Baldridge, J. A. Boatz, J. H. Jensen, S. Koseki, M. S. Gordon, K. A. Nguyen, T. L. Windus, and T. S. Elbert, *QCPE Bull*, **10**, 52(1990).

(33) T. K. Minton, G. M. Nathanson, and Y.T. Lee, *J. Chem. Phys.* **86**, 1991(1987).

(34) E. J. Hintsa, X. Zhao, and Y. T. Lee, *J. Chem. Phys.* **92**, 2280(1990).

(35) X. Zhao, Ph.D. thesis, University of California, Berkeley, CA, 1988.

(36) L. J. Butler, E. J. Hintsa, S. F. Shane, and Y. T. Lee, *J. Chem. Phys.* **86**, 2051(1987).

(37) M. J. Frisch et al., GAUSSIAN 90, Gaussian, Pittsburgh, Pennsylvania, 1990; M. J. Frisch et. al. GAUSSIAN 92, Revision C, Gaussian, Pittsburgh, Pennsylvania. 1992.

(38) S.-W. Chiu, W.-K Li, W.-B. Tzeng, and C. Y. Ng, *J. Chem. Phys.* **97**, 6557(1992).

(39) S. G. Lias, J. E. Bartmess, J. F. Liebman, J.L. Holmes, R. D. Levin, and W. G. Mallard. *J. Phys. Chem*. Ref. Data 17, Suppl. No. 1(1988).

(40) L. A. Curtiss, K. Raghavchari, and J. A. Pople, *J. Chem. Phys.* **93**, 2537(1990).

(41) J. M. Nichovich, K. D. Kreutter, C. A. can Dijk, and P. H. Wine, *J. Phys. Chem*. **96** 2518(1992).

(42) P. H. Wine(private communication).

(43) C.-W-Hsu, C.-L. Liao, Z.-X. Ma, and C.Y. Ng, *J. Phys. Chem*. **99**, 1760(1995).

(44) S.-C. Yang and R. Bersohn, *J. Chem. Phys.* **61**, 4400(1974).

THIOPHENE BIRADICAL DECAY OF THE PRIMARY LASER PHOTOFRAGMENTATION PRODUCT AT 193 NM

A paper to be submitted to the Journal of Chemical Physics

H.-Q. Zhao and C. Y. Ng

Abstract

Thiophene biradical decay dynamics as the primary laser photofragmentation product at 193 nm has been studied. Five product processes are identified as follows:

$$C_4H_4S(\text{Thiophene}) \rightarrow HC{\equiv}CH + C_2H_2S \quad (1)$$

$$C_4H_4S(\text{Thiophene}) \rightarrow S + C_4H_4 \quad (2)$$

$$C_4H_4S(\text{Thiophene}) \rightarrow C_3H_3 + HCS \quad (3)$$

$$C_4H_4S(\text{Thiophene}) \rightarrow CS + C_3H_4 \quad (4)$$

$$C_4H_4S(\text{Thiophene}) \rightarrow SH + C_4H_3 \quad (5)$$

The derived $P(E_{c.m})$ for these processes show characteristics of unimolecular decay. For process (1), two isomer products: •CHCHS• and *c*-CH=CHS have been deduced from the TOF spectra for C_2H_2S. By observing the maximum release of translational energy, the bond energies for *c*-CH=CHS + HC≡CH, •CHCHS• + HC≡CH and SH + C=CH-CH=CH have been determined to be 113.5 ± 2, 133.5±2 and 138±2 kcal/mol. These values are in agreement with the literature data. Furthermore, due to stepwise photodissociation, it is not surprising that the angular distribution for all of these processes is isotropic.

Introduction

Photodissociation of cyclic organic compounds has attracted great interest. [1,2,3,4] In general, its mechanism involves a single bond cleavage as the primary step, and the transient biradical may further dissociate via different pathways by breakage of various bonds. [1] In translational photofragmentation spectroscopy, the primary product continues in the direction of the molecular beam due to momentum conservation. Therefore, only the subsequent dissociation of the transient biradical can be observed. The measurement of translational energy release reveals the biradical decay dynamics. Furthermore, the bond energy, including primary and secondary bond breakage, can be inferred by the observation of the maximum translational energy release.

Thiophene is a basic cyclic organic compound in which a sulfur atom is included in the ring. Due to its strong photochemical activity , it is suitable for studying the biradical decay process. Furthermore, thiophene exists in fossil fuels and is a strong poison in many petrochemical engineering processes. Study of this biradical decay provides some insight into the mechanism of this sulfur compound elimination. In this paper, thiophene biradical decay has been studied as the primary laser photofragmentation product at 193 nm.

Experimental

The rotatable beam source laser photofragmentation apparatus used in this study has been described in detail. [5-6] The apparatus consists of three main components: an ArF or KrF excimer laser, a photodissociation chamber in which a rotatable supersonic molecular beam

intersects the laser beam, and a linearly movable ultrahigh vacuum electron ionization mass spectrometric detector.

In this experiment, a pulsed beam of Thiophene (5% seeded in He) is produced by supersonic expansion through a commercial pulsed valve(General Valve, No. 9 nozzle diameter 0.5 mm at 323K with a total stagnation pressure of approximately 1535 torr. The pulsed valve is operated at 30 Hz. The seeded thiophene beam has an angular divergence of three degrees which is defined by the opening of the conical skimmer and the circular aperture between the differential chamber and the photodissociation chamber. The three degree angular spread of the beam corresponds to a beam width of 3 mm in the photodissociation region. The photodissociation chamber is maintained at pressure of $1x10^{-8}$ torr.

The laser (Compact model 205) was operated at approximately 15 mJ during the experiment, with the light focused to a roughly $5mm^2$ spot size at the crossing region of the laser and molecular beams.

The TOF spectra are taken at a flight path distance of 65.5 cm between the photodissociation region and the ionizer. The emission current of the ionizer is ~1mA and the ionization electron energy is ~76 eV.

The TOF spectra presented here were recorded on a multi process scaler (Stanford Research model SRT430) with a process width of 1.28μs. The ion drift times through the quadruple mass filter were determined to be 4.114 $m^{1/2}$ μs, where m is the ion mass. The actual flight times of photofragments were corrected for the corresponding ion drift times.

The velocity distribution of the parent thiophene beam was determined by taking laser hole burning spectra of thiophene ion at θ_{lab} =0°. The measured speed profile of species was then fitted to an assumed functional form [5,7], $f(v) \sim v^2 \exp[-(v-v_0)/\alpha^2]$, where v_0 and α have been determined in these experiments to be 1.35×10^5 cm/s and 2.1×10^4 cm/s respectively.

The analysis of the TOF data was performed by a forward simulation method [8-10]. Briefly, the procedure began with a trial kinetic energy distribution $P(E_{c.m.})$, which was transformed to a TOF spectrum for comparison with the experimental TOF spectrum. Here, $E_{c.m.}$ represents the center-of-mass kinetic energy of the photofragments. The $P(E_{c.m.})$ distribution was adjusted until satisfactory agreement between the experimental and calculated TOF data was obtained.

In the measurements of the angular distribution, the laser light was polarized by a stack of ten quartz plates set at the Brewster angle. The electronic vector E of the polarized laser beam was set perpendicular to the detector and then rotated into the desired direction with a half-wave retarder. The laser energy was measured by a pyroelectric detector, and was kept at 10 mJ/pulse.

Results and Discussion

Thiophene belongs to the aromatic group because the lone pair electrons in the sulfur atom join in the conjugated π diene system. The lowest electronic transitions upon excitation at 193 nm are postulated to involve the π-π^* transition. [11] The absence of local mode excitation at 193 nm for this molecule indicates that formation of the transient biradical does not support the pathway via bond selective dissociation. However, due to the weak bond of

C-S, the major transient biradical product is expected to involve C-S bond breakage, as shown in eq. 1. The identification of all dissociation processes in our experiment involved C-S bond breakage, further supporting the hypothesis of the transient state via C-S bond breakage. [12] Although the detection of fragment C_4H_2S at beam angle 13° is assigned to the process of dimer dissociation or hydrogen (H_2) elimination C_4H_4S(Thiophene) $\rightarrow$ C_4H_2S + H_2 in the primary study of the photodissociation of thiophene in the absence of H_2 fragment detection, [3] the strong signal at m/e$^+$ 84(C_4H_4S), 83(C_4H_3S), and 82(C_4H_2S) at beam angle 10° in our experiment provides further evidence to identify this process as dimer dissociation.

(Thiophene) $\rightarrow$

(opening ring) $\Delta H = 99.7$ kcal/mol (1)

1. HC≡CH + C_2H_2S process

The fragment C_2H_2S from dissociation of the transient biradical C_4H_4S may exist in several isomers. The heats of formation for three stable isomers of C_2H_2S vary greatly (eq. (2), (3) and (4).) [2, 3, 13]

C_4H_4S(Thiopene) → •CHCHS• + HC≡CH ΔH=128 (133.2) kcal/mol (2)

C_4H_4S(Thiophene) → *c*-CH=CHS + HC≡CH ΔH=114 kcal/mol (3)

C_4H_4S(Thiophene) → CH_2=C=S + HC≡CH ΔH= 66 kcal/mol (4)

Due to the kinematic constraint, different populations of translational energy, $P(E_{c.m.})$, which results in separated /partially overlapped TOF peaks , is expected to be observed when the different isomers are formed. The TOF spectrum for C_2H_2S at θ_{lab}=25° shows a very small fast peak (Fig 2.b), which is amplified at θ_{lab}=30° (fig 2.d) by truncating the slow part of the peak as the Newton diagram shows (fig. 1). The fitting of these two spectra gives two peaks for the population of translational energy (fig. 3). The maximum of the slow peak is around 5 kcal/mol and the $p(E_{c.m})$ below this value can not be observed at beam angle 25° . Due to the influence of dimers and clusters, the detection of the slow part of the $P(E_{c.m})$ results in a large uncertainty, but the maximum of this $p(E_{c.m})$ can be expected to be extended to zero. The maximum of the fast peak is around 21 kcal/mol and its abundance drops to zero at 16.5 kcal/mol. and 36.5 kcal/mol. The threshold values of 16.5 and 36.5 kcal/mol are estimated for the slow and the fast peak, respectively. (fig. 3) This observation of the thresholds strongly suggests that the isomers c-CH=CHS and •CHCHS• are formed during the dissociation process. Isomer c- CH=CHS may result from the reconfiguration of •CHCHS•, since the molecule *c*-CH=CHS is much more stable than the biradical •CHCHS•. In that case, the transitional barrier from •CHCHS• to *c*-CH=CHS is inferred to be small.

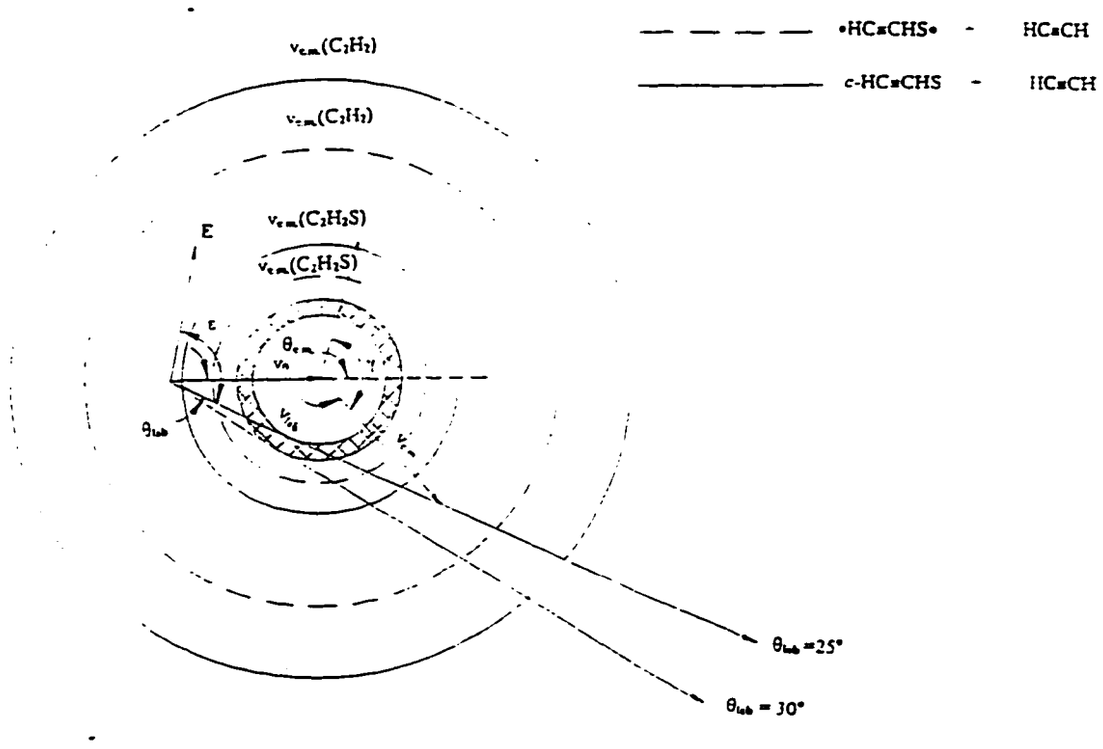

Figure 1. Kinematics for the formation of *c*-CH=CHS + HC≡CH and •HC=CHS• + HC≡CH . V_o is the laboratory velocity for C_4H_4S, and $v_{c.m}(C_2H_2S)$ and $v_{c.m}(C_2H_2)$ are the maximum c.m. velocities for C_2H_2S and C_2H_2., respectively. The truncated part has been shaded when the molecular beam angle increases from 25° to 30°. The diagrams also show the relationship $\gamma=\theta_{c.m.} + \varepsilon - \theta_{lab.}$, where γ is the angle between the laser electric field (**E**) and the c.m. photofragment velocity; $\theta_{c.m.}$ is the angle between the molecular beam velocity and the fragment recoil c.m. velocity; ε is the angle between **E** and detector axis; and θ_{lab} is the angle between the molecular beam velocity and the detector axis.

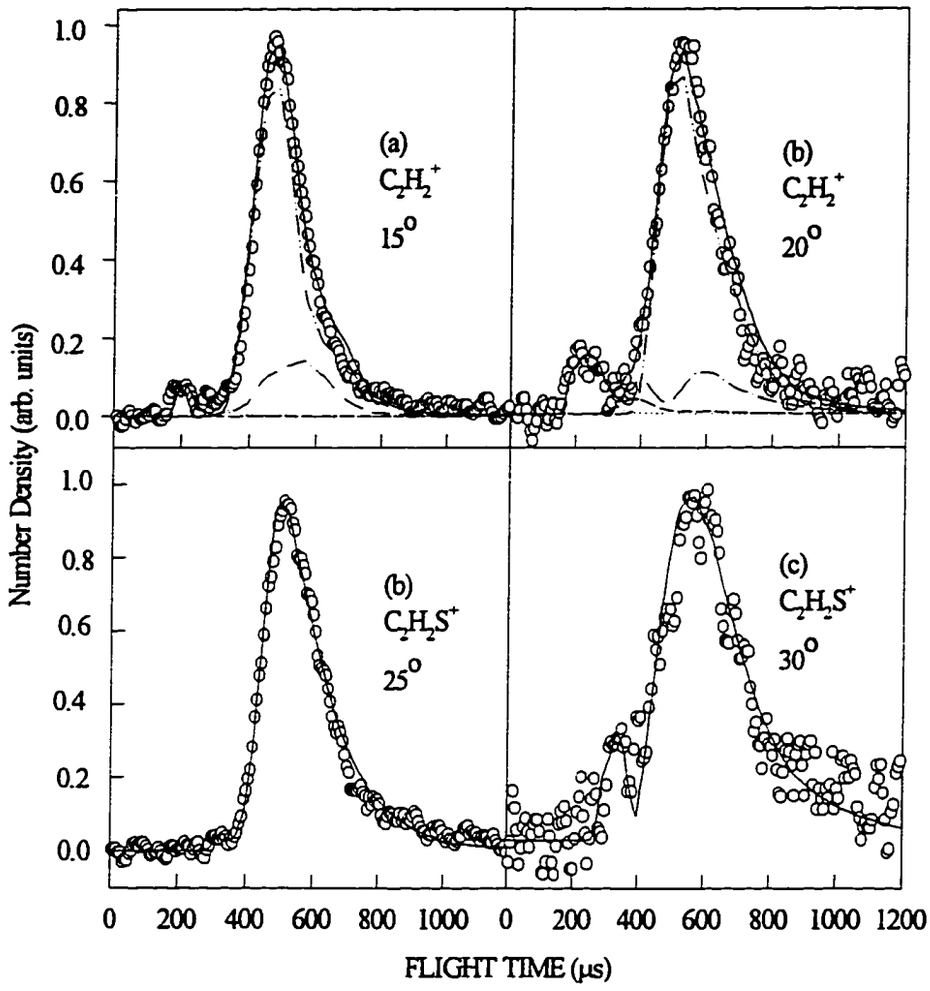

Figure 2. TOF spectra obtained for C_2H_2 and C_2H_2S at θ_{lab} = 15°, 20°, 25°, and 30°. Circles represent the experimental data. The solid line is a best fit. Contributions are shown in fig. 2 (a) and (b) for C_3H_3 (dot-dot-dash line), C_2H_2S (dot-dash line), C_2H_2 (dashed line), C_2H_2 from secondary dissociation (dotted line).

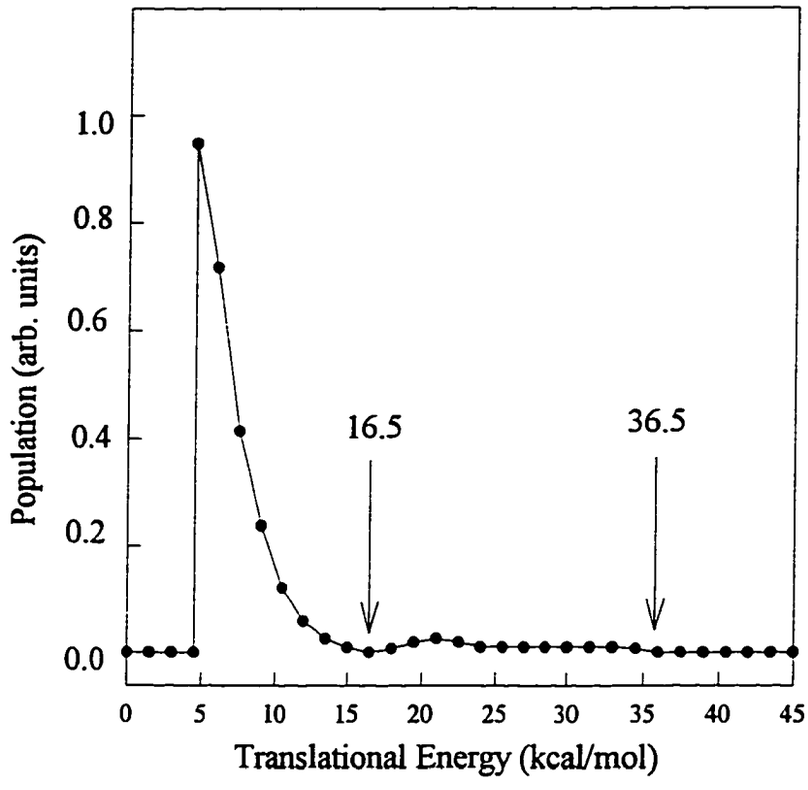

Figure 3. $E_{c.m}$ distribution[$P(E_{c.m})$] for process (1) derived by fitting the TOF spectra for C_2H_2S and C_2H_2.

TOF spectra for C_2H_2 , a counterpart of C_2H_2S, are much weaker. This may be due to the lower ionization efficiency of HC≡CH. The TOF spectra for C_2H_2 can not be fit by $P(E_{c.m.})$ derived from TOF spectra for C_2H_2S (dashed curve), indicating that other processes are involved in the spectra. We expect that $C_2H_2^+$ fragment ions formed in the electron ionization of C_2H_2S contribute to the spectra for C_2H_2:

$$C_2H_2S + e^- \rightarrow C_2H_2^+ + S + 2e^- \qquad (5)$$

However, this contribution (dot-dash curve) does not fit the slow, large peak. We note that the photofragment C_3H_3 can be ionized to form $C_2H_2^+$:

$$C_3H_3 + e^- \rightarrow C_2H_2^+ + CH + 2e^- \qquad (6)$$

Therefore, the $P(E_{c.m.})$ derived from TOF spectra for C_3H_3 is used to fit the spectra for C_2H_2 (dot-dot-dash curve). A very fast peak appears in fig.2a and fig.2b., and shows laser energy independence, excluding the two photo effects. Only the secondary dissociation of the radical *c*-CH=CHS can produce the fast signal by abandoning the sulfur atom. Therefore, this fast peak (dotted line) is assigned to the secondary dissociation :

$$c\text{-}CH{=}CHS \rightarrow HC{\equiv}CH + S \qquad (7)$$

It is very interesting that the fastest signals are observed in TOF spectra for S and SH in both our and J. D. Mayers's experiments [3], and that this secondary $P(E_{c.m.})$ (fig. 4) fits the fastest signal of SH quite well due to the S mass leakage.

2. S + C_4H_4 Process

A $P(E_{c.m.})$ of S + C_4H_4 Process can be derived from TOF spectra for C_4H_4 (fig.5). The signal from C_4H_3 may also contribute to this spectrum due to the mass leakage. However, since the mass leakage ratio is unknown and the signal from C_4H_3 resides in the slow part of TOF spectra for C_4H_4, the contribution from C_4H_3 is ignored in fitting the TOF spectra for C_4H_4. A threshold of this $P(E_{c.m})$ (fig. 6) is accurately determined at 15.5 kcal/mol, and the $P(E_{c.m})$ can be measured down to 2 kcal/mol, but is expected to extend to zero. The heats of formation of three stable isomers are shown in eq. 8, 9, 10, [2] and the measurement $P(E_{c.m.})$ for S + C_4H_4 Process suggests that the biradical fragment preferably forms the stable molecule $CH_2=C=C=CH_2$.

$$C_4H_4S(\text{Thiophene}) \rightarrow CH_2=CH-C\equiv CH + S(^3P) \quad \Delta H=12 \text{ kcal/mol} \qquad (8)$$

$$C_4H_4S(\text{Thiopene}) \rightarrow CH_2=C=C=CH_2 + S(^3P) \quad \Delta H=122 \text{ kcal/mol} \qquad (9)$$

$$C_4H_4S(\text{Thiophene}) \rightarrow H_2C=C-C=CH_2 + S(^3P) \quad \Delta H=140 \text{ kcal/mol} \qquad (10)$$

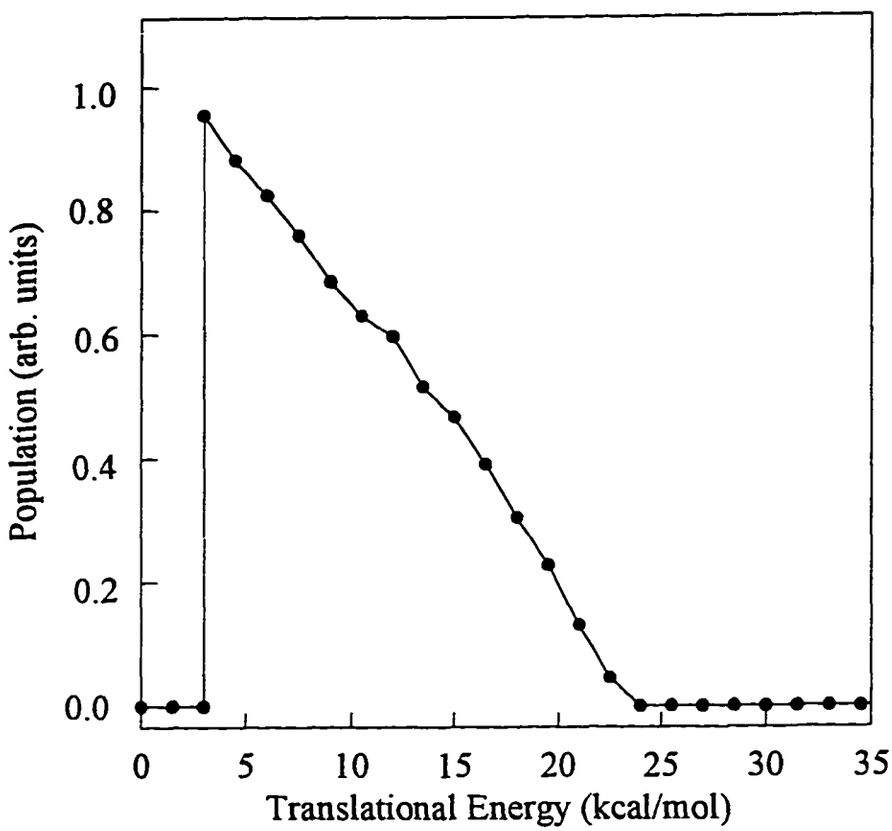

Figure 4. $P(E_{c.m})$ for the secondary dissociation process (7).

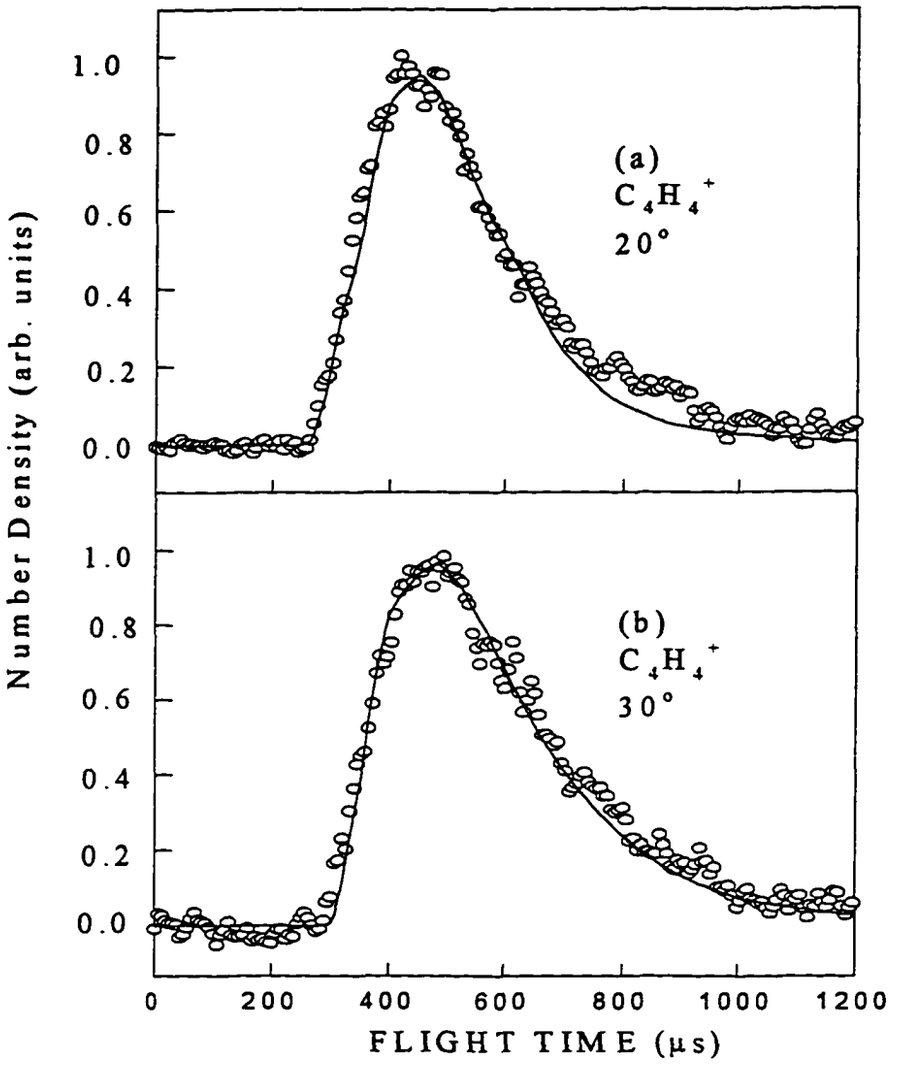

Figure 5. TOF spectra for S obtained at (a) θ_{lab}=20° and (b) θ_{lab}=30°. Circles represent experimental data. The solid line is a best fit using P($E_{c.m}$) from fig.6.

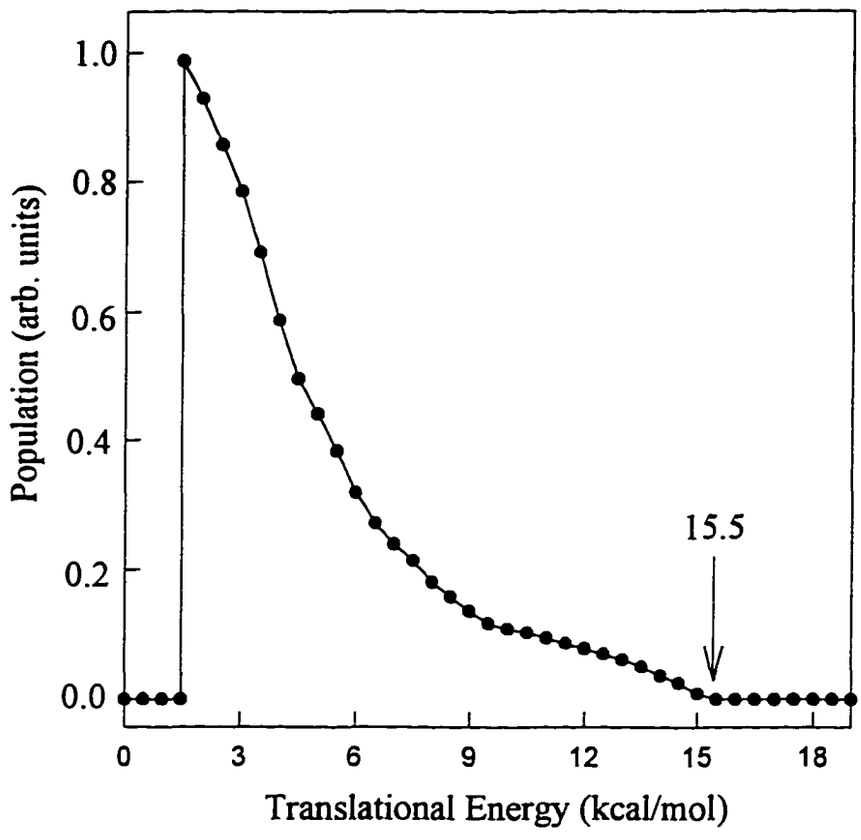

Figure 6. $E_{c.m}$ distribution [$P(E_{c.m})$] for process (2) derived by fitting the TOF spectra for S at θ_{lab}=20° and θ=30°.

The detection of the signal for S was unsuccessful, due to strong background from O_2. However, the information for S can be further obtained from TOF spectra for SH due to the mass leakage.

3. C_3H_3 + HCS Process

TOF spectra for C_3H_3 and HCS are shown in fig.7, and the $P(E_{c.m})$ (fig. 8) derived from TOF spectra for HCS fits the TOF spectra for C_3H_3 quite well (dashed curve), indicating that only one process has happened. The possible processes and their heats of formation are listed in eq.11, 12, 13.[13]

$C_4H_4S(\text{Thiophene}) \rightarrow HCS + HC{\equiv}C{-}CH_2$ ΔH=110 kcal/mol (11)

$C_4H_4S(\text{Thiophene}) \rightarrow HCS + HC{=}CH{-}CH\bullet$ ΔH=144 kcal/mol (12)

$C_4H_4S(\text{Thiophene}) \rightarrow HCS + HC{=}C{-}CH_2$ ΔH=153 kcal/mol (13)

The translational energy release can be measured down to 1 kcal/mol and probably extends to zero. The maximum translational energy release occurs at 4 kcal/mol, supporting that the isomer HC=CH–CH• is formed in the photodissociation process. A very small fast peak in the TOF spectra for C_3H_3 has been observed, and this peak can be fit by $P(E_{c.m})$ for C_3H_4 due the mass leakage (dot-dash curve).

4. CS + C_3H_4 Process

TOF spectra for CS and C_3H_4 are depicted in fig. 9. Since the signal from CS is hard to detect due to the large background from CO_2, the mass has been tuned up to $\approx$ 44.3 in

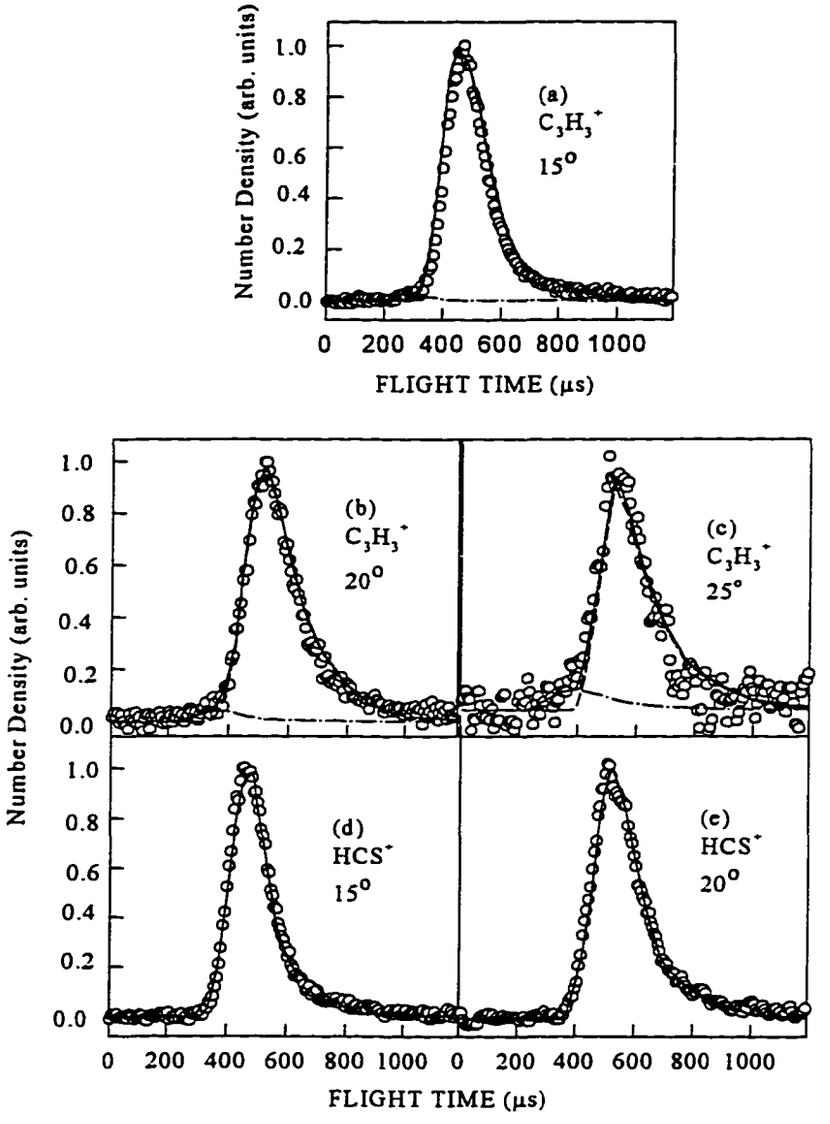

Figure 7. TOF spectra obtained for C_3H_3 and HCS at $\theta_{lab} = 15°$, 20°, and 25°. Circles represent the experimental data. The solid line is a best fit. Contributions are shown in fig. 7 (a), (b), and (c) for C_3H_3 (dashed line), and C_3H_4 (dot-dash line).

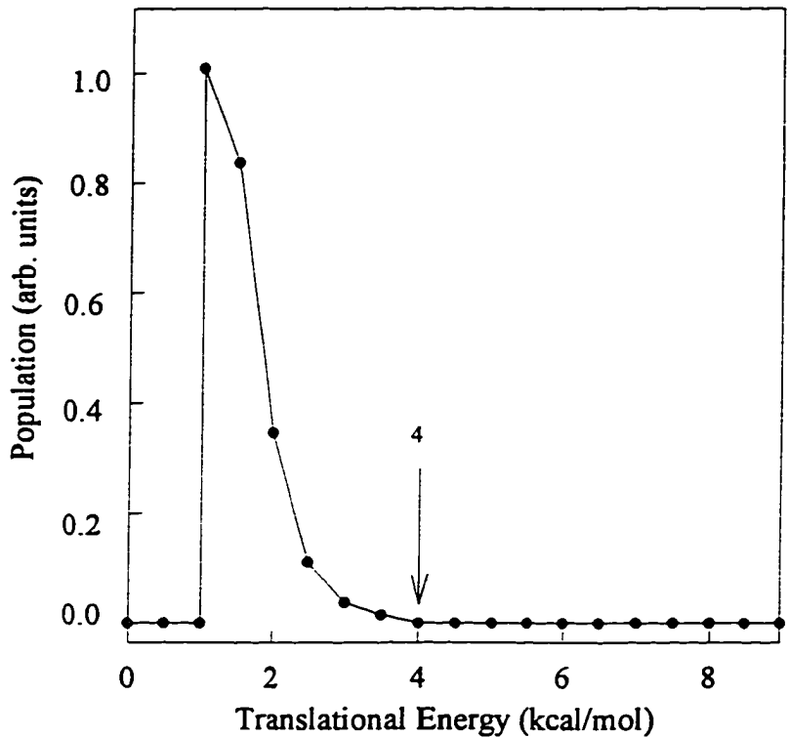

Figure 8. $E_{c.m}$ distribution [$P(E_{c.m})$] for process (3) derived by fitting the TOF spectra for C_3H_3 and HCS

order to avoid the large noise. Therefore, it is not surprising that the big slow peak (dot-dash curve) can be fit by the $P(E_{c.m.})$ derived from HCS due to the large mass leakage. The derived $P(E_{c.m.})$ from the fast peak (dashed line) is shown in (fig.10). TOF spectra for C_3H_4 only show a small fast peak (dashed curve), indicating that this is a minor process. The large slow peak (dot-dash curve) is fit by the $P(E_{c.m.})$ derived from C_3H_3. The maximum translational energy release is ≈30 kcal/mol, and $P(E_{c.m.})$ peaks near zero. All of these observations are consistent with J. D. Myers results.[3]

5. SH + C_4H_3 Process

TOF spectra for C_4H_3 are shown in fig. 11 (c) and fig. 11(d). The fitting shows that the contribution from C_4H_4 is small, due to mass leakage (dot-dash line). The derived $P(E_{c.m.})$ (fig.12) peaks at 1 kcal/mol and is expected to extend to zero. The threshold of this $P(E_{c.m.})$ is ≈12 kcal/mol, indicating that process (14) occurs.

$$C_4H_4S(\text{Thiophene}) \rightarrow SH + C{=}CH{-}CH{=}CH \qquad \Delta H{=}140.2 \text{ kcal/mol} \quad (14)$$

The fitting of TOF spectra for SH is much more complex due to the mass leakage. The fitting shows contributions are made from SH(dashed curve), S (dot-dash curve), and HCS (dot-dot-dash curve) due to ionization process (15):

$$HCS + e^- \rightarrow S^+ + HC + 2e^- \qquad (15)$$

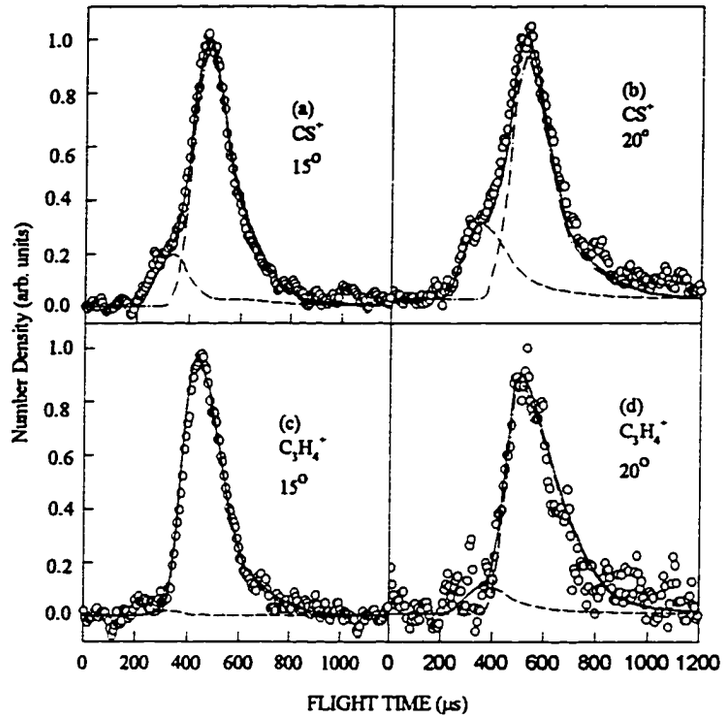

Figure 9. TOF spectra for CS and C_3H_4 at $\theta_{lab.} = 15°$, and 20°. Circles represent the experimental data. The solid line is a best fit. Contributions are shown in fig.9 (a) and (b) for CS (dashed line), and HCS (dot-dash line). Contributions are shown in fig.9 (c) and (d) for C_3H_4 (dashed line), and C_3H_3 (dot-dash line).

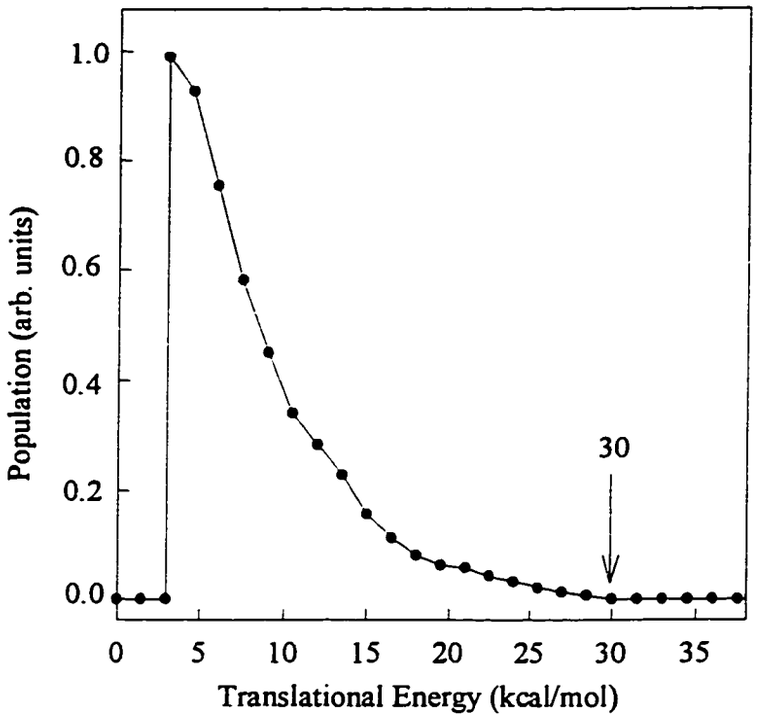

Figure 10. $E_{c.m}$ distribution [$P(E_{c.m})$] for process (4) derived by fitting the TOF spectra for CS and C_3H_4 at θ_{lab}=15 and 20° .

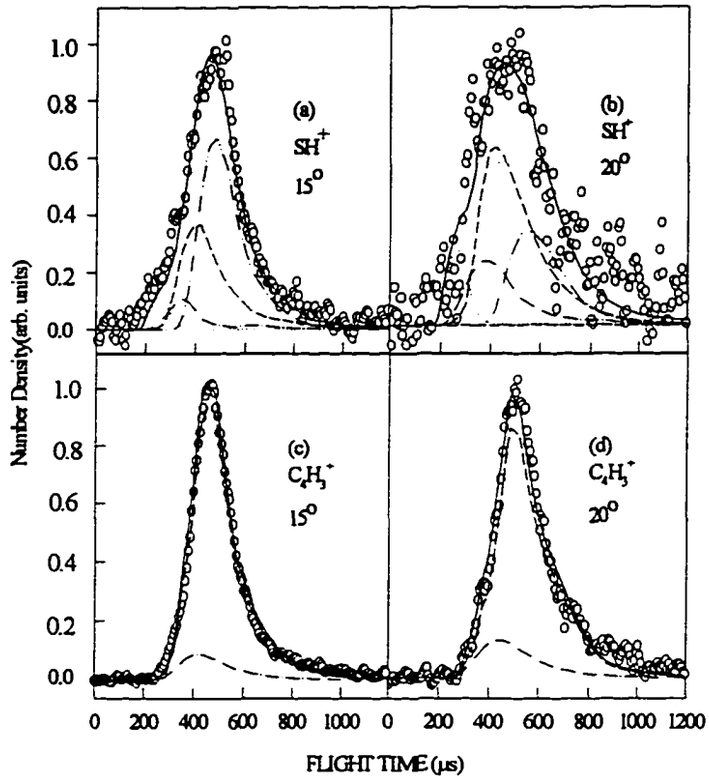

Figure 11. TOF spectra for SH and C_4H_3 at θ_{lab}=15° and 20°. Circles represent the experimental data. The solid line is a best fit. Contributions are shown in fig.11 (a) and (b) for SH (dashed line), S(dot-dash line), HCS(dot-dot-dash line), and S from process (7) (dotted line). Contributions are shown in fig. 11 (c) and (d) for C_4H_3 (dashed line), and C_4H_4 (dot-dash line).

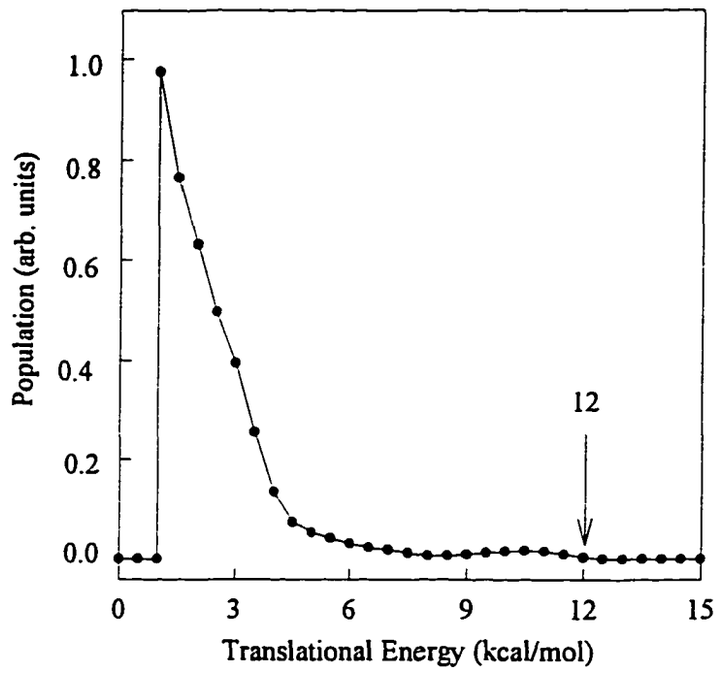

Figure 12. $E_{c.m}$ distribution [$P(E_{c.m})$] for process (5) derived by fitting the TOF spectra for SH and C_3H_4 at θ_{lab}=15 and 20°

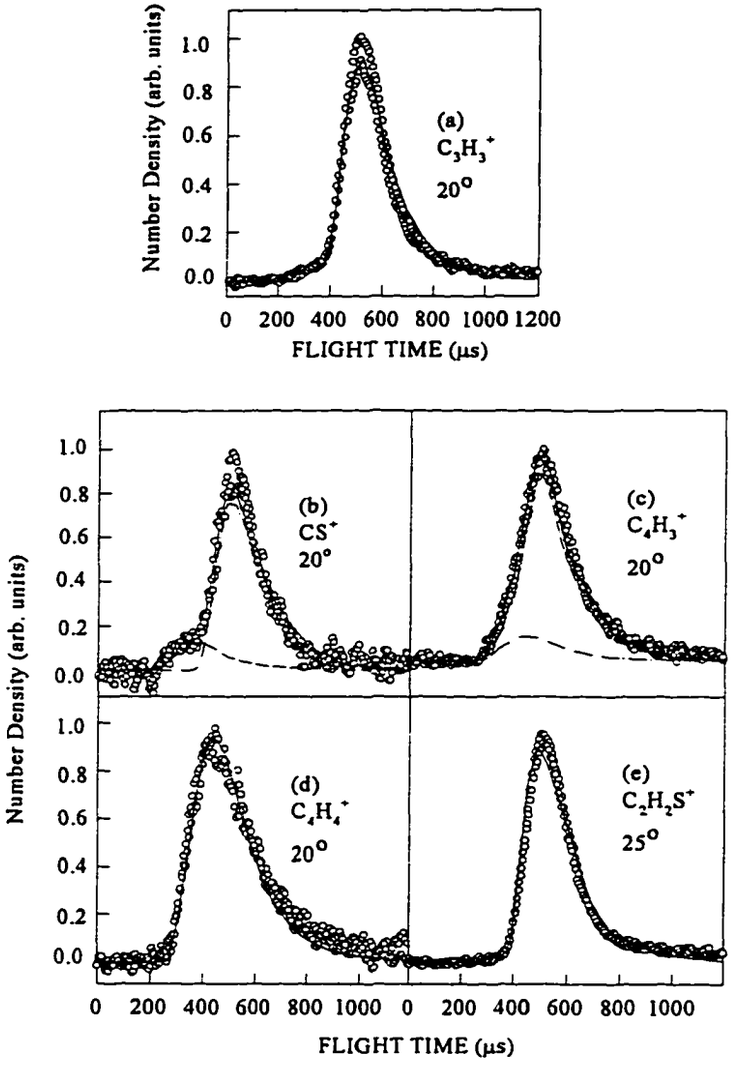

Figure 13. The TOF spectra observed at ε=0°, and 90° for C_3H_3, CS, C_4H_3, and C_4H_4 at $\theta_{lab.}$ =20°, and C_2H_2S at $\theta_{lab.}$ =25°

The S from minor process (CS + C_3H_4) appears in the same position as S from process (C_4H_4) + S) and is neglected in the fitting. A small fast peak appears in the TOF spectra for SH and cannot fit by the primary processes. It is interesting that J. D. Mayers's TOF spectra[3] for SH and S also show a small fast peak that does not fit. We note that J. D. Mayers excluded the secondary dissociation (7) in the fitting. However, this small peak can be fit by the $P(E_{c.m})$ of the dissociation process (7) derived from TOF spectra for C_2H_2 in our experiment.

The Angular Distribution

The stepwise photodissociation mechanism for cyclic compounds is further confirmed by the measurements of the angular distribution for the above processes. The isotropy results of the above processes are expected if the stepwise photodissociation processes occur. TOF spectra for fragments (a) C_3H_3, (b) CS, (c) C_4H_3, (d) C_4H_4, and (e) C_2H_2S have been measured at $\varepsilon=0°$ and $\varepsilon=90°$ (fig. 13). The intensities of TOF spectra for the five fragments remain constant, indicating that all five processes are isotropic.

Conclusion

The photodissociation of thiophene, a cyclic organic compound, reveals the different pathways that the transient biradical decays by breakage of different bonds. Five dissociation processes have been identified as follows:

$$C_4H_4S(\text{Thiophene}) \rightarrow HC{\equiv}CH + C_2H_2S \qquad (1)$$

$$C_4H_4S(\text{Thiophene}) \rightarrow S + C_4H_4 \qquad (2)$$

$$C_4H_4S(\text{Thiophene}) \rightarrow C_3H_3 + HCS \qquad (3)$$

$$C_4H_4S(\text{Thiophene}) \rightarrow CS + C_3H_4 \qquad (4)$$

$$C_4H_4S(\text{Thiophene}) \rightarrow SH + C_4H_3 \qquad (5)$$

The derived $P(E_{c.m})$ for these processes show characteristics of unimolecular decay. For process (1), two isomer products: •CHCHS• and *c*-CH=CHS have been observed from TOF spectra for C_2H_2S. By observing the maximum release of translational energy, the bond energies, including bond cleavages of a primary step and a secondary step, have been determined to be 113.5 ± 2, 133.5±2 and 138±2 kcal/mol for *c*-CH=CHS + HC≡CH, •CHCHS• + HC≡CH and SH + C=CH-CH=CH, respectively, which is in agreement with the literature data. Furthermore, the isotropic angular distributions for all these processes are consistent with the fact that photodissociation processes occur via a stepwise mechanism.

References

(1) S. Braslavsky and J. Heicklen; *Chemical Reviews*, 77, 473 (1977).

(2) C. W. Hsu, C.-L. Liao, Z.-X. Ma, and C.Y. Ng; *J. Phys. Chem.* **99**, 1760 (1995).

(3) Myers, J.D. Ph.D. Thesis, University of California at Berkeley (1993).

(4) H. A. Wiebe and J. Heicklen; *Ca. J. Chem.* **47**, 2964 (1969).

(5) W.-B. Tzeng, H.-M. Yin, W.-Y. Leung, J.-Y. Luo, S. Nourbakhsh, G. D. Flesch, and C. Y. Ng, *J. Chem. Phys.* **88**, 1658(1988).

(6) S. Nourbakhsh, C.-L. Liao, and C. Y. Ng, *J. Chem. Phys.* **92**, 6587(1990).

(7) T. K. Minton, G. M. Nathanson, and Y. T. Lee, *J. Chem. Phys.* **86**, 1991(1987).

(8) E. J. Hintsa, X. Zhao, and Y. T. Lee, *J. Chem. Phys.* **92**, 2280(1990).

(9) X. Zhao, Ph.D. thesis, University of California, Berkeley, CA, 1988.

(10) L. J. Butler, E. J. Hintsa, S. F. Shane, and Y. T. Lee, *J. Chem. Phys.* **86**, 2051(1987).

(11) S. F. Mason, Physical Methods in Heterocyclic Chemistry, Katritzky, Academic Press, New York (1963).

(12) E. E. van Tamalen and T. H. Whitesides, *J. Am. Chem. Soc.*, **93**, 6129(1971).

(13) A. K. Nayak, S. K. Sarkar, R. S. Karve, V. Parthasarathy, K. V. S. Rama Rao, J. P. Mittal, S. L. N. G. Krishnamachari, and T. V. Venkitachalam, *Appl. Phys.* **B 48**, 437(1989).

SCATTERING CROSS SECTIONS FOR $O(^3P)[SO(X,^3\Sigma^-)]$ + He[Ne, Ar, Kr]

A paper to be submitted to the Journal of Chemical Physics

H.-Q. Zhao and C. Y. Ng

Abstract

Scattering cross sections for $O(^3P)[SO(X,^3\Sigma^-)]$ + He[Ne, Ar, Kr] have been measured in a photodissociation apparatus. The scattering for $O(^3P)$ + He[Ne, Ar, Kr] obeys the rigid sphere model inthe high velocity range. The measurements of impact parameters, r_0, for the scattering of $O(^3P)$ + He[Ne] are close to the summation of van der Waals radii of the colliding particles. The measurements for $SO(X,^3\Sigma^-)$ + He[Ne, Ar, Kr] show that the interaction potential is of the form $V(r)=\pm C_n/r^n$. Values for C_n and n were also determined.

Introduction

Measurement of elastic scattering cross sections can be used to determine the interaction potential of the colliding particles.[1,2] Knowledge of these interactions provides information for understanding van der Waals forces and the sizes of colliding particles. Furthermore, the interactions between radicals and molecules are involved in many processes, such as UV laser action and photochemical reactions. Therefore, the knowledge of these interactions is of interest to understanding these processes.

Due to their high chemical reactivity, radicals are also involved in many reactive scattering studies.[3,4] The determination of these interactions can also provide information for understanding orientation and alignment of these radicals in reactive collision. In the past years, the measurement of such interactions mainly employ thermal dissociation, microwave discharge

or electron bombardment to produce radicals.[5-7] However, due to the limitations of the method, only some of the radical states can be produced, and the experimental velocity range covers only a part of the potential energy curve. The photodissociation of molecules is another important source of radicals and can produce a pure state. Moreover, the photodissociation processes of many molecules have been studied in detail[8-14]. This knowledge helps us to select radicals in the desired electronic state. For example, the photodissociation processes (1) and (2)[15,16]

$$SO_2 + h\nu(193\ nm) \rightarrow O(^3P) + SO(^3\Sigma^-) \quad (1)$$

$$N_2O + h\nu(193\ nm) \rightarrow O(^1D) + N_2(^1\Sigma) \quad (2)$$

can be used to study the scattering behavior of different O states. In this study, we present our results using laser photodissociation to measure the scattering cross sections between $O(^3P)[SO(^3S^-]$ and He[Ne, Ar, Kr) due to the photodissociation process (1).

Experimental

The rotatable beam source laser photofragmentation apparatus used in this study has been described in detail.[8-14] The apparatus consists of three main components: an ArF or KrF excimer laser, a photodissociation chamber in which a rotatable supersonic molecular beam intersects with the laser beam, and a linearly movable ultrahigh vacuum electron ionization mass spectrometric detector.

For scattering purposes, a gas cell with a 4.45 cm long and 3 mm diameter opening was mounted at the exit of main chamber along the axis of the photodissociation and detector. In order to maintain a constant pressure throughout the experiment, a very stable leak valve (Varian model No. 951-5100) was used. Two gas lines were connected with the gas cell. One line

connects the cylinder to the gas cell through a leak valve. The other line connects the gas cell to a baratron pressure gauge and also to a valve that leads to the main chamber. By using this design, the gas cell can be pumped down very quickly with the valve open. The gas cell pressure was maintained below 10^{-6} Torr with the leak valve closed, and in the 10^{-4} Torr range with it open. All of the rare gases used were UHP grade.

The measurement of scattering cross sections required a TOF spectrum with an attenuation due to the rare gas in the gas cell. However, the rare gas increased the background TOF signal, resulting in a large error. Therefore, a pulsed beam with lower background was used to get better results.

In this experiment, a pulsed beam of SO_2 (20% seeded in He) is produced by supersonic expansion through a commercial pulsed valve (General Valve, No. 9 nozzle diameter 0.5 mm) at 298 K and a total stagnation pressure of approximately 1465 torr. The pulsed valve is operated at 50 Hz. The seeded SO_2 beam has an angular divergence of 3° which is defined by the opening of the conical skimmer and the circular aperture between the differential chamber and the photodissociation chamber. The 3° angular spread of the beam corresponds to a beam width of 3 mm in the photodissociation region. The photodissociation chambers are maintained at pressures of approximately $1x10^{-8}$ torr when the leak valve is closed, and $3x10^{-8}$ torr when it is open.

The laser (Questek model 2460) energy was kept constant at 70 mJ during the experiment, with the light focused to a roughly 5 mm^2 spot size at the crossing region of the laser and molecular beams.

The TOF spectra were taken at a flight path distance of 65.5 cm between the photodissociation region and the ionizer. The emission current of the ionizer was 1.60 mA and the ionization electron energy was 76 eV.

The TOF spectrum was recorded on a Stanford Research model SRT430 multichannel scaler. The bin widths were set to 0.32 ms and 0.16 μs for $O(^3P)$ and $SO(^3\Sigma^-)$, respectively.

The calculation of the scattering cross section follows the general rule:[2]

$$s=/n_kL*Ln(I_0/I) \qquad (3)$$

where I_0 and I are the incoming and outgoing beam intensities, respectively, n_kL is the product of scattering gas density and length of the scattering region. Due to the gas flow of the gas cell, n_kL should be substituted by $(n_kL)_{eff}$. The general method to calibrate this value is to use the internal standard method wherein a known scattering system in the gas pressure range is used to calibrate the value of (n_kL). In our experiment, a second barrier with many small holes is used to introduce the rare gas into the scattering region uniformly. The gas cell exit hole is much smaller than the tube connected with the baratron, so the gas fluence is not a significant factor.

To assist the analysis of TOF data, a forward simulation method was employed.[17-19] The procedure involved a trial kinetic energy distribution $P(E_{c.m})$, which was transformed to a TOF spectrum for comparison with the experimental TOF spectrum. Here, $E_{c.m}$ was the center-of-mass kinetic energy of the photofragments. The $P(E_{c.m})$ distribution was adjusted until satisfactory agreement between the experimental and calculated TOF data was obtained.

The velocity distribution of the pulsed parent molecular beam, which was used in a forward simulation method, was measured after the experiments by taking the laser hole burning spectra of SO or SO_2 at lab angle $\theta_{lab}=0^o$ and using the background subtraction method. A very stable pulse generator (SRS DG535) was used to drive the experiment and the multi-channel scaler was operated in the toggle mode, which has addition and subtraction states. One of the TTL output signals of the pulse generator was used to trigger the pulsed valve controller. Another TTL output signal, delayed 450 μs from the pulsed valve firing, was divided between the trigger of the MCS and a synchronous box controlled by the toggle mode output of the MCS. Only the TTL output signal of that box was permitted to trigger the laser when the MCS was in the addition state of toggle mode. The holing burning spectrum was thus recorded. The measured speed profile of the species was then fitted to an assumed functional form:[8]

$$f(v) \sim v^2 \exp[-(v-v_0)^2/\alpha^2] \quad (4)$$

where V_0 is the most probable speed and α is a measure of the width of speed profile. In this experiment, these constants were determined to be $v_0=9.79\times10^4$ cm/s and $\alpha=0.62\times10^4$ cm/s, respectively. The ion drift times through the quadrupole mass filter were determined to be $4.114m^{1/2}$ μs, where m is the ion mass. The actual flight times of photofragments were corrected for the corresponding ion drift times.

Results and Data Analysis

I. Scattering cross sections for $O(^3P)$ + He[Ne, Ar, Kr]

Scattering cross sections for $O(^3P)$ + He[Ne, Ar, Kr] are shown in fig. 1. Our results are in agreement with the results using a microwave discharge[9], and the same rules of the scattering cross section dependence on the velocity are followed. However, due to the high velocity range in our experiment, a flat curve is observed in all of the scattering of O-He, O-Ne, O-Ar and O-Kr. For the O-He system, that flat curve covers almost the entire velocity range. The fitting of the open valve TOF spectra shown in fig.2 (using the translational distribution of process (1) shown in fig.3) are pretty good, further indicating that the scattering of $O(^3P)$ by He is uniform.

These results can be explained by the fact that in the high velocity range, the collision objects approach very close and repulsive potential energy plays an important role. Therefore, the rigid-sphere model is obeyed;[20]

$$\sigma=2\pi r_0^2 \qquad (5)$$

where the total cross section is twice the geometrical cross section of the spheres. From Eq. 4, the value of r_0 can be inferred to be 324 nm, 339 nm, 460 nm and 535 nm for O-He, O-Ne, O-Ar and O-Kr, respectively. For O-He and O-Ne, this value is in agreement with the summation of van der Waals radii of O-He (330 nm) and O-Ne (310 nm),[21] respectively.

II. Scattering cross sections for $SO(^3\Sigma^-)$ + He[Ne, Ar, Kr]

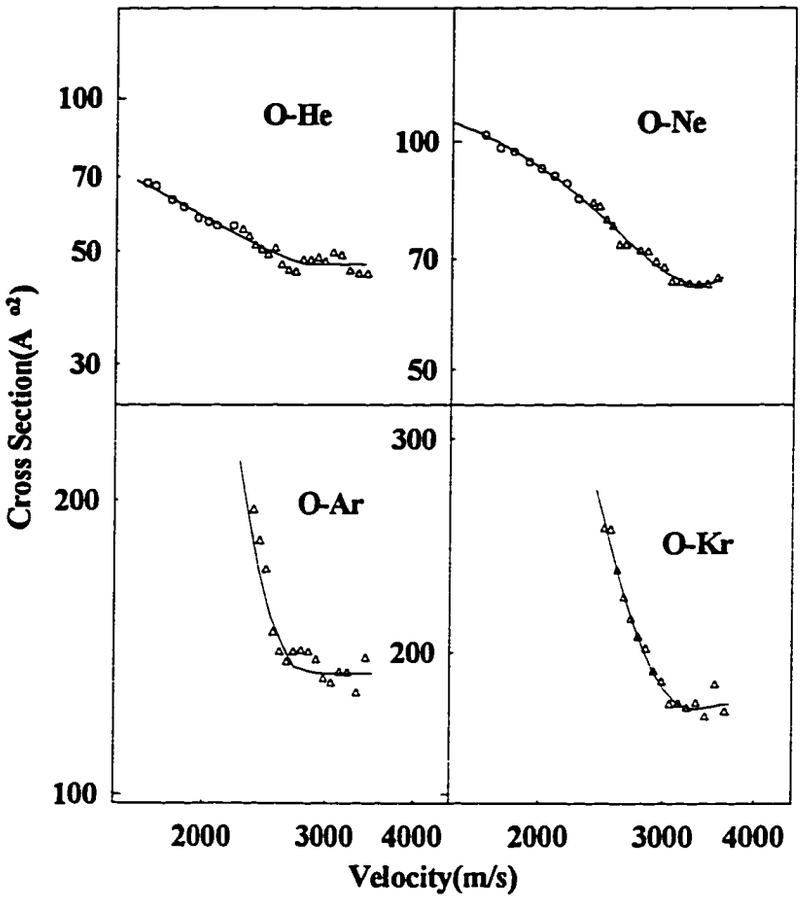

Figure 1. The scattering cross sections for $O(^3P)$ + He[Ne, Ar, Kr] as a function of the velocity. Circles represent the data abstracted from reference (9).

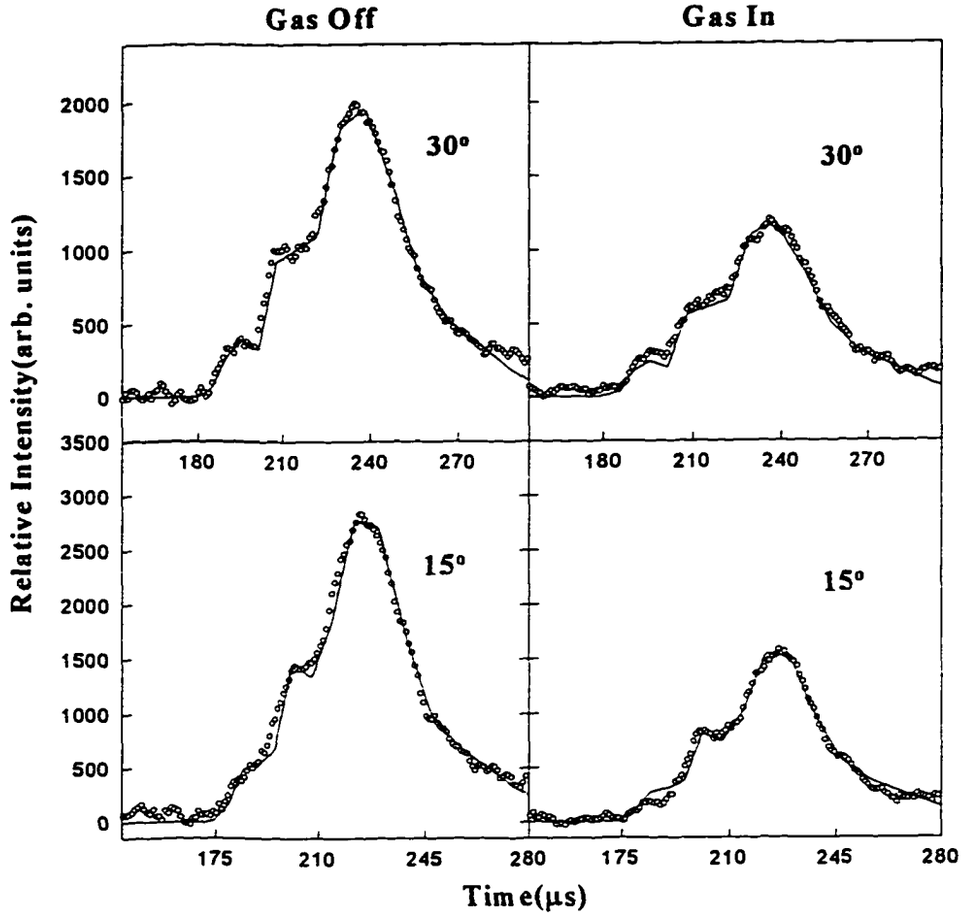

Figure 2. TOF spectra of $O(^3P)$ for $O(^3P)$-He with the leak valve closed and open.

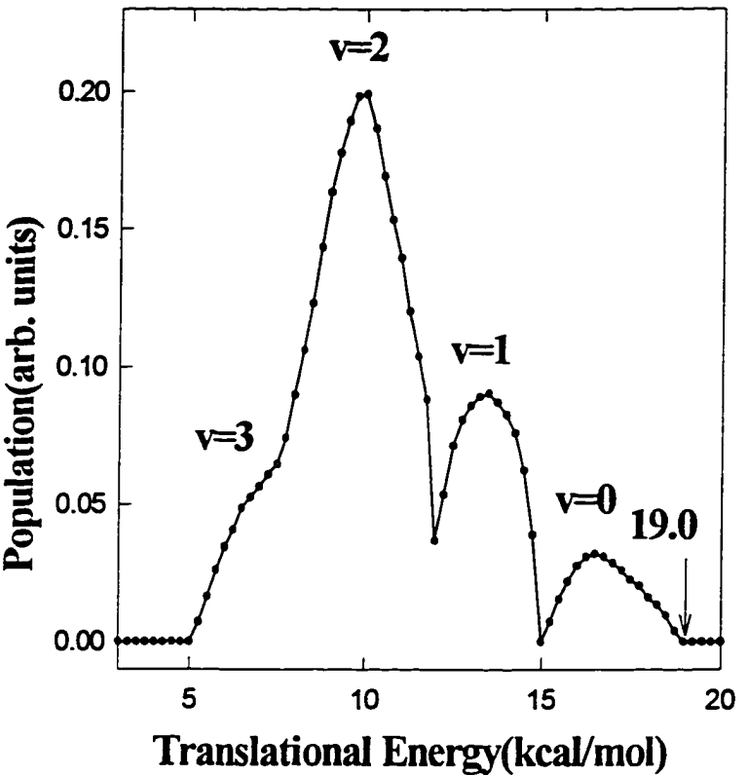

Figure 3. Translational energy of the process: $SO_2 + h\nu(193\ nm) \rightarrow O(^3P) + SO(^3\Sigma^-)$

Scattering cross sections for $SO(^3\Sigma^-)$ + He[Ne, Ar, Kr] are shown in fig. 4. They clearly show that the log of the cross sections decreases linearly with the log of the velocity. This velocity range covers the attractive part of potential energy. However, in SO-Ar system, the repulsive part of potential energy is also observed in high velocity range. Moreover, the fitting of the TOF spectra also supports the above results. The TOF spectra (fig.5) after scattering clearly show that the SO signal is scattered more in the low velocity range (θ_{Lab}=45°) than in the high velocity range. By using the van der Waals form of potential energy:

$$V(r)=\pm C_n/r^n \qquad (6)$$

the scattering cross section has the form:[2,22]

$$s=F(n)(C_n/hv)^{2/(n-1)} \qquad (7)$$

where $F(n)=p^2(2K_n/(n-1))^{2/(n-1)}[G(2/(n-1)\sin(p/(n-1))]^{-1}$ and $K_n=p^{1/2}G(n+1/2)/G(n/2)$.
The van der Waals potential energy parameters C_n and r_n obtained by simulating our data (indicated by solid line of the fig.4) are given in Table 1. In the attractive portion of the potential, n is no more than 4. This may due to the fact that SO is a polar radical. Its attractive potential is greater than that of the normal van der Waals force (n=6). The repulsive part of SO-Ar has a large n indicates that its repulsive potential energy rapidly increases as r_0 decreases. The interaction potential is shown in fig.6.

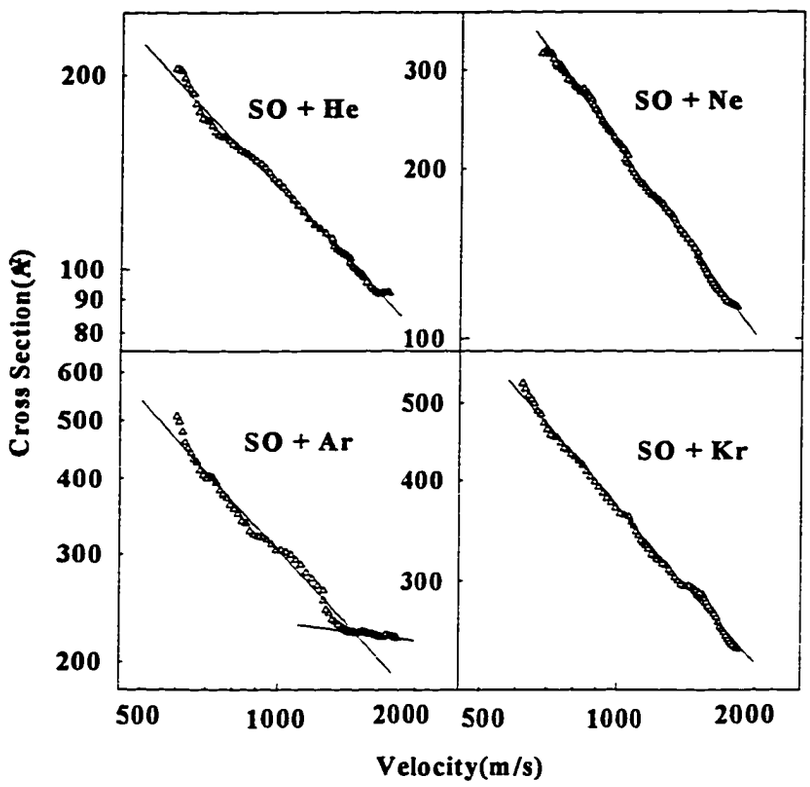

Figure 4. The scattering cross sections for $SO(^3S^-)$ + He[Ne, Ar, Kr] as a function of the velocity.

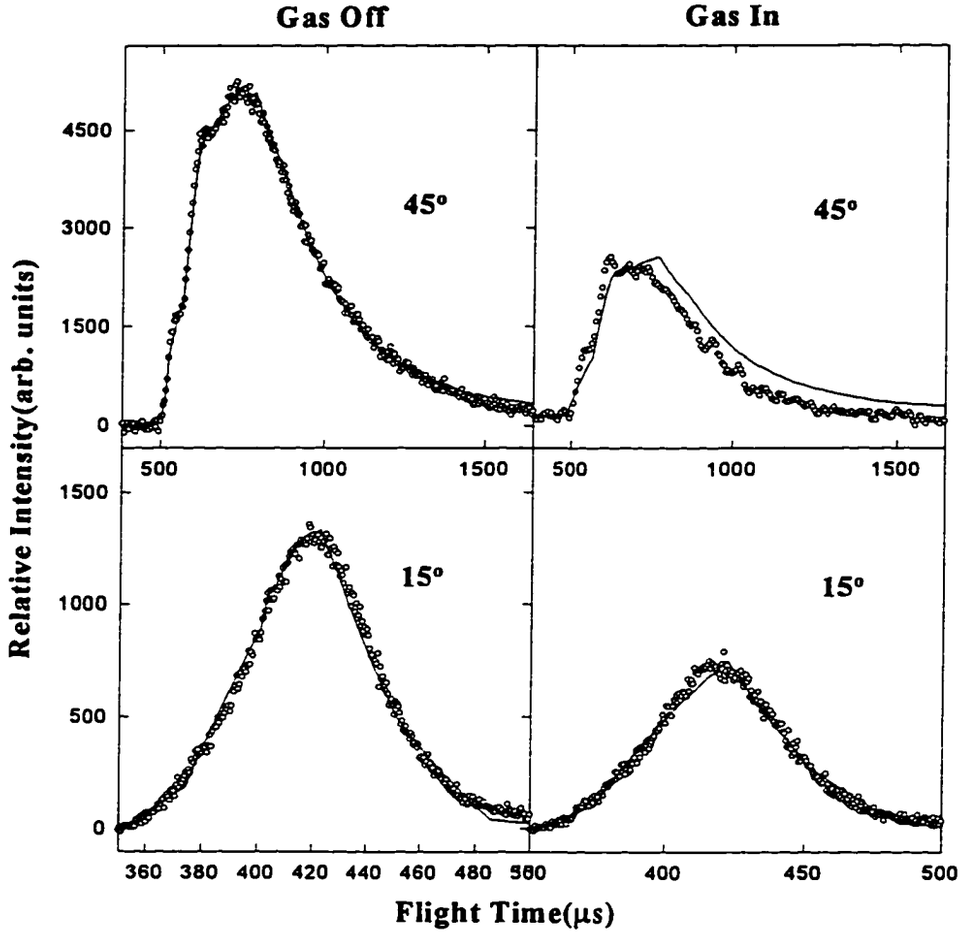

Figure 5. TOF spectra of $SO(^3\Sigma^-)$ for $SO(^3\Sigma^-)$-He with leak valve closed and open.

Table I. Potential parameters for for $SO(^3S^-)$ + He[Ne, Ar, Kr]

	SO-He	SO-Ne	SO-Ar		SO-Kr
	Attr.	Attr.	Attr.	Rep.	Attr.
n	3.7	2.8	3.4	20.8	4.1
$C_n(mevA^{on})$	162	48.1	229	4.43E+16	1834
$r_0(A^o)$ Range	3.8-5.7	4.3-7.1	5.9-9.0		6.3-9.2

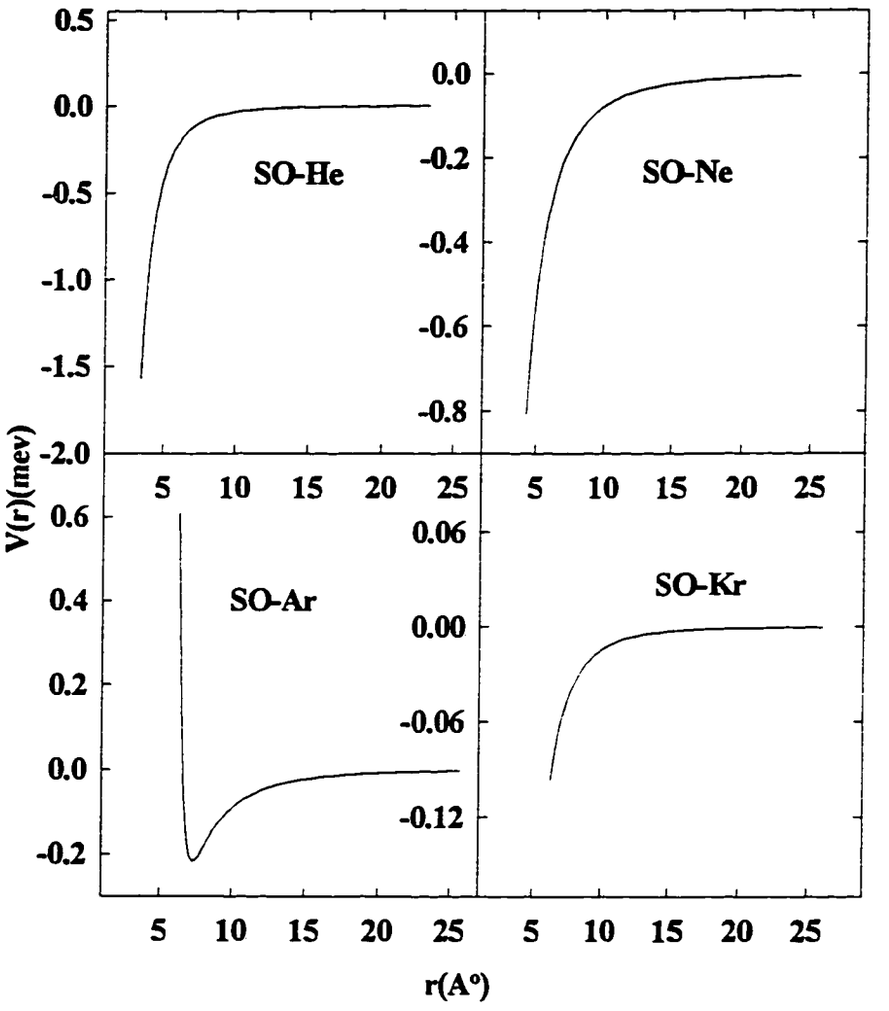

Figure 6 The interaction potential for $SO(^3\Sigma^-)$ + He[Ne, Ar, Kr] at the probing distance.

Discussion

I. Probing Distance

It is conventional to regard the average cross section as probing the potential at a distance of $r_0=(s/2p)^{1/2}$. Since the cross section is a function of velocity, a large velocity range can probe a long distance range of the interaction potential. Due to the relationship:

$$V_{lab}=V_p + V_{c.m} \qquad (8)$$

it is evident that the lab velocity (V_{lab}) can cover a broad range in our experiment by changing the parent velocity v_0 and lab angle θ, which is defined to be the angle between the seeded SO_2 molecular beam and the detector axis,

Based on the energy conservation:

$$h\nu(193) + E^*_{int} = D_0(OS\text{-}O) + E_e + E_v + E_r + E_{c.m} \qquad (9)$$

where $h\nu$ is the photon energy of the laser (147.9kcal/mol); E^*_{int} is the initial internal energy of the parent SO_2 molecule (assumed to be negligible due to supersonic cooling); $D_0(OS\text{-}O)$ is the dissociation energy for the OS-O bond at 0 K; and E_e, E_v, E_r, and $E_{c.m}$ are the electronic, vibrational, rotational, and c.m. translational energies of the photofragments, respectively. A value of 132 kcal/mol has been given previously for the dissociation energy of the OS-O bond at 298 K.[15] Using this value, we have constructed a Newton diagram, shown in fig. 6, for the formation

of SO and O by process (1) using Eq. (9). Here $V_{c.m}(O)$ and $V_{Lab}(O)$ represent the maximum c.m. and laboratory velocities. From the Newton diagram, the maximum $V_{c.m}(O)$, which is 2~3 times V_0, dominates $V_{lab}(O)$. Therefore, the experiments have been performed over only a high velocity range for $O(^3P)$.

The Newton diagram for SO, which is shown in fig. 7, is different from that for O. It clearly shows that the beam angle has a tremendous influence on V_0due to the small maximum $V_{c.m}(SO)$. Fig. 5 shows that the TOF spectrum for SO at θ_{lab}=45° covers twice the velocity range of that for SO at θ_{lab}=15° and goes to a slow velocity range.

It is noticed that V_0 also can be changed by changing the carrier gas. For example, in the photodissociation of SO_2[15] using Ne, V_0 is about 10 times smaller compared to that He is used. In that way, the velocity (V_{lab}) is extended to very slow velocity range, which is important for observing glory undulations.

II. Resolution

The resolution angle is simply given by the detector viewing angle. In our experimental setup, this angle is about one degree. This angle is limited due to the long flight distance (gas cell center to detector distance is about 43 cm) in our apparatus. In our experimental velocity range, ϑ is smaller than the limiting angle characteristic of the system. This is given by $\vartheta \sim \pi h/\mu g(\sigma/2\pi)^{1/2}$.[2] Since the ambient gas cell temperature is about 40 °C in our experiment. it is necessary to cool the gas cell to increase the resolution.

In summary, photodissociation processes can be used to study the interaction between radical and molecules. The radical velocity range can be extended by changing the parent molecular beam angle and carrier gas. In this study, the Scattering Cross Sections For

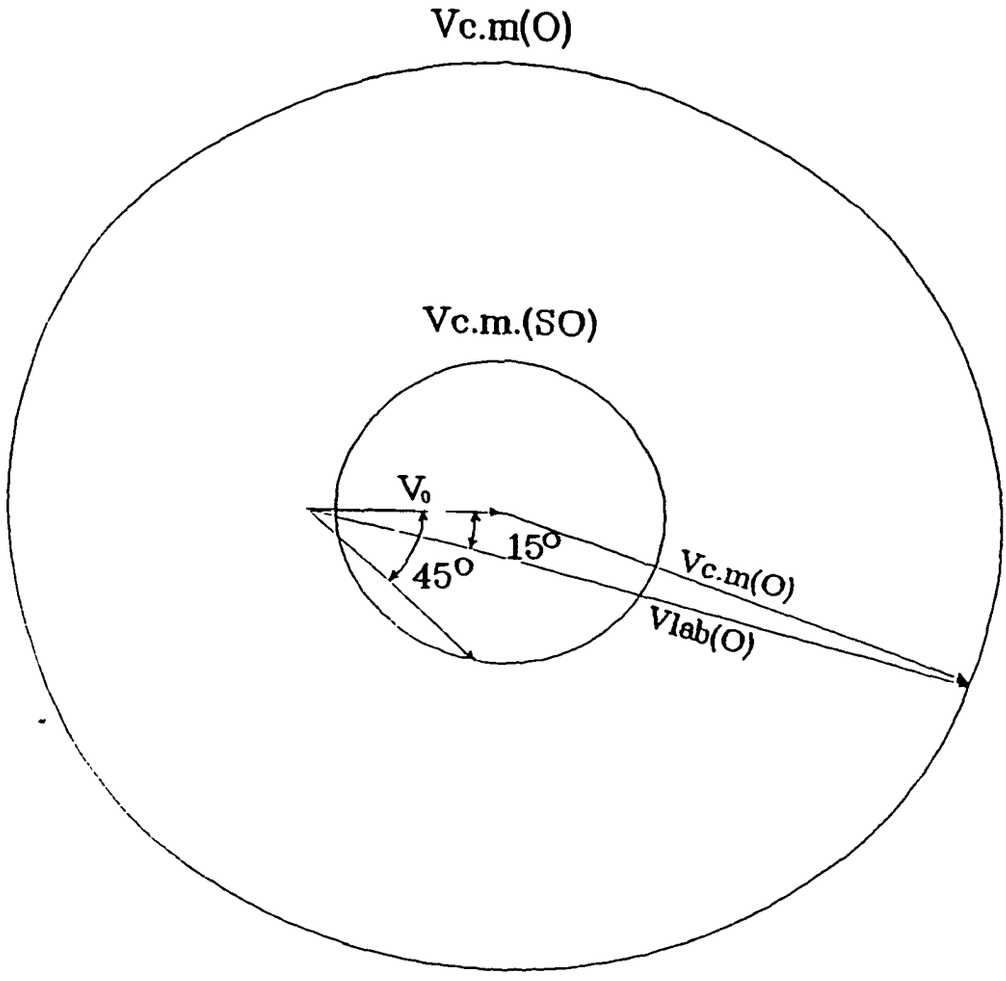

Figure 7. Kinematics for the formation of $SO_2 \rightarrow O(^3P) + SO(^3\Sigma^-)$ by the 193 nm photodissociation of SO_2. V_p is the laboratory velocity for SO_2. $V_{c.m}(O)$ and $V_{c.m}(SO)$ are the maximum c.m. velocities for $O(^3P)$ and $SO(^3\Sigma^-)$, respectively.

$O(^3P)[SO(X,^3\Sigma^-)]$ + He[Ne, Ar, Kr] have been measured, and the interaction potential has been derived.

Conclusion

Scattering cross sections for $O(^3P)[SO(X,^3\Sigma^-)]$ + He[Ne, Ar, Kr] have been measured in photodissociation apparatus. In comparison with other methods, the scattering particles can be prepared in a pure state, but the measurement of velocity range is limited by the nature of the molecule photodissociation.. The scattering for $O(^3P)$ + He[Ne, Ar, Kr] obeys the rigid sphere model at high velocity range. The measurement of impact parameters, r_0, for the scattering of $O(^3P)$ + He[Ne] are close to the summation of van der Waals radii of the colliding particles. The measurements for $SO(X,^3\Sigma^-)$ + He[Ne, Ar, Kr] show that the interaction potential is of the form $V(r)=\pm C_n/r^n$. Values for C_n and n are also presented.

References

(1) R. D. Levine and R. B. Berstein, Molecular reaction dynamics and chemical reactivity (Oxford, New York, 1987).

(2) G. Scoles, D. Bassi, U. Buck and D. Laine, Atomic and Molecular beam method. Vol.I (Oxford, New York, 1988)

(3) D. M. Neumark, A. M. Wodtke, G. N. Robinson, C. C. Hayden, and Y. T. Lee, *J. Chem. Phys.* **82**, 3045(1985).

(4) D. -C Che and K. Liu, *J. Chem. Phys.* **103**, 5164(1995).

(5) V. Aquilanti, R. Candori, and F. Pirani, *J. Chem. Phys.* **89**, 6157(1988).

(6) B.G.Brunetti, S. Falcinelli, E. Giaquinto, A. Sassara, M. Prieto-Mazanares and F. Vecchiocattivi, *Phys. Rev.* A vol. 52, (1)855.

(7) W. E. Lamb, Jr., and R. C. Retherford, *Phys. Rev.* **79**, 549; **81**, 333(1950).

(8) W. -B Tzeng, H.-M Yin, W.-Y. Leung, J.-Y. Luo, S. Nourbakhsh, G. D. Flesch, and C. Y. Ng, *J. Chem. Phys.* **88**, 1658(1988).

(9) S. Nourbakhsh, C.-L. Liao and C. Y. Ng, *J. Chem. Phys.* **92**, 6587(1990).

(10) S Nourbakhsh, K. Norwood, H.-M. Yin, C.-L. Liao and C. Y. Ng, *J. Chem. Phys.* **95**, 5014(1991).

(11) S. Nourbakhsh, K. Norwood, H.-M. Yin, C.-L. Liao, and C. Y. Ng, *J. Chem. Phys.* **95**, 946(1991)

(12) S. Nourbakhsh, H.-M. Yin, C.-L. Liao, and C. Y. Ng, *Chem. Phys. Lett.* **183**, 348(1991).

(13) S. Nourbakhsh, K. Norwood, G.-Z. He, and C. Y. Ng, *J. Am. Chem. Soc.* **113**, 6311(1991).

(14) S. Nourbakhsh, H.-M. Yin, C.-L. Liao and C. Y. Ng, *Chem. Phys. Lett.* **190**, 469(1992).

(15) P. Felder, C. S. Effenhauser, B. M. Haas and J. R. Huber, *Chem. Phys. Lett.* **148**,417(1988).

(16) P. felder, B.-M. Haas and J. R. Huber, *Chem. Phys. Lett.* **186**, 177(1991).

(17) E. J. Hintsa, X. Zhao, and Y. T. Lee, *J. Chem. Phys.* **92**, 2280(1990).

18. X. Zhao, Ph.D. Thesis, University of California, Berkeley, CA(1988).

19. L. J. Butler, E. J. Hintsa, S. F. Shane, and Y. T. Lee, J. Chem. Phys. 86, 2051(1987).

20. H. S. W. Massey and C. B. O. Mohr, Proc. Roy. Soc. (LonDon) A141(1933)434.

21. L. Pauling, The nature of the chemical bond(Ithaca, New York)(1960).

22. E.A. Mason, and V. D. Maijdenberg, Physica 117A, 139.

GENERAL CONCLUSION

Photodissociation dynamics of polyatomic molecules for $C_6H_5COCH_3$, $(CH_3)_2SO$, $HSCH_2CH_2SH$, and C_4H_4S(Thiophene) have been studied by using photofragment translational spectroscopy. The TOF spectra for CH_3 and C_6H_5 resulting from photofragmentation of $C_6H_5COCH_3$ show that the branching ratio of $C_6H_5 + COCH_3$ to $C_6H_5CO + CH_3$ is ≈ 1 for 193 nm excitation, but that ratio decreases to ≈ 0.01 at 248 nm excitation,. The secondary dissociation, $C_6H_5CO^* \rightarrow C_6H_5 + CO$ and $CH_3CO^* \rightarrow CH_3 + CO$, is only observed at 193 nm excitation. However, the minor process, $CH_3COC_6H_5 \rightarrow CH_3C_6H_5 + CO$, is detected at both 193 nm and 248 nm excitation. The maximum release of translational energy for process $CH_3COC_6H_5 \rightarrow C_6H_5CO + CH_3$ at 248 nm indicates that the C_6H_5CO-CH_3 bond energy is 80.2 ± 3 kcal/mol. The product processes resulting from the 193.3 nm photofragmentation of $(CH_3)_2SO$ show that CH_3SO, CH_3 and SO are the dominant photoproducts. The $E_{c.m.}$ energy distribution for photofragments of $(CH_3)_2SO \rightarrow CH_3 + CH_3SO$ peaks at $E_{c.m.} \approx 3$ kcal/mol, indicating that CH_3SO and CH_3 are formed with considerable internal energies. Data analysis suggests that $\approx 53\%$ of the CH_3SO radicals initially formed by process $(CH_3)_2SO \rightarrow CH_3 + CH_3SO$ at 193 nm excitation undergo spontaneous dissociation to $CH_3 + SO$, with a quantum yield of ≈ 1.53 for CH_3. The product processes resulting from the 193 nm photofragmentation of $HSCH_2CH_2SH$ have shown that the C-S scission to yield $SH + CH_2CH_2SH$ constitutes the overwhelmingly dominant product process. On the basis of the $E_{c.m}$ threshold for the $P(E_{c.m})$ distribution of $HS + CH_2CH_2SH$, we obtain a value of 74 ± 2 kcal/mol for $D_0(HS\text{-}CH_2CH_2SH)$. The angular distribution measurements of SH gives β=-

0.4±0.1 for process: $HSCH_2CH_2SH \rightarrow HS + CH_2CH_2SH$, indicating that the C-S bond fission is fast with respect to molecular rotation. Photodissociation of thiophene, a cyclic organic compound, revealed different pathways of transient biradical decay by breakage of different bonds. Five dissociation processes have been identified as follows:

$$C_4H_4S(\text{Thiophene}) \rightarrow HC{\equiv}CH + C_2H_2S \quad (1)$$

$$C_4H_4S(\text{Thiophene}) \rightarrow S + C_4H_4 \quad (2)$$

$$C_4H_4S(\text{Thiophene}) \rightarrow C_3H_3 + HCS \quad (3)$$

$$C_4H_4S(\text{Thiophene}) \rightarrow CS + C_3H_4 \quad (4)$$

$$C_4H_4S(\text{Thiophene}) \rightarrow SH + C_4H_3 \quad (5)$$

The derived $P(E_{c.m})$ for these processes shows characteristics of unimolecular decay. For process (1), two isomer products: •CHCHS• and *c*-CH=CHS are observed from TOF spectra for C_2H_2S. By observing the maximum release of translational energy, the bond energies, including bond cleavages of a primary step and a secondary step, have been determined to be 113.5 ± 2, 133.5±2 and 138±2 kcal/mol for *c*-CH=CHS + HC≡CH, •CHCHS• + HC≡CH, and SH + C=CH-CH=CH, respectively, which is in agreement with literature data. Furthermore, the isotropic angular distribution for all of these processes is consistent with the fact that photodissociation processes occur via a stepwise mechanism.

Scattering cross sections for $O(^3P)[SO(X,^3\Sigma^-)]$ + He[Ne, Ar, Kr] have been measured in the modified photofragment translational spectroscopy apparatus. In comparison with other

methods, the scattering particles can be prepared in a pure state, but measurement of the velocity range is limited by the nature of the molecule photodissociation.. The scattering for $O(^3P)$ + He[Ne, Ar, Kr] obeys the rigid sphere model at high velocity range. The measurements of impact parameters, r_0, for the scattering of $O(^3P)$ + He[Ne] are close to the summation of van der Waals radii of the colliding particles. The measurements for $SO(X,^3\Sigma^-)$ + He[Ne, Ar, Kr] show that the interaction potential is of the form $V(r)=\pm C_n/r^n$. Values for C_n and n have also been determined.